DETECTION AND CHARACTERIZATION OF MALATHION ADHERENCE TO PIPING MATERIALS USED IN WATER DISTRIBUTION SYSTEMS

THESIS

William D. Flemings, CPT, USA
AFIT-ENV-MS-15-M-096

DISTRIBUTION STATEMENT A.

APPROVED FOR PUBLIC RELEASE; DISTRIBUTION UNLIMITED.

AFIT-ENV-MS-15-M-096

DETECTION AND CHARACTERIZATION OF MALATHION ADHERENCE TO PIPING MATERIALS USED IN WATER DISTRIBUTION SYSTEMS

THESIS

Presented to the Faculty

Department of Engineering Physics

Graduate School of Engineering and Management

Air Force Institute of Technology

Air University

Air Education and Training Command

In Partial Fulfillment of the Requirements for the

Degree of Master of Science in Combating Weapons of Mass Destruction

William D. Flemings, BS

CPT, USA

March 2015

AFIT-ENV-MS-15-M-096

DETECTION AND CHARACTERIZATION OF MALATHION ADHERENCE TO PIPING MATERIALS USED IN WATER DISTRIBUTION SYSTEMS

William D. Flemings, BS
CPT, USA

Committee:

Dr. Willie Harper, PhD
Chairman

LTC Douglas Lewis, PhD
Member

Dr. Michael Shelley, PhD
Member

Abstract

"Protection of the public water supply is a national security priority, and as such, it is important to better understand the fate of a chemical weapons agent injection into a public water distribution system. This study investigated the adherence of malathion to pipe materials that are used in public water distribution systems, with malathion serving as a chemical representative of the organophosphorus nerve agent VX. Copper and iron specimen were exposed to malathion solutions for periods of 4, 8, and 24 hours and then tested for evidence of chemical adherence to the metal surfaces. Nonlinear desiccation profiles revealed total mass losses that were typically between 0.01-0.02% but notable mass increases were also observed during desiccation, likely due to surface reactions involving oxygen. Normalized mass differences were poorly correlated with the malathion concentrations (R^2 typically < 0.6), which suggests that mass-based measurements are not sufficient to determine malathion exposure to pipe materials. X-ray photoelectron spectroscopy was also used in an effort to detect shifts in the adsorptive spectra that appeared to be attributable to the presence of trace levels of malathion on the surface of the exposed pipe materials. The spectra observed from the XPS analysis of the copper and iron specimen suggests that the presence of malathion on the surface of the pipe material can sufficiently be detected and measured by XPS analysis. To the author's knowledge, this is the first study to investigate malathion adherence to pipe materials with mass measurements and XPS."

Acknowledgements

First, I would like to thank the United States Environmental Protection Agency's National Homeland Security Research Center for sponsoring this project. Next I would like to thank Dr. Willie Harper for his continual guidance and encouragement over the course of the project. I would like to thank LTC Douglas Lewis and Dr. Michael Shelley for their willingness to serve as part of my committee. I would like to thank Dr. Daniel Felker for taking time out of his day on numerous occasions to assist in my understanding of the XPS as well as setting me up with the correct lab equipment. Capt Walter Lee and CPT Shamaun Holston were instrumental in both helping me prepare for the performance of this study, as well as in the preparation of this document. Finally, I would like to thank my wife for all of her support along the way.

William D. Flemings

Table of Contents Page

List of Figures

List of Tables

Table Page

DETECTION AND CHARACTERIZATION OF MALATHION ADHERENCE TO PIPING MATERIALS USED IN WATER DISTRIBUTION SYSTEMS

I. Introduction

1.1 Background

Chemical contamination of water supply systems as a means of a chemical weapons attack has long been a national security concern, particularly the use of chemicals such as VX, given its high persistence in the environment [1]. The Bioterrorism Act of 2002 set the requirement that drinking water utilities serving more than 3,300 people conduct vulnerability assessments and develop emergency response plans. The EPA is tasked with assisting utilities in their effort to meet these requirements by developing tools and methodologies capable of (1) identifying and prioritizing threats to drinking water and wastewater infrastructure, (2) evaluating vulnerabilities, (3) creating standard frameworks for risk management, and (4) planning for countermeasures to reduce the risk of intentional contamination [2]. This tasking is derived from Homeland Security Presidential Directive 9, which triggered the EPA's establishment of the Water Security Initiative. This initiative is a program that is intended to assist drinking water utilities in identifying and responding to water quality problems, including contamination, in the distribution system. Water quality concerns for drinking water utilities include, but are not limited to, that of intentional contamination by way of terrorist activity. There is much interest in technologies that can be used to detect a contamination event as well as dispel or confirm the credibility of such a threat. Currently, there are several methods in existence that are capable of detecting Chemical Agents (CA) such as VX and Soman, but these

methods are limited in their ability to characterize the existence and/or level of contamination of these agents within a water distribution system. In response to these limitations and the responsibilities maintained by the EPA, water and waste water research is conducted regularly by the US Environmental Protection Agency (EPA) Homeland Security Program (HSRP). In late 2005, the EPA conducted an evaluation of four different enzymatic test kits in an effort to determine their ability to accurately detect the presence of chemical agents, carbamate pesticides, and organophosphate pesticides through a cholinesterase enzyme reaction [2]. The EPA concluded that given the enzymatic test kits' inability to produce any results other than those of a qualitative nature, that while the test kits were capable of validating the presence of the tested chemicals, they could not be used to distinguish between contaminants [2]. While this capability is useful, it is not sufficient for characterization and/or the determination of contamination levels. This inefficiency in current technology is driven by current knowledge gaps that limit the evolution of water quality technology. The current study is tasked with providing some of the knowledge necessary to bridge the current gap, and further enhance the research into water quality technologies. Furthermore, higher accuracy in detection and classification by quantification is not only a sought after analytical technique, but it is advantageous to future water distribution contamination studies from a Weapons of Mass Destruction perspective.

1.2 Malathion

The chemical Malathion will be used in this study as a direct representative of the chemical agent VX, given its similar chemical properties as an organophosphate. This decision was made for safety purposes based on the significantly lower level of toxicity associated with Malathion versus that of the chemical agent VX. The chemical name for Malathion is (*diethyl*

(*dimethoxyphosphinothioylthio*) *succinate*). It is an organophosphate that has historically been used as an insecticide and is considered a neurotoxin. The molecular formula for Malathion is $C_{10}H_{19}O_6PS_2$ [3].

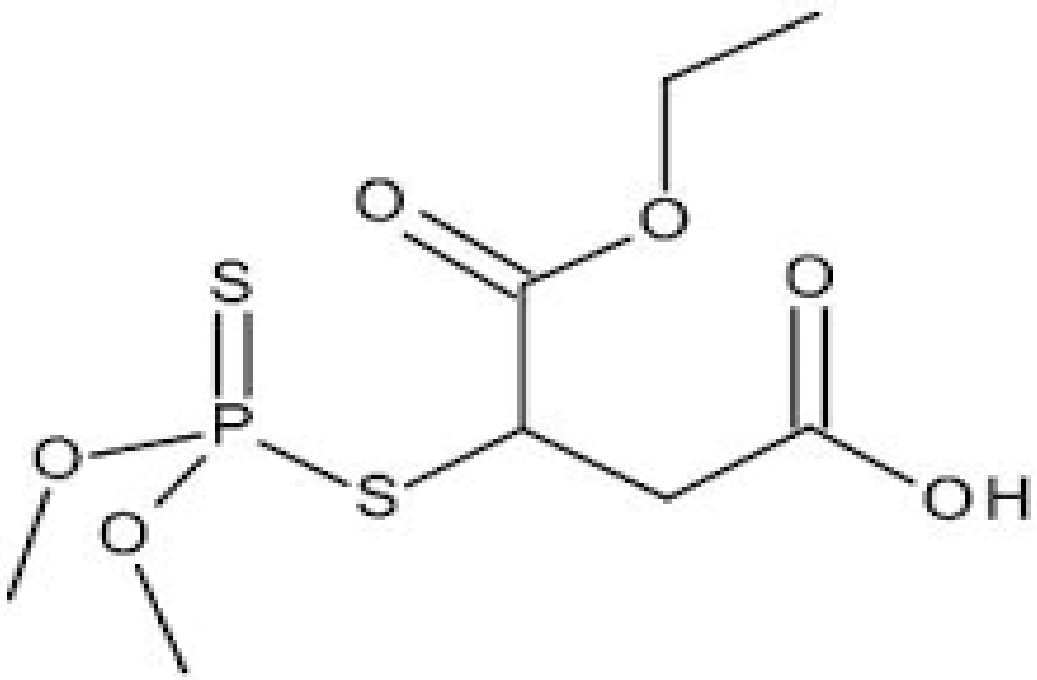

Figure 1. Chemical Structure of Malathion [74]

As a chemical substance, it was first registered in 1956 [3]. As an organophosphate (phosphate ester), it is a substance from a family of esters of phosphoric acid. Some examples of other organophosphorus compounds are that of DNA, RNA, and many co-factors that are essential for life [3]. As a result of their biochemical properties, organophosphorus compounds form the basis for many of the insecticides, as well as that of many of the nerve agents. Their use in these particular substances is based on taking advantage not only of their, on average, high acute toxicity level, but also the adverse neurobehavioral effects they cause [4]. The employment of organophosphorus compounds as effective insecticides and nerve agents is subject to their ability to act on the enzyme Acetyl cholinesterase (AChE); a process that will be discussed later in detail. The interaction with AChE by these compounds provides them with the ability to adversely affect the nerve function of insects and humans. For this reason, many organophosphorus compounds, such as Parathion and Malathion, have been used as insecticides, while other organophosphorus compounds, such as VX and Sarin, have been used as nerve agents. Malathion specifically, has been used as an insecticide in combating the Mediterranean fruit-fly, as well as the West-Nile virus transmitting mosquitoes. Nerve agents are considerably more toxic than pesticides, as the pesticides tend to degrade rapidly through exposure to sunlight, air, and soil. However, this degradation does not undermine the substance's overall level of toxicity. Malathion is a commonly used pesticide, therefore, regularly exposing the general public to its relatively low level of toxicity. It is the exposure to these low levels of toxicity that are the major concern with chemicals such as pesticides. A more specific concern is the exposure of children to the pesticide since it is widely used at playgrounds and recreational areas to control pests in areas where children play. And it was this concern that lead to the EPA ban of the residential use of these pesticides in 2001 [5].

1.3 VX

The chemical name for VX is O-ethyl S-[2-(*diisopropylamino*)*ethyl*] *methylphosphonothioate*. VX is an organophosphate with a much higher level of toxicity than that of Malathion. The only known use for VX is as a chemical weapon. The molecular formula for VX is $C_{11}H_{26}NO_2PS$ [6].

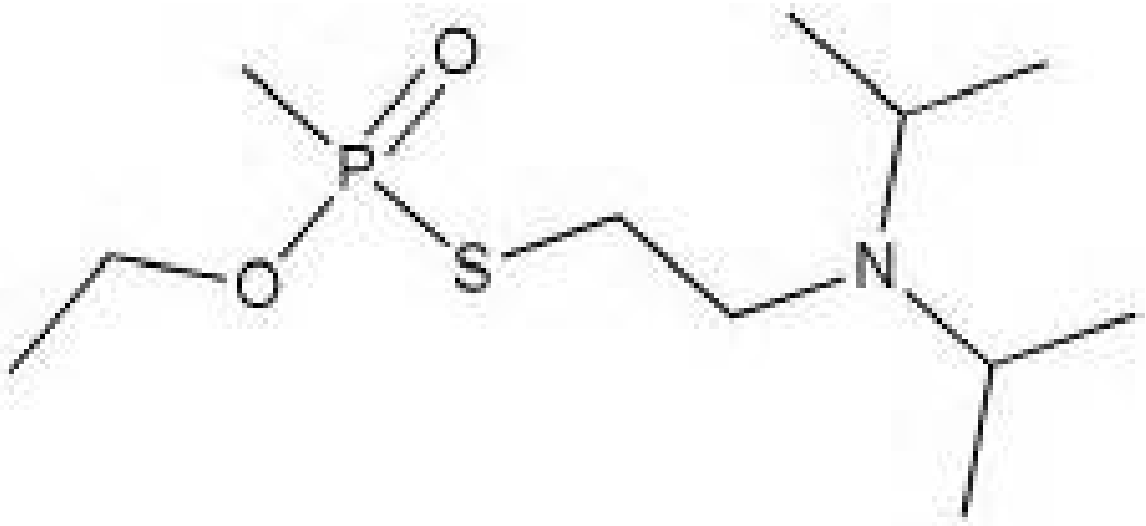

Figure 2. Chemical Structure of VX [6]

Due to the nature of its primary use, the production and stockpiling of VX was outlawed by the Chemical Weapons Convention of 1993 [7]. As an organophosphate, VX is similar to Malathion in that its toxic effect is the result of its *acetylcholinesterase* (AChE) inhibition. VX has a higher level of toxicity than that of Malathion as a result of the much higher affinity its R-group has for the active site of the AChE. Although, Malathion has the same mechanism of toxicity as that of VX, it is far less toxic to human beings [8]. This phenomenon is responsible for the effectiveness of VX as a chemical weapon. VX can take the form of both a liquid and a

gas, and given its high persistence in the environment; as a result of its low volatility, along with its colorless and odorless characteristics, it is a major concern for introduction into an American water distribution system.

1.4 Water Distribution Systems

A water distribution system consists of a vast amount of interconnected pipes, storage facilities, and other components necessary to meet the drinking water supply and fire protection requirements for the majority of the facilities found in any town, city, state, or nation. Such a system is required to provide an uninterrupted source of pressurized drinking water to all consumers. In the United States, this system consists of almost one million miles of interconnected piping and components. Water distribution systems are constructed with mains that are used to carry the water from the water treatment plant (or source if no treatment is required) to the consumer. To protect the water distribution systems across the United States, the Environmental Protection Agency (EPA) has implemented distribution system regulations [5]. These regulations consists of the Surface Water Treatment Rules (disinfectant residual and sanitary survey requirements), the Stage 1 and 2 Disinfectants and Disinfection Byproducts Rules (DBPR) (monitoring for DBPs in the distribution system), the Ground Water Rule (sanitary surveys), and the Total Coliform Rule (monitoring for bacterial contamination in distribution systems).

1.5 Chemical Agent Detection

The capability of detecting the presence of Chemical Agents (CA) has been available for some time. At present, there is a wide variety of detectors commercially available, however, due to their individual capabilities, not all are suitable for use in every potential threat scenario [9].

The numerous detectors available will vary based on factors such as selectivity, sensitivity, and response time. A good detector will offer a sufficient and effective balance between these factors in an effort to provide maximum detection capability, minimum false alarm actuation, and protect the user from unnecessary exposure. One example of such a detection capability is that of Ion Mobility Spectroscopy (IMS). IMS is a separation technique that allows ionized analyte molecules to be distinguished on the basis of their mass, charge, and mobility in the gas phase [9]. An IMS device operates by drawing a sample vapor into the detector inlet, where the chemical will diffuse through a membrane into an ionization region. After entering the ionization region, the vapor will be ionized under atmospheric conditions. This ionization will result in the migration of a cloud of ions in an electric field into the drift region, where the ions will be separated based on their ionic mobility. The ions will then be accelerated towards a collector located at the end of the drift tube. At the collector, the ions will collide and release their charge, generating a current that will be registered as a signal by a signal processor. The generated signal will be a series of peaks that represent the relative drift times for the various substances that are present in the vapor. A plot of the current generated by a series of peaks over time is referred to as an ion mobility spectrum. The spectrum will be compared to the detector's internal library and an alarm will be generated when there is a match to any archived spectrum for a chemical agent [9]. While this is certainly a sufficient technology for detecting a chemical agent, it will prove ineffective in the case of the scenario presented in this study. The scenario presented here is based on a CA exposure to a drinking water distribution system, in which case, no vapor would be available for sampling within the distribution system itself. The requirement for this study is that detection is possible within the distribution system during operation. Most of the chemical agent detection technology currently available is incapable of meeting this requirement, and

those that are capable of sampling a chemical agent in liquid form are not applicable during water distribution operation. This lack of chemical agent detection capability is the basis of the current study. The intent of this study is to provide a baseline of knowledge with respect to characteristic nature of the adsorption of a chemical agent; an organophosphate in this case, to the pipe material used in a drinking water distribution system.

1.6 US Environmental Protection Agency (EPA)

Malathion is considered by the EPA to have a low level of toxicity threat to human beings. It is actually much more toxic to aquatic organisms and bees. This low level of toxicity with respect to human beings does not mean that its use is not regulated. The Food and Drug Administration (FDA) and the EPA have set a maximum level of Malathion residue allowed on food crops to that of 8 parts per million (ppm), giving the impression that there is some level of concern with respect to the toxicity of Malathion. The toxicity of any substance is based upon a particular mechanism(s) by which the substance causes adverse effects external and/or internal to an organism. For Malathion, the mechanism of toxicity is similar to that of many organophosphates; it is that of cholinesterase inhibition. Malathion is considered to be an irreversible AChE inhibitor. This implies that Malathion inhibits the enzyme AChE from breaking down Acetylcholine (ACh). The AChE enzyme is used to hydrolyze the neurotransmitter ACh. This enzyme is mostly found at neuromuscular junctions and cholinergic brain synapses where it is used to terminate a requested and generated synaptic transmission. This signal termination is vital to the proper biological function of the human body, as well as other mammals and insects. The process of communication between neurons is called neurotransmission. This process takes place as a result of a threshold action potential, causing the release of a neurotransmitter at the pre-synaptic terminal. This neurotransmitter will move along

the synapse until it reaches the post-synaptic neuron where it will bind with its receptor, which will cause either an inhibition or an excitation of the post-synaptic neuron. This induction can lead to information passage through electrical signals to other neurons, or muscle cell contraction via electrical signals as well. In addition to the presence of the neurotransmitter at the post-synaptic terminal is the presence of the enzyme AChE. The enzyme will act to terminate the signal by hydrolyzing the ACh. This reduces the concentration of ACh at the post-synaptic membrane. In order to allow for another signal to be transmitted and received, the concentration of ACh must be lowered at the post-synaptic cleft, and this is only possible via the release of Ach from its receptors. The release of the Ach by the receptors is conducted via the hydrolyzation of the AChE. Therefore, if the AChE is inhibited, there will be build-up of ACh at the post-synaptic cleft. This build-up will block the transmission of any new signals to the neuron, and subsequently lock in any previously transmitted signal due to the over-presence of ACh. If this occurs at a neuromuscular junction, it can lead to a continuous muscle spasm. This continuous muscle spasm will eventually lead to muscle fatigue, or in the case of a reverse operating neuromuscular junction, paralysis [4]. Other possible side effects created by the process of AChE inhibition are that of convulsions, bronchia constriction, and death by asphyxiation. According to the EPA, the human health risk assessment incorporates potential exposure risks from all sources, which include food, drinking water, residential (if applicable), and occupational scenarios [4]. The assessment is designed such that it can determine the likelihood of adverse health effects caused as a result of exposure to the substance. These adverse effects take into account that of acute, as well as that of chronic. In addition to the given scenarios, the assessment is also designed to take into account that of all population subgroups (i.e. women, men, children, and infants). The Agency issued a Data Call-In in October, 2004 requiring the special

cholinesterase assay [4]. A measure of the cholinesterase inhibition ability of Malathion was observed in several species of mammals with respect to different methods of exposure. The possible methods of exposure for Malathion are inhalation, ingestion, dermal, and eye exposure. The most likely of which is that of inhalation and ingestion due to the nature of the use of Malathion as pesticide. The assessment studies did reveal some observed adverse health effects at the lowest tested levels. However, these effects were minimal in severity, as well as occurrence. The result of the assessment was the determination that “Malathion exhibits low acute toxicity via the oral, dermal, and inhalation routes” [4]. As there have been no previous efforts to study the adherence of Malathion to pipe materials; to the author's knowledge, other studies in the area of the characteristic properties of Malathion must be researched and related to that of the current water infrastructure study as it pertains to that of the behavior of Malathion in a water distribution system. There have been previous efforts to study Malathion adsorption to soil, Konrad et al., related rates of Malathion degradation directly to the extent of Malathion adsorption to soil. Eugene E. Kemaga, 1979, calculated the soil sorption coefficients (K_{oc}) for numerous pesticides. Wauchope et al., 2002, examined the theory, uses, measurement or estimation, limitations and reliability if the soil sorption coefficient (K_d) and the soil organic carbon sorption coefficient (K_{oc}) of pesticides, and provided some rules of thumb for the use of the parameters in describing the behavior and fate of pesticides in the environment, including analysis by modeling. Kermit S. Lafleur, 1979, reported on the pesticide adsorption ratios (=amount sorbed/amount supplied) for inorganic, as well as organic substrates with respect to the pesticide concentrations. Not only has Malathion adsorption to soil been studied by numerous individuals and groups, many of these studies have resulted in the calculation, verification, or development of some variant of the soil sorption coefficient for Malathion.

1.7 Homeland Security Research Program (HSRP)

The terrorist attacks of September 11, 2001 was a significant event that triggered a series of both military and legislative actions on the part of the United States. One of such actions was the passing of the Public Health and Bio terrorism Preparedness and Response Act of 2002. Responses to applicable incidents of this nature have lead to the realization that scientific research is a requirement in order to improve the effectiveness and efficiency of the US government's response to such incidents [2]. As a result of this conclusion, the EPA established the Homeland Security Program (HSRP) in an effort to meet this newly developed requirement. The HRSP is tasked with assuming some of the EPA's responsibilities in the given areas [2]:

- maintaining the security of water and waste water systems
- remediation following contamination incidents and natural disasters
- development of a nationwide laboratory network with the capacity to analyze samples for the presence of chemicals and bio toxins, microbial pathogens, or radiological agents

These responsibilities provide an insight to the connection between the nature of this water infrastructure study and that of the role of the US government. The EPA lists the current HSRP research efforts as being aimed at answering the following questions [2]:

- What strategies are needed to make communities, including their water systems, more resilient?
- What information is needed about contaminant behavior and associated exposure/risk to inform mitigation?
- What tools and information are needed to detect contamination and mitigate initial impacts?

- What sampling and analysis methods, protocols, and strategies are needed to enable and inform response and remediation decisions?
- What are the best approaches to communicate risks associated with environmental contamination?
- What are the techniques to minimize impacts and decontaminate following a contamination incident?
- What are the techniques to manage and dispose of contaminated water and waste generated during cleanup?
- What are the systems approaches for integration of overall response and remediation strategies?
- What expertise and consultation is provided to HSRP customers to assist them in their preparedness, response and remediation activities?

These research questions express the need for information from studies like that of the water infrastructure study in which this thesis is based. The first research question specifically speaks to the need to increase the resiliency of community water systems. This needed resiliency will be supported by some of the questions that may be answered by this study, as well as by some of the questions that may be generated.

1.8 RAND National Security Research Division (NSRD)

The RAND National Security Research Division (NSRD) conducts research and analysis for all national security sponsors other than the US Air Force and the US Army [10]. The research conducted by the NSRD spans a vast number of areas, and is conducted within five different centers: (1) the Acquisition and Technology Policy Center, (2) the Forces and

Resources Policy Center, (3) the Homeland Security and Defense Center, (4) the Intelligence Policy Center, and (5) the International Security and Defense Policy Center. The center of concern here is that of the Homeland Security and Defense Center (HSDC). The purpose of this center is to conduct analyses to prepare and protect communities and critical infrastructure from natural disasters and terrorism[[10]. The notable responsibility here being that of the protection of communities from terrorism. This responsibility serves as a bridge between the HSRP and the NSRD, as the NSRD is a tool employed in an effort to meet the needs of the HSRP. And the specific application of this employment is that of the HSDC. The HSDC is responsible for several publications that fall into the following categories [10]:

- Critical Infrastructure Protection
- Domestic Threat Assessment
- Emergency Management
- Intelligence
- Terrorism Risk Management

Despite this broad spectrum of publications, the different research division centers, and the numerous analyses that have been conducted to date, there is currently no ongoing efforts that mirror that of the nature of this water infrastructure study. This is a confirmation of the direct need and applicability of the water infrastructure study itself.

1.9 Objective

The objective of this project is to study the adherence of Malathion to piping materials using sorption experiments, mass-based measurements and X-ray Photoelectron Spectroscopic analysis (XPS). The assumption is that this study will provide a basis for the detection of a

chemical agent such as VX after it has been introduced into a water distribution system. In an effort to accomplish this objective, the following questions will be evaluated:

1. To determine whether mass-based differences can be used to detect Malathion adherence to water distribution piping materials.
2. To determine whether adherence of Malathion to water distribution piping materials can be detected using XPS analysis.

II. Theory

2.1 Adsorption

Adsorption is the adhesion of atoms, ions, or molecules from a gas, liquid, or dissolved solid to a surface [11]. The process is defined by the presence of an adsorbate (the solid surface performing the adsorption) and an adsorbent (the gas or liquid being sorbed). The process of adsorption is surface based, unlike that of the process of absorption where the absorbent is dissolved within the chemical structure of the adsorbate [12]. There are two descriptive forms of adsorption, physisorption and chemisorption , which are based on the interactions of a particular type of chemical bond. In the case of physisorption the characteristic bonds that are responsible for this type of adsorption are that of weak van der Waals forces. In the case of chemisorption, the characteristic bonding is that of covalent bonds [13]. The adsorption process is driven by the existence of an excess of surface energy with respect to that of the adsorbent. This excess surface energy exists due to the physical characteristics of the adsorbent at its surface. At its surface, the atoms are not surrounded by other atoms within the material. This situation allows for a scenario where the surface atoms have the ability to attract other adsorbates in an effort to fill the gaps that exist as a result of the lack of surrounding material at the surface edge [14]. Adsorption is best described via that of an isotherm. The nature of an isotherm is based on the development of a relationship between an adsorbate and an adsorbent in a constant temperature process [15]. For the purposes of this particular study, the relationship of concern is that of the concentration of the adsorbate versus that of the adsorbent. In the case of an isotherm, the quantity adsorbed is nearly always normalized by the mass of the adsorbent. For environmental modeling, three specific types of isotherms have been used in explaining experimental adsorption data [15]. The three isotherms are the Langmuir, BET, and Freundlich. While each model is useful, it is the

Freundlich isotherm that is the most applicable to the scenario presented within this study. The Freundlich isotherm is typically used as an empirical adsorption model for solid-liquid systems. This is in contrast to the other two isotherms models that are more applicable to a gas-liquid system. The Freundlich isotherm model is used to fit data rather than to verify an adsorption mechanism [15]. The Freundlich is modeled by the following equation [15]:

$$q_e = K_f C_e^{1/n} \quad (1)$$

K_f is an empirical constant related to the capacity of the adsorbent material to adsorb the adsorbate, and n is a constant related to the affinity of the adsorbate for the surface The determination of the empirical parameters K_f and 1/n can be accomplished by linearizing the equation and taking the logarithm of both sides of that result to produce the following equation [15]:

$$\log q_e = \log K_f + \frac{1}{n} \log C_e \quad (2)$$

In a study conducted by Vinay K. Singh et al., fly ash obtained from a thermal power plant was used as an adsorbent for the removal of Malathion from aqueous solution. In this particular study, the adsorption dynamics were modeled by way of the Lagergren equation: $\ln(q_e - q) = \ln q_e - k_{ad} * t$; where q_e represented the amount of solute at equilibrium per unit weight of the adsorbent, and k_{ad} represented the rate constant of adsorption (removal of Malathion). From the data, a plot of ln(q_e - q) vs. t was generated at an initial concentration, pH, particle size, and temperature. The generated plot maintained a linear behavior that was perceived to indicate that the adsorption behavior was in-line with the equation used for the kinetic modeling. This allowed for the calculation of the k_{ad} value from the slope of the straight line generated by the plot. The calculation of the k_{ad} value in the study conducted by Vinay K. Singh et al., is consistent with the

method that will be used to calculate a similar value for the current study. The difference will take place in the form of the adsorption isotherm model that is used. As previously mentioned, the adsorption isotherm model that will be used is that of the Freundlich isotherm model. However, the same principles will apply, as the expected linear behavior of the data generated plot will serve as the basis for the calculation of the adsorption rate constant for the current study.

2.2 Volatilization

Volatilization is a process where a chemical substance is converted from a liquid or a solid state to a gaseous or vapor state. One substance can be separated from another by the process of volatilization, and can then be recovered by the condensation of the separated vapor. The volatility of a substance is directly dependent on temperature, and thus, the vapor pressure of that substance [16]. Malathion itself is not very volatile, and thus, would not be expected to become separated from the de-ionized water that it is in solution with in regards to this study. A good measure of this volatility would be based on that of the Henry's constant for malathion in water. Henry's law, was first proposed in 1800 by J.W. Henry as an empirical law well before the development of our modern ideas of chemical equilibrium. The law states that at a constant temperature, the amount of a given gas that dissolves in a given type and volume of liquid is directly proportional to the partial pressure of that gas in equilibrium with that liquid. An equivalent way of stating the law is that the solubility of a gas in a liquid is directly proportional to the partial pressure of the gas above the liquid [17]. The Henry's Law constant for malathion is 4.9×10^{-9} atm-cu m/mole [17]. This Henry's Law constant indicates that malathion is expected to be essentially nonvolatile from water surfaces [18].

Solubility is a property of a solid, liquid, or gaseous chemical substance that describes its ability to dissolve in solution with another solid, liquid, or gas to form one homogeneous chemical compound [19]. The solubility of Malathion is 145 mg/L at 20ºC [5]. This property is a limiting factor in the determination of the concentration of the Malathion/water solution that can be used in this study. The specific Malathion/water solution concentrations (100, 75, 50, and 25 mg/L) chosen for this study were based on this limitation.

2.3 Partitioning Coefficient

A partitioning coefficient is a ratio of concentrations of a compound in a mixture of two immiscible phases at equilibrium [15]. For the purposes of this study, the two phases will be solid (pipe material) and liquid (Malathion). The partitioning coefficient for adsorption will be calculated as follows [5]:

$$K_{ad} = \left(\frac{Mass\ of\ Adsorbate\ Sorbed}{Mass\ of\ Adsorbate\ in\ Solution}\right) = \frac{A_i}{C_i} \quad (3)$$

$$A + C_i = A_i \quad (4)$$

where A = free or unoccupied surface adsorption sites, C_i = total dissolved adsorbate remaining in solution at equilibrium, and A_i = amount of a sorbate on the solid at equilibrium.

2.4 X-ray Photoelectron Spectroscopy

XPS is a surface sensitive quantitative spectroscopic technique that measures the elemental composition at the parts per thousand range, empirical formula, chemical sate, and electronic state of the elements that exist within a material [20]. Essentially, this spectroscopic

technique uses an irradiation method to produce an XPS spectrum that can then be used to determine the chemical composition of the material that has been analyzed. The technique is based on the principle of the photoelectric effect that was first documented by Heinrich Hertz in 1887. This principle describes the phenomenon that takes place when the energy from an incident photon is completely absorbed by an orbital electron. The increase in energy causes the ejection of the orbital electron form its original atom with an energy level as such:

$$E = E_{\gamma} - \phi \tag{5}$$

where E_{γ} is the energy of the incident photon and ϕ is the binding energy for electrons in this particular atomic shell. As a result of this interaction, the incident photon is completely absorbed and its energy is is carried off by the photoelectron. The XPS irradiation method is based on this principle and is conducted by directing a beam of X-rays at the material to be analyzed, while simultaneously measuring the kinetic energy and number of electrons that escape from the top 0 to 10 nm of the material surface. Each atom within the material being analyzed will consists of core electrons with binding energies that are conceptually equal to the ionization energy of that core electron. Therefore, if the photon energy of the incident photon that is directed at the surface of the material is sufficient, it will be absorbed by the core electron, causing its ejection from the orbital, and thus from the surface of the material. The photoelectron will be ejected with an amount of kinetic energy that can be expressed by the following equation:

$$KE = h\nu - E_b - \phi \tag{6}$$

where KE is the kinetic energy of the photoelectron, hν is Plank's constant (h) multiplied by the frequency of the electromagnetic radiation (ν), and ϕ is the binding energy of the core electron.

Due to the short range that these electrons can travel and thus be detected for analysis, the XPS technique requires a high vacuum, on the order of 10^{-8} milli bar, in order to achieve successful operational capability [21]. Although the XPS is capable of detecting all elements in principle, it is however, limited in its ability to detect those elements with an atomic number of 3 or higher. Therefore, limiting its capability to detect Hydrogen and Helium. The XPS spectrum that is produced as a result of material irradiation is a plot of the number of electrons detected versus the binding energy of the detected electrons. The spectra will consist of a series of peaks that coincide with the characteristic binding energies of each element present on the surface of the material being analyzed. The spectral peaks correspond to the electron configuration of the electrons within each of the present atoms. A direct relationship exists between the number of electrons detected in each of the characteristic peaks and the amount of that particular element within the sampling volume of the XPS. The raw data is used to produce atomic percentage values, and therefore, the data must be corrected by dividing the signal intensity by a "relative sensitivity factor" and then normalized over all of the detected elements [21]. It should be noted that the XPS is only capable of detecting those electrons that escape from the surface of the sample material and reach the detector [21]. This is the driving factor behind the high vacuum requirement for proper operation. Therefore, the higher the applied vacuum, the more sensitive the analysis that can be conducted by XPS. Additionally, it should also be noted that as the electrons escape the material being analyzed, they will experience numerous interactions (i.e. inelastic collisions, recombination, and excitation of the sample) that will significantly reduce the number of electrons that can escape the material and reach the detector. As a result, an exponential attenuation factor exists as the depth of the material increases. This results in a significant increase in the detected signal at the surface of the material versus that detected

deeper within the material. Consequently, the XPS is an exponentially surface-weighted signal, and therefore, an optimal analytical technique to use in an effort to detect chemical adsorption to the surface of a given material.

III. Literature Review

3.1 Pesticides in Drinking Water Systems

The presence of Malathion in water distribution systems has received limited attention in previous research projects. There have been some research efforts made with the purpose of understanding, analyzing, and characterizing the health effects associated with the existence of pesticides in water distribution systems and/or their sources. However, those efforts have, for the most part, been directed at the interactions and hazardous behavior of pesticides with the water itself, as opposed to that of the materials associated with the water distribution system(s). In 2004, the World Health Organization (WHO) published a background document for the development of "Guidelines for Drinking-water Quality" [22]. This document described the approaches used in deriving guideline values and presents critical reviews and evaluations of the effects on human health of Malathion in drinking-water. The report concluded that based on the occurrence of Malathion in drinking-water at concentrations much lower than the health-based value, the presence of Malathion in drinking-water under usual conditions is unlikely to represent a hazard to human health. Kolpin et al., (1998), collaborated in a comprehensive review, on behalf of the National Water Quality Assessment Program of the U.S. Geological survey, in an effort to assess the understanding of the occurrence and distribution of pesticides in surface waters; accepted as sources of drinking-water [23]. Coupe et al., (2004), evaluated the effectiveness of the drinking-water treatment process on pesticide concentrations, and found that with respect to that of Malathion, the treatment process either removed or degraded the pesticide completely [24]. This conclusion has opened the door to the possibility that a chemical such as VX would experience the same fate. Bondarenko et al., (2009), reviewed monitoring studies concerned with the pesticide, carbamate, and organophosphate contamination in urban surface

streams in the U.S. The review concluded that Malathion was quickly degraded under aerobic or anaerobic conditions, and that the sorption coefficient consistently increased with exposure time [25].

3.2 Other Chemicals in Water Distribution Systems

The presence of recalcitrant or dangerous organic chemicals in water distribution systems has received considerable attention in previous research efforts. Matilainen et al., (2010), studied the effectiveness of coagulation and flocculation followed by sedimentation/flotation and sand filtration as a water treatment process in the removal of natural organic matter (NOM) from drinking-water [26]. Providenti et al., (1993), examined some of the reasons that bio degradation of recalcitrant compounds may not take place in the environment, despite its proven occurrence in a laboratory environment [27]. Kornaros et al., (2006), examined the effectiveness of a biological trickling filter in a waste water treatment plant at removing dangerous chemicals concentrated in the waste water, produced as a by-product of a company manufacturing organic dyes and varnishes [28]. Due to the obvious health concerns involved, the presence of recalcitrants or dangerous organic chemicals in water distribution systems has received a great deal of attention, to include that of field and laboratory research efforts.

3.3 Chemical Adsorption to Pipe Materials

The adsorption of chemicals to pipe materials has been studied in previous research. Stephanie S. Watson, (2010), reported the results of a pipe material chemical contamination and decontamination research project aimed at evaluating the accumulation of the chemicals in the building's water supply, as well as the methods of removal. The results of the project were used to establish adsorption isotherms for the chemical and the pipe materials [29]. The U.S.

Environmental Protection Agency's (EPA) National Security Research Division (NSRD), 2012, conducted research for the purpose of developing and testing the standardized Persistence and Decontamination Experimental Design Protocol (PDEDP) to quantitatively determine the persistence of individual contaminants to various drinking-water pipe materials, as well as the testing of techniques for decontaminating affected pipe surfaces if the contaminant persists [10]. Kun Li et al., (1999), studied the sorption potential of drainage and water supply piping material with respect to three specific organic chemicals in an effort to obtain a better understanding of the environmental fate and transport of such chemicals when used on a golf course [30]. Wendong et al., studied the effects of humic acid on the adsorption of Zn^{+2} on amorphous $Al(OH)_3$ [31]. The study was conducted as a result of the common existence of Zinc (II) in drinking-water. There are numerous chemicals that will come in contact with water distribution system piping materials, and many of these chemicals will generate adverse effects as a result of this exposure. Based on the concern for these adverse effects, many studies have been conducted and much research effort has been placed in obtaining a better understanding of them, the chemical interactions, treatment, and possible techniques for prevention.

3.4 Water Crystallization

Water crystallization is a phenomenon that may play a role in the results that are observed during this study. It is therefore imperative that this phenomenon is reviewed in order to achieve a better understanding of the behavior as well as its possible impact on the sorption experiment. Igor M. Scishchev et al., (1994), conducted multiple molecular dynamics simulations involving the crystallization of a bulk sample of liquid water. The simulations consisted of a supercooled liquid at 250K that was subjected to a homogeneous static electric field. The results of the simulations suggested that the existence of electric fields near the surface

of various materials can play a role in promoting the crystallization of water [32]. P. Jenniskens et al., (1996), describe a model of water crystallization over long timescales that can be applied to a wide range of impure water ices under typical astrophysical conditions if the fragility factor D can be estimated. The model is based on electron diffraction studies of vapor-deposited water ice that have characterized the dynamical structural changes during crystallization that affect volatile retention in cometary materials [33]. This research is directly applicable as it characterized the affect of water crystallization on chemical retention at the surface of a material. R. Scott Smith et al., (1997), reported on molecular diffusion in amorphous solid water. The results of the study gave indication of a long-range translational diffusion occurring with the amorphous to crystalline ice phase transition, which suggests that the amorphous material exhibits liquid-like translational diffusion prior to crystallization at temperatures near 155K [34]. The described translational diffusion can provide some insight into the behavior of the interaction between water and the surface of a material where a chemical reaction is taking place. Surya Devarakonda et al., (1999), studied supersaturated solutions of THF-water hydrate systems before and during crystallization in an effort to examine the system's behavior in the metastable zone and any anomalies suggesting cluster formation. The study resulted in the production of crystal size distribution (CSD) measurements that were used to compute the hydrate crystal growth rates [35]. M. Strub et al., (2003), modeled the crystallization of a water droplet into a cold humid airflow. The purpose of the study was to examine the behavior of the droplet as it is transformed from the supercooled liquid phase to the liquid-solid phase and finally to the solid phase [36]. The various heat transfer processes were observed as well, which could provide some insight into the nature of the relationship between the water crystallization and heat transfer processes that may have taken place during the desiccation portion of the sorption experiment.

3.5 Chemical Reactions

It is important to note that copper does not react with water due to the nature of the bond between the two hydrogen atoms and the oxygen atom. This arrangement is much more chemically favorable to the oxygen atom than that of which would require an interaction with the copper [37]. The interaction between copper and water will take place under the conditions in which a copper salt (i.e. $CuCl_2$) is placed in the presence of water. A chemical reaction between that of the water and the copper will take place as a result of the dissociation of the copper salt. This dissociation allows for the following interaction between the copper and the water: $Cu^{+2} + 6H_2O(l) \rightarrow [Cu(H_2O)_6]^{+2}(aq)$ [38]. However, this condition is not necessary when considering copper in the presence of moist air. Such a scenario will result in the formation of the compound Copper oxide on the surface of the copper material. The equation for this reaction is as follows: $4Cu(s)+ O_2(g) \rightarrow 2Cu_2O(s)$. The formation of Copper oxide on the surface of the copper material is a phenomenon that will certainly add to the molecular weight of the copper and should be taken into consideration during this study.

Similar to that of the behavior of copper in moist air, iron will react with oxygen in moist air as well. Although, the iron oxide layer that is formed does not serve as a protective coating for the metal from further reaction, rather, the oxide layer will flake off and expose more of the iron metal to the moist air. This process is known as rusting and its formation is as follows: $4Fe(s) + 3O_2(g) \rightarrow 2Fe_2O_3(s)$ and $3Fe(s) + 2O_2(g) \rightarrow 2Fe_3O_4(s)$.

3.6 Contaminant Detection in Water Systems

Rafi Schwartz et al., (2014), conducted a study with the goal of providing a step towards solving the general event detection problem of water distribution systems. Organophosphate

pesticides *Chlorpyrifos* (CP) and *Parathion* (PA) were injected into a water distribution network at various locations under the control and observation of various hydraulic parameters such as pH, alkalinity, and acidity. The results of the study indicated that the injection of these substances could be detected under certain conditions by the observance of a rapid drop in the chlorine level [39]. These results are directly related to those derived from the current study, and can provide a substantial link to the purpose of this study.

Jun Li et al., (2014), conducted a study of the presence of nine selected organophosphate flame retardants (OPFRs) in drinking water in China [40]. Although, the study concluded that the risk of ingesting OPFRs through drinking water was not a major health concern for either adults or children in China, the study itself could provide some insight into the persistence and behavior of organophosphates within a water distribution system. Jaime Nacher-Mastre et al., (2011), conducted an analysis of organophosphate esters (OPEs) via gas chromatography coupled to a high resolution time-in-flight mass analyzer (GC-TOF-MS). The purpose of this analysis was to determine the capability of detecting the presence of the OPEs in environmental water, marine salts, and brine samples at very low concentration levels [41]. The results of the analysis provided confirmation of the capability of detecting several of the OPEs without the need for additional analysis, which is an important link to the current study with respect to understanding the analysis most capable of low level organophosphate detection in water systems. In a similar study, Chunyan Hao et al., (2010), developed and validated a scientific methods using SPE followed by HPLC/MS/MS analysis for the determination of 39 pesticides in different aquatic environmental matrices. Their work resulted in accreditation by the Canadian Association for Laboratory Accreditation and license sure by the Ontario government for drinking water analysis. Elizabeth Flynt et al., (2005), reviewed a method for screening water pollutants called

solid-phase micro extraction (SPME) [42]. The review highlighted the development of a method that uses SPME for the detection of seven specific organophosphate pesticides in drinking water treatment source waters.

The literature suggests that numerous research efforts have been directed in a broad spectrum with respect to that of the detection of chemical contaminants in water distribution systems. While these efforts do not appear to point directly at chemical warfare agents, there is evidence to support the link between the chemical contaminants of concern in the studies and the chemical warfare agents. The chemical similarities between organophosphate pesticides like Malathion and chemical warfare agents like VX provide a means for theoretical analysis that can be supported, and possibly even substantiated by the vast array of research that has already been performed.

IV. Experimentation

4.1 Sorption Experiment

The in-situ sorption experiments were conducted at The Air Force Institute of Technology in the Environmental Science laboratories. The objective of the sorption experiments was to determine the partitioning coefficient associated with the chemical sorption of malathion to copper and iron piping materials. The sorption experiment protocol steps are as follows:

1. Malathion solutions. Make a 1 g/L solution of malathion and perform serial dilutions to achieve the solution concentrations of 1000, 750, 500, and 250 mg/L.
2. Sorbents. Two sorbents will be used for these experiments, copper coupons and iron coupons. Five experimental solutions will be needed for each sorbent.
3. Sorption. Submerge one of each type of coupon in 100 ml of solution in a 500 ml open-mouth flask. Use a magnetic stir bar. Allow mixing to occur for 4 hours and cover flask with para film.
4. Retrieve samples. Use a syringe and plastic tubing to retrieve three 5 ml samples every hour for 4 hours. Filter the samples and place them in labeled vials. Store vials in the refrigerator and carry out HPLC analysis as soon as possible.
5. Stop. Rinse and clean the glassware. Dispose of waste malathion in marked containers.

Several adjustments to the protocol steps were made, and those adjustments are as follows:

1. 100 mg/L of malathion solution was originally prepared instead of 1 g/L due to the realization of the solubility of malathion in water. This solubility is a maximum of 145 mg/L. This change also altered the solution concentrations previously specified.
2. The number of solutions was reduced from five to four due to the decrease in solution concentrations by a factor of 10, and the resulting solution concentrations were 100 mg/L, 75 mg/L, 50 mg/L, and 25 mg/L.
3. A *shaker* was used to adequately mix the malathion solutions instead of a magnetic stir bar.
4. The solutions were allowed to mix for 24 hours instead of 4 hours.
5. The fluid samples using a syringe and plastic tubing were not retrieved. Instead the coupons were retrieved from their respective solutions after soaking for a specified period of time and they were weighed prior to and after their submersion in the malathion solutions.

The 100 mg/L Malathion/water solution was prepared using 1 g of 95% Malathion with a density of 1.23 g/mL as follows:

$$\frac{1g}{1.23g} = 0.813mL \tag{7}$$

81.3 μL of 95% Malathion were added to 1 L of deionized water (the closest pipette measurement was 82 μL). The resulting solution had an assumed concentration of 100 mg/L. This solution was then placed in a shaker for a 24 hour period. After removal from the shaker, the 100 mg/L solution was diluted to 75 mg/L, 50 mg/L, and 25 mg/L.

4.1.1 Equipment

The sorption experiment was conducting using fairly basic laboratory equipment. The laboratory equipment that was used consisted of the following: twenty-four 10 mL test tubes, four 500 mL glass jars, para film, an Excellence Plus Micro Balance, a silicon-gel desiccator, plastic tubing, a 10 mL syringe, and one hundred and twenty copper and iron coupon samples. The twenty-four test tubes were cleaned using soap and deionized water after each sample run. The four 500 mL glass jars were used to store the four Malathion/water solutions during the sorption experiment. The para film was used to cover the opening of each of the glass jars. The micro balance was used to measure the weight of the samples during the sorption experiment. The desiccator was used to remove the moisture from the samples after they were removed from the Malathion/water solutions. The plastic tubing and the syringe were used to siphon 5 mL of the Malathion/water solution from the glass jars into the test tubes. The one hundred and twenty copper and iron samples were submerged in the different Malathion/water solutions, placed in the desiccator, weighed on the micro balance, and analyzed via the XPS. The copper and iron coupons were not handled with exposed skin at any time during the sorption experiment.

4.1.2 Data

The data collected from the sorption experiment consisted of weight measurements via the Excellence Plus Micro Balance. The weight measurements were taken at predetermined times, based on predetermined intervals. Each run included three iron and copper samples submerged in a Malathion/water solution for each of the four different solution concentrations, which equates to twenty-four submerged samples per run. Each sample was weighed and recorded prior to its submergence in its Malathion/water solution. After removal from the Malathion/water solution, each sample was wiped off, weighed, and recorded prior to being

placed into the desiccator. After removal from the desiccator, each sample was weighed and recorded.

4.2 X-ray Photoelectron Spectroscopy (XPS)

The XPS analysis was performed at the Air Force Institute of Technology in the Environmental Services Laboratory. As a result of the level of operational expertise required to use the XPS, the analysis was performed by the Environmental Engineering department chemist Dr. Daniel Felker. The analysis was performed on a sample of an unexposed copper coupon, an unexposed iron coupon, a Malathion exposed copper coupon, and a Malathion exposed iron coupon. Each analysis was performed separately for a period of close to twelve hours. The samples were removed directly from a desiccator prior to their introduction to the XPS, and were not handled with any exposed bare skin. Additionally, the analysis was performed in accordance with an approved scientific procedure.

4.2.1 Equipment

The XPS itself is an instrument that is made of several individual components, and a brief description of some of the more important components is provided in this section. To begin, the XPS has two alpha sources; one is a Mg K-α, with a photon energy (hν) ~ 1253.6 eV , and the other is a Al K-α, with a photon energy (hν) ~ 1486.6 eV . The X-ray beam has an energy level of 10-15 kV . The filament that is used to carry the current has a current of 5-30 mA . The system contains an ultra-high vacuum stainless steel chamber with UHV pumps, an electron collection lens, an electron energy analyzer, Mu-metal magnetic field shielding, an electron detector system, a moderate vacuum sample introduction chamber, sample mounts, a sample stage, and a set of stage manipulators.

4.2.2 Calibration

There a few methods that can be used in order to calibrate an XPS. The most often used and most obvious of them all is the use of a known binding energy standard. This can be conducted with a number of different calibrants, but gold (Au), silver (Ag), and copper (Cu) are the most frequently used. For these three calibrants, there associated structure and binding energies are as follows: $Au4f_{7/2}$ = 3.96 eV , $Ag3d_{5/2}$ = 368.21 eV , and $Cu2p_{3/2}$ = 932.62 eV . However, it should be pointed out that these binding energy values are applicable only for the monochromatic Al K-α source. These values will differ for any other alpha source that is used. For the purposes of the calibration of the XPS used in the current study, the calibrant used was C1s.

The other techniques that can be used to calibrate an XPS are that of the Fermi Level (FL), where by the instrument is calibrated via the determination of the zero binding energy scale from a measurement of the Fermi edge of a metal. The Onset (ON) method can be used, which allows for the calibration of the XPS via the determination of the zero kinetic energy scale from the onset of electron emission. And finally, the Digital Voltmeter (DVM) method, in which the voltages is used to determine the energy scale are calibrated directly by way of an accurate digital voltmeter [21]. The International Organization for Standardization (ISO) has developed and published a brief description of the method used in calibrating the binding energy scales of an XPS instrument equipped with unmonochromated Al and Mg-α sources, as well as those equipped with monochromated Al-α sources [21].

4.2.3 Data

Sample analysis by way of X-ray Photoelectron Spectroscopy generates a spectra graph that is specific to the individual sample and its constituents. The spectra graph consists of a number of peaks and valleys on a graph plotting binding energy versus signal strength. Each peak on the graph is representative of an electron emission at a given binding energy [21]. XPS spectral lines are identified by the shell from which the electron is ejected (1s, 2s, 2p, etc.). The emission peaks are a characteristic of each elements final state configuration, with the exception of elements that are within compounds where ionic or covalent bonding occurs. This particular scenario will produce what is called a chemical shift, where a difference in the binding energy, from that produced by the pure element, can be observed as a result of the breaking of the ionic or covalent bond [21]. Once any chemical shift has been accounted for, the XPS spectra for the analyzed sample is compared with those spectra available in the XPS library for confirmation of element(s) or compound(s) that are present on the surface of the sample.

It is worth noting that the emission of the photoelectron from its orbital will be followed by the emission of an Auger electron. This takes place as a result of the falling of an orbital electron to replace the vacancy created by the emitted photoelectron. In order to maintain conservation of energy, once the orbital electron falls to the lower orbital, an Auger electron is emitted. The XPS will measure the kinetic energy of both the photoelectrons, as well as the Auger electrons. Therefore, the signal produced by the electrons will include both photoelectron and Auger electron lines. The photoelectron line energies are dependent on the incident photon energy, whereas the Auger electron line energies are not. This means that if the XPS spectra was presented on a kinetic energy scale, knowledge of the X-ray source used to collect the data would be required in order to compare the chemical states in different samples using different

sources. To avoid this issue the binding energy scale was derived to make uniform comparisons of chemical states possible without the additional source information requirement.

V. Results

5.1 The Effect of Malathion Exposure on the Mass of Copper and Iron Specimen

The following graphs display two distinct relationships of concern. The first set of graphs was generated from the weight measurements of the copper and iron specimen during the desiccation period. Each group of four measurements were graphed in comparison to the time period in which they were taken. This process produced a Mass Loss vs. Time graph for each specimen coupon with respect to the type of coupon (copper or iron), the malathion concentration (100, 75, 50, or 25 mg/L), and the specific iteration (run 1, 2, 3, 4, or 5). Each graph contains four data points that coincide with the four chosen desiccation time periods (15 min, 1 hr, 4 hr, and 24 hr). The data points were graphed and the curve connecting the data points was fit to a linear model. In an effort to obtain this linear fit, a single data point on each graph was excluded as an outlier. This data point was considered an outlier only for the purposes of fitting the curve.

The second set of graphs display the effects of the immersion of the specimen coupons in the malathion solution on the mass loss of each specimen. The graphical relationship depicted on each of these graphs is that of a comparison of the Normalized Mass Loss values for both the copper and the iron specimen for a specific immersion time period to that of each of the malathion solution concentrations. This relationship was evaluated using the coefficient of regression. This value was overlaid on each of the graphs and assessed at the end of the section.

Figure 3 shows the effect of desiccation times of 15 minutes, 1 hour, 4 hours, and 24 hours on the mass loss of a copper specimen that had been submerged for 24 hours (run 2) in a 100 mg/L solution of malathion in water. The curve of the copper specimen mass loss verse time

relationships is nonlinear, with a relatively sharp decrease in mass in the time 15 min-1 hour time interval. A more moderate decrease was observed in the 1hr-24hr time interval. The graph features an apparent outlier at the 4 hour point; this point was omitted from the regression in order to develop a smooth curve ($R^2 = 0.9875$). Approx. 0.00017 g (< 0.02%) were lost in 24 hours of desiccation. This result showed that copper specimen exposed to 100 mg/L of malathion solution had a non-linear desiccation profile, featuring what appeared to be an apparent outlier.

Figure 4 shows the effect of desiccation times on mass loss for a copper specimen submerged for 24 hours (run 2) in a 75 mg/L solution of malathion in water. A nonlinear curve was observed, the data was fitted to an exponential function with a coefficient of determination (R^2) of 0.9495. The graph features an apparent outlier at the 4 hour point; this point was omitted from the regression in order to develop a smooth curve. The total mass loss observed during the desiccation experiment was approx. 0.00018 g (0.01%). This result showed that copper specimen exposed to 75 mg/L of malathion solution had a desiccation profile showing exponential mass loss and an apparent outlier.

Figure 5 shows the effect of desiccation times on mass loss for a copper specimen submerged for 24 hours (run 2) in a 50 mg/L solution of malathion in water. A nonlinear curve was observed, the data was fitted to an exponential function with a coefficient of determination (R^2) of 0.8662. The 1 hour mass measurement was an apparent outlier. The total mass loss observed during the desiccation experiment was approx. 0.0001 g (0.01%). This result showed that copper specimen exposed to 50 mg/L of malathion solution had a desiccation profile showing exponential mass loss and an apparent outlier.

Figure 6 shows the effect of desiccation times on mass loss for a copper specimen submerged for 24 hours (run 2) in a 25 mg/L solution of malathion in water. A nonlinear curve was observed, the data was fitted to an exponential function with a coefficient of determination (R^2) of 0.9558. The 1 hour mass measurement was an apparent outlier. The total mass loss observed during the desiccation experiment was approx. 0.00012 g (0.01%). This result showed that copper specimen exposed to 25 mg/L of malathion solution had a desiccation profile showing exponential mass loss and an apparent outlier.

Figure 7 shows the effect of desiccation times on mass loss for an iron specimen submerged for 24 hours (run 2) in a 100 mg/L solution of malathion in water. A nonlinear curve was observed, the data was fitted to an exponential function with a coefficient of determination (R^2) of 0.9934. The 1 hour mass measurement was an apparent outlier. The total mass loss observed during the desiccation experiment was approx. 0.00013 g (0.01%). This result showed that iron specimen exposed to 100 mg/L of malathion solution had a desiccation profile showing exponential mass loss and an apparent outlier.

Figure 8 shows the effect of desiccation times on mass loss for an iron specimen submerged for 24 hours (run 2) in a 75 mg/L solution of malathion in water. A nonlinear curve was observed, the data was fitted to an exponential function with a coefficient of determination (R^2) of 1. The 15 min and 4 hour mass measurements were apparent outliers. The total mass loss observed during the desiccation experiment was approx. 0.00013 g (0.01%). This result showed that iron specimen exposed to 75 mg/L of malathion solution had a desiccation profile showing exponential mass loss and two apparent outliers.

Figure 9 shows the effect of desiccation times on mass loss for an iron specimen submerged for 24 hours (run 2) in a 50 mg/L solution of malathion in water. A nonlinear curve was observed, the data was fitted to an exponential function with a coefficient of determination (R^2) of 0.9975. The 1 hour mass measurement was an apparent outlier. The total mass loss observed during the desiccation experiment was approx. 0.00012 g (0.01%). This result showed that iron specimen exposed to 50 mg/L of malathion solution had a desiccation profile showing exponential mass loss and an apparent outlier.

Figure 10 shows the effect of desiccation times on mass loss for an iron specimen submerged for 24 hours (run 2) in a 25 mg/L solution of malathion in water. A nonlinear curve was observed, the data was fitted to an exponential function with a coefficient of determination (R^2) of 0.8212. The 15-min mass measurement was an apparent outlier. The total mass loss observed during the desiccation experiment was approx. 0.00008 g (0.01%). This result showed that iron specimen exposed to 25 mg/L of malathion solution had a desiccation profile showing exponential mass loss and an apparent outlier.

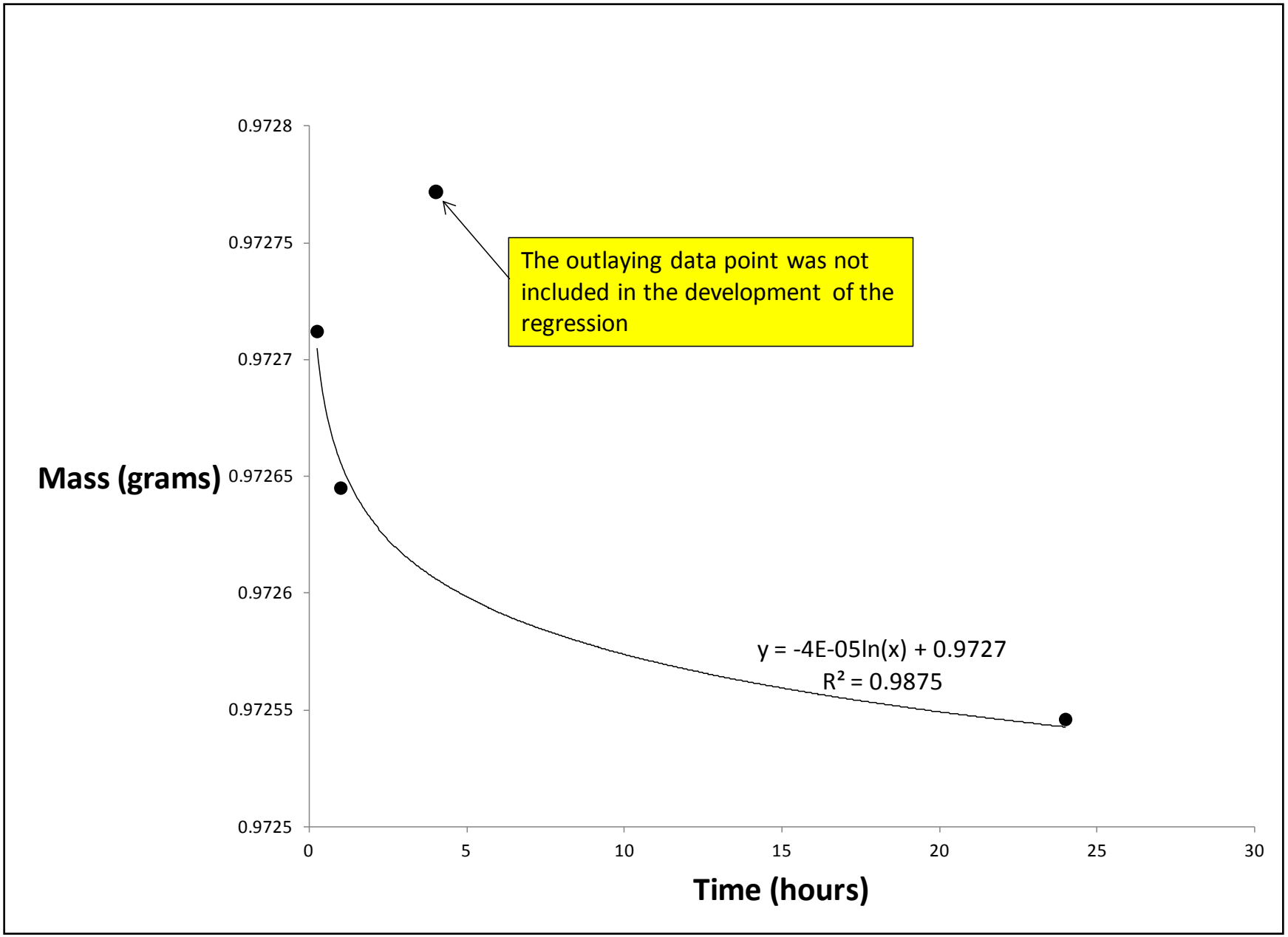

Figure 3. The Effect of Desiccation Time on Mass Loss for Copper Specimen Exposed to100 mg/L Malathion (run 2)

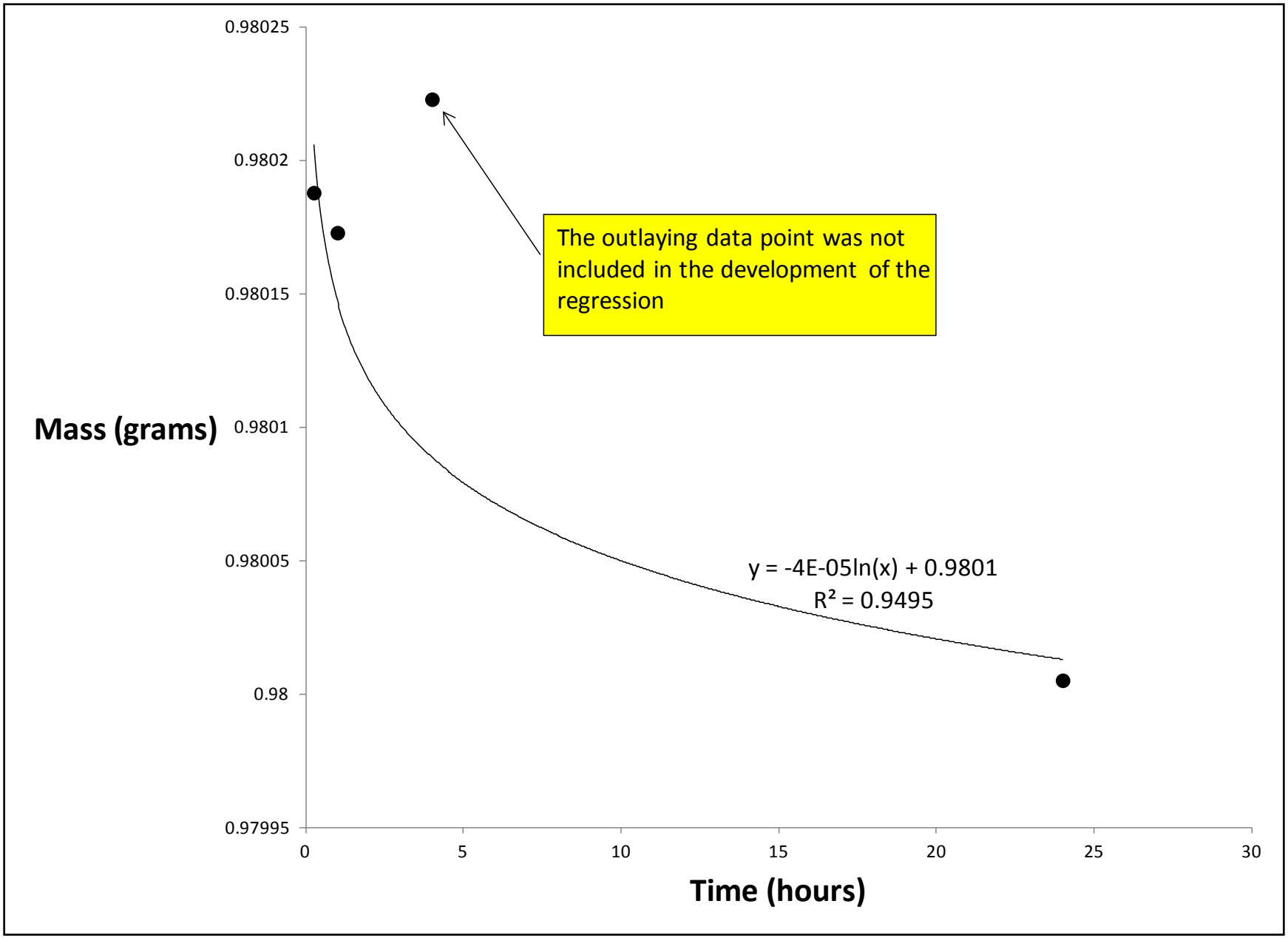

Figure 4. The Effect of Desiccation Time on Mass Loss for Copper Specimen Exposed to 75 mg/L Malathion (run 2)

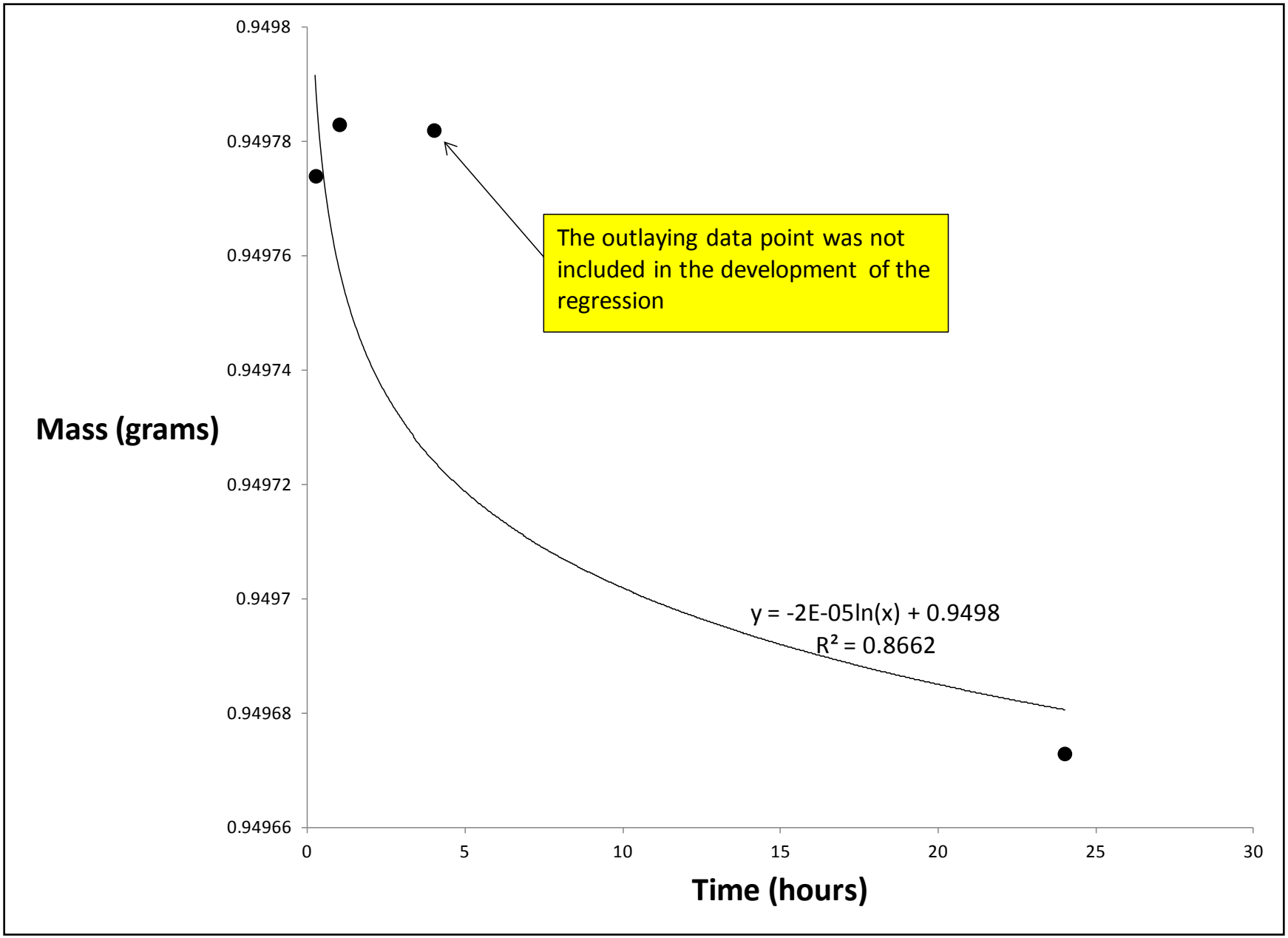

Figure 5. The Effect of Desiccation Time on Mass Loss on Copper Specimen Exposed to 50 mg/L Malathion (run 2)

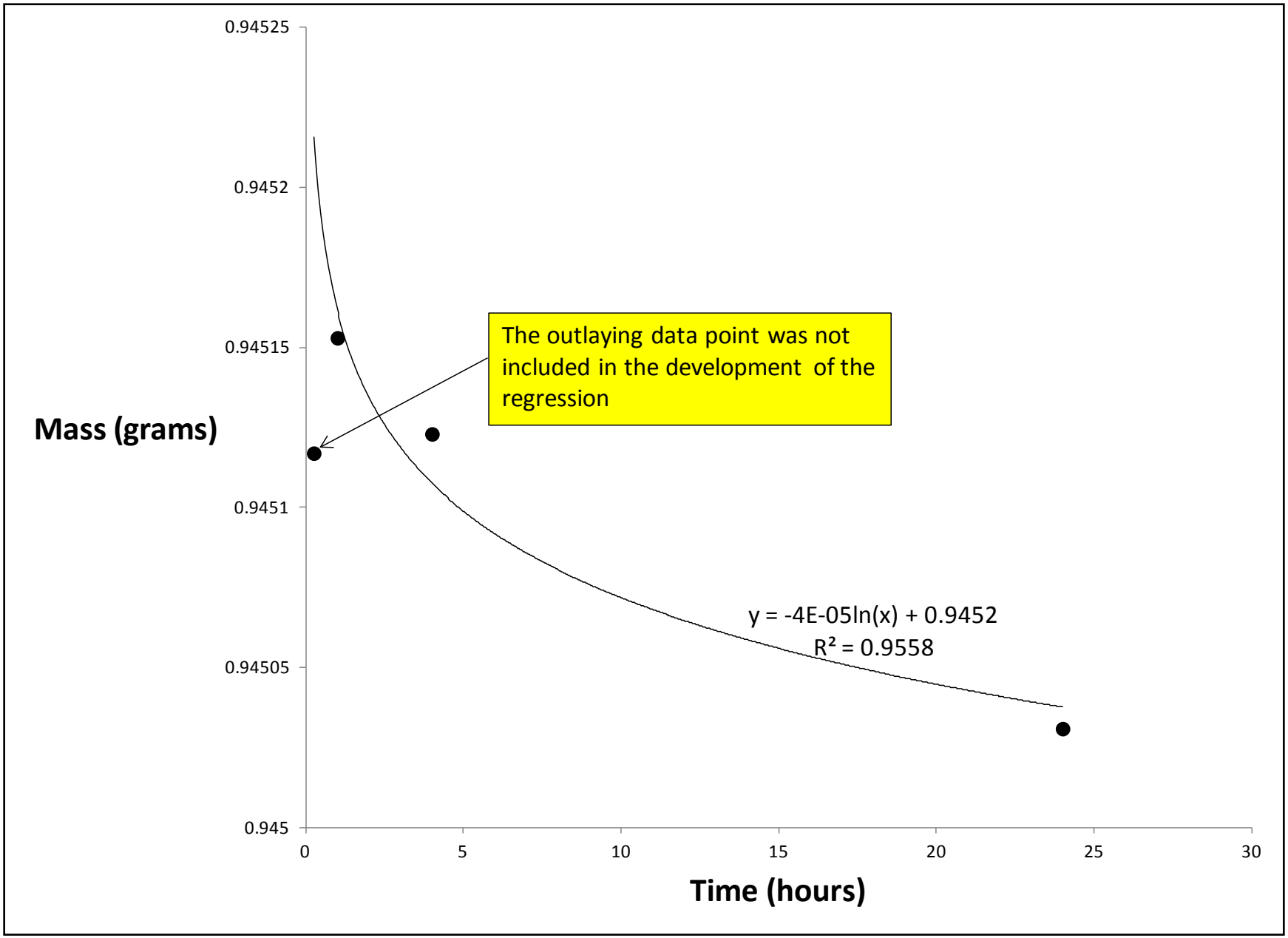

Figure 6. The Effect of Desiccation Time on Mass Loss on Copper Specimen Exposed to 25 mg/L Malathion (run 2)

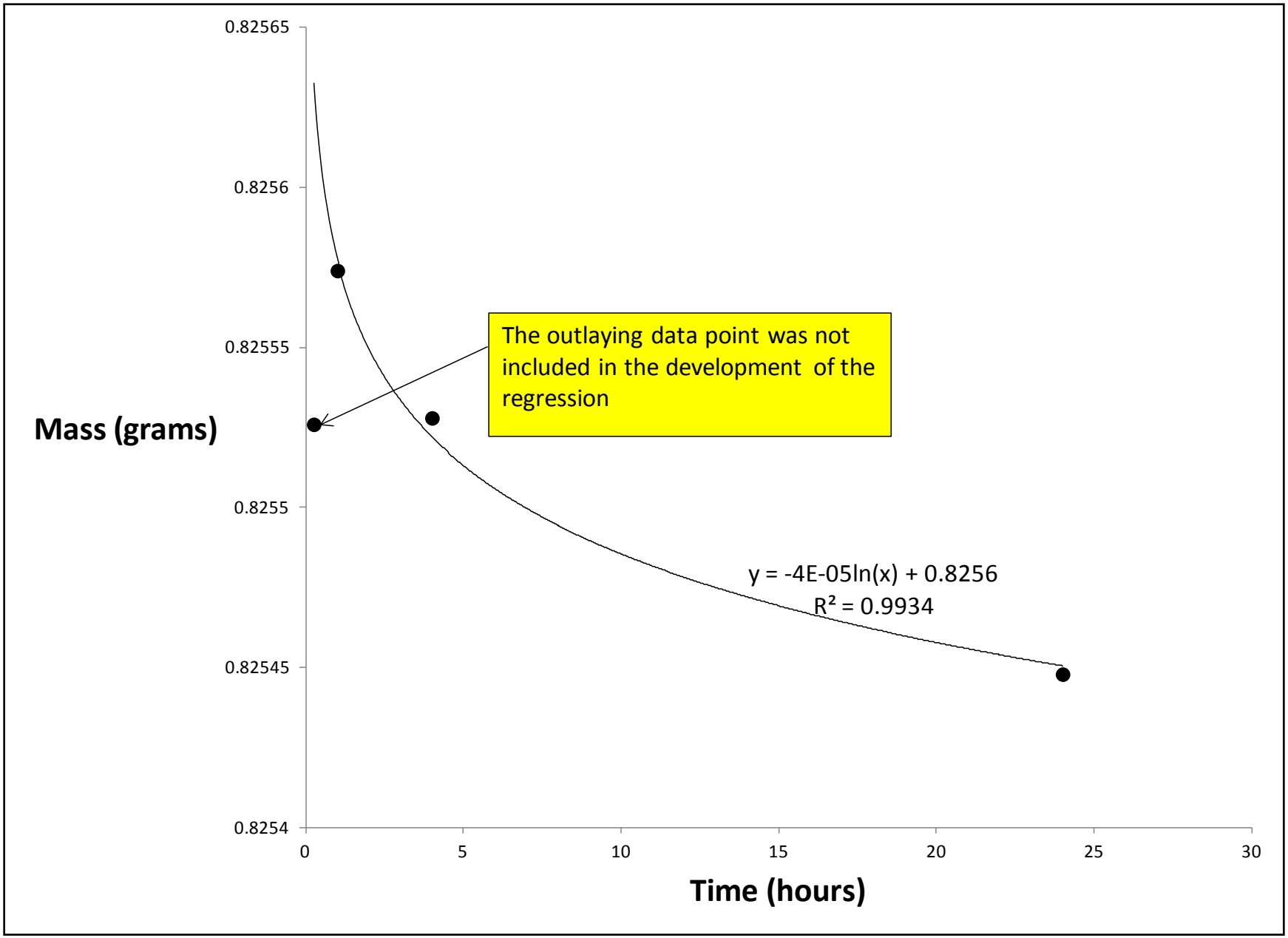

Figure 7. The Effect of Desiccation Time on Mass Loss for Iron Specimen Exposed to 100 mg/L Malathion (run 2)

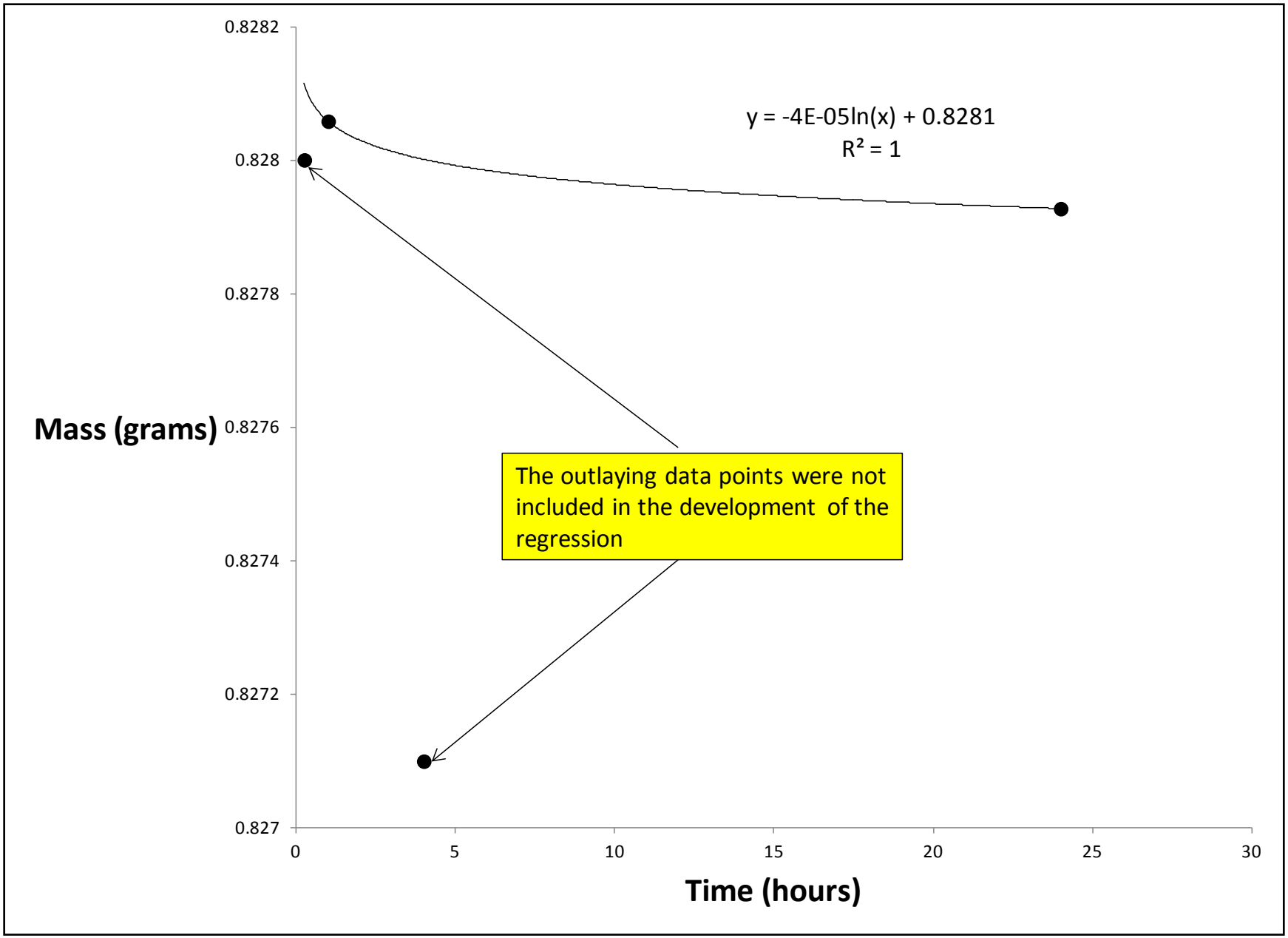

Figure 8. The Effect of Desiccation Time on Mass Loss for Iron Specimen Exposed to 75 mg/L Malathion (run 2)

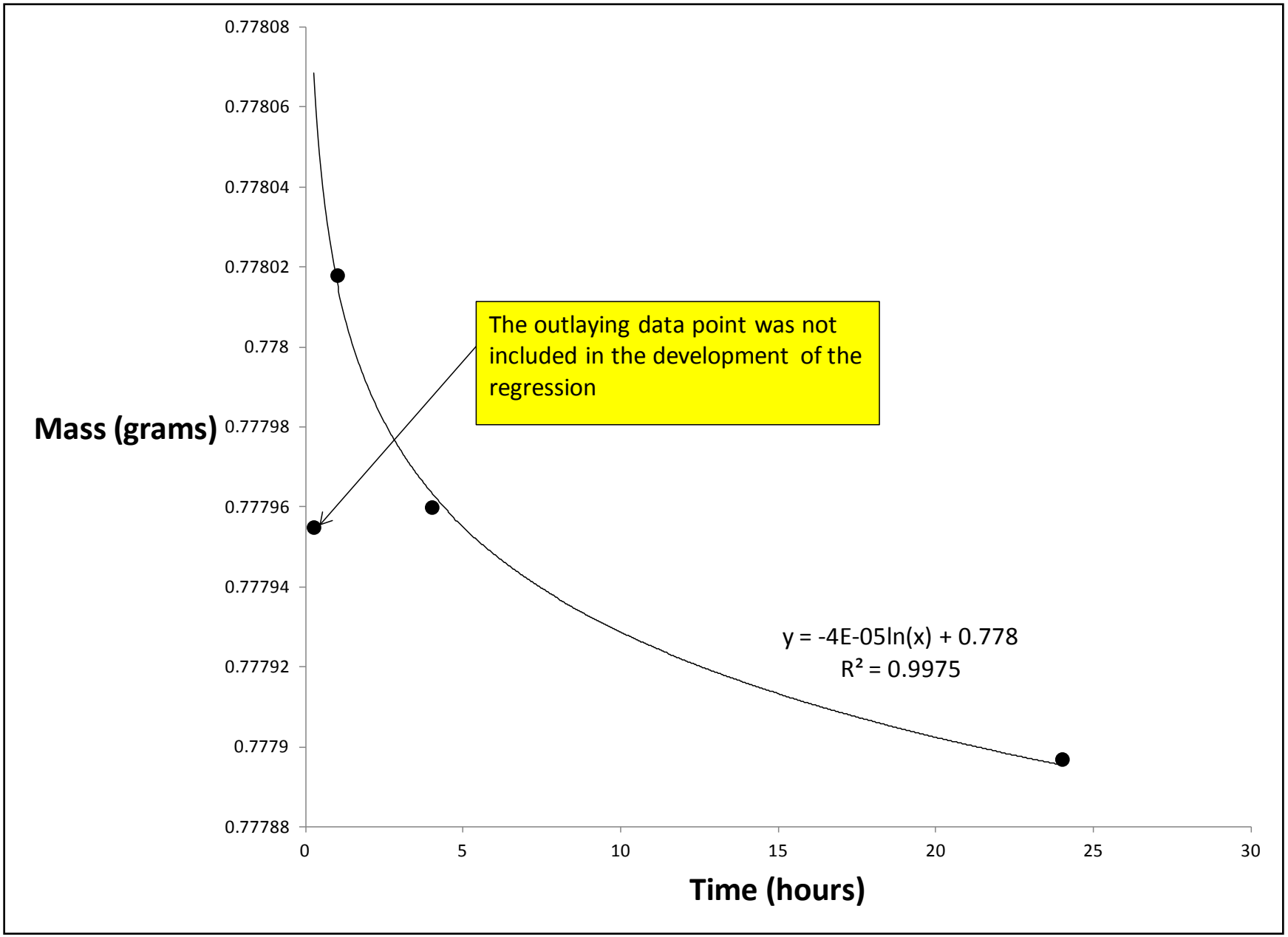

Figure 9. The Effect of Desiccation Time on Mass Loss for Iron Specimen Exposed to 50 mg/L Malathion (run 2)

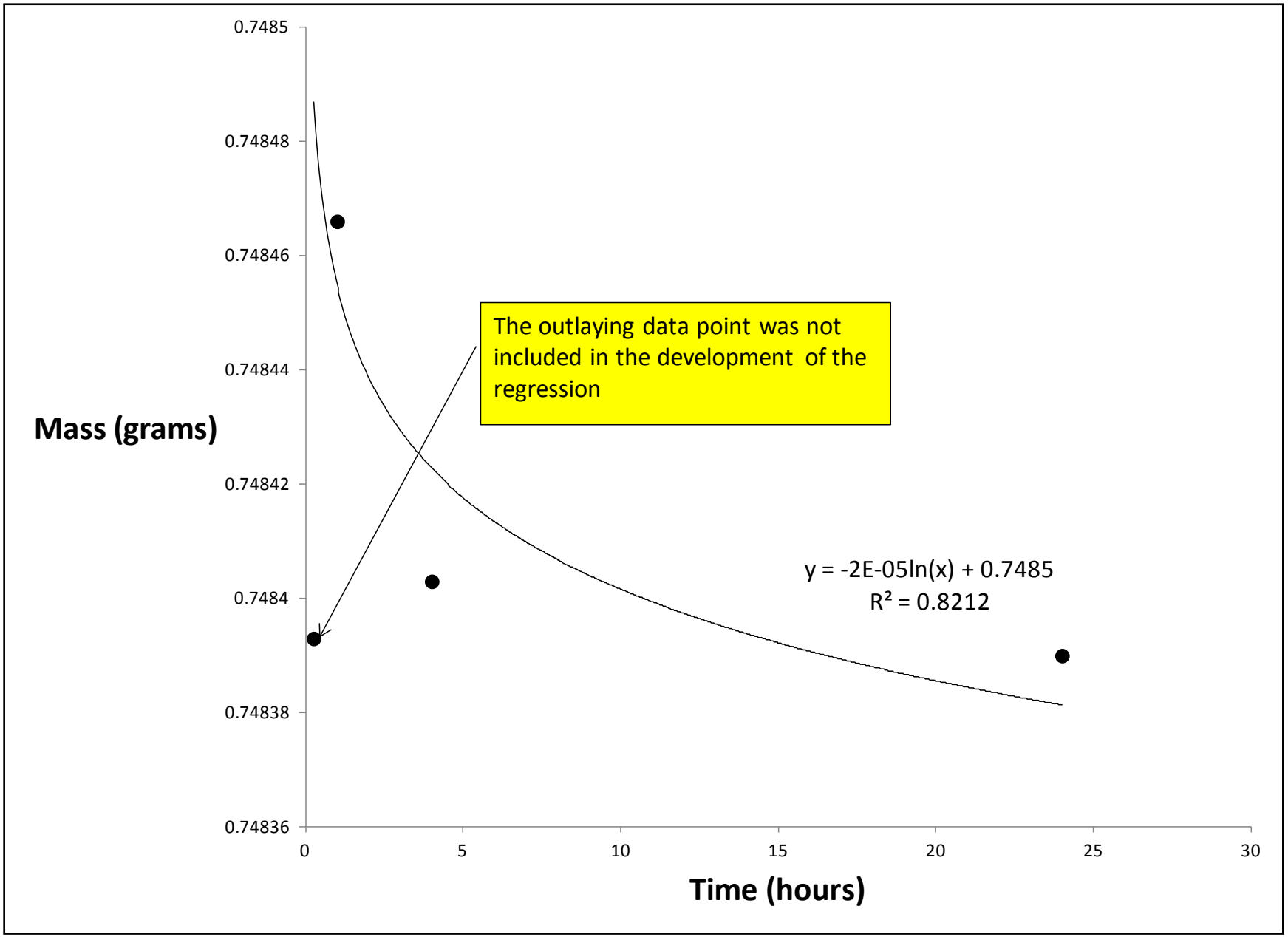

Figure 10. The Effect of Desiccation Time on Mass Loss for Iron Specimen Exposed to 25 mg/L Malathion (run 2)

Figure 11 shows the effect of immersion in DI water on specimen mass. The normalized mass difference was determined based on the following:

$$\Delta m = m_f - m_i / m_i \quad (8)$$

where m_i = initial mass and m_f = mass after immersion in DI water

The normalized mass difference was approx. 0.000038 g for copper and 0.000013 g for iron. The 3-fold difference in the normalized mass differentials can be partially explained by the loss of iron particles during the DI immersion. The positive mass differentials are an indication that water molecules may bind to the surface of the specimen. Fe and Cu are also known to react with soluble oxygen producing metal oxide compounds [43]. These results show that immersion in water increases the mass of copper and iron specimen.

Figure 12 shows the effect of immersion in malathion solution on specimen mass (24 hour, run 2). The normalized mass differences were positive for copper specimen but negative for iron specimen and the relationships between the normalized mass differences and the malathion concentrations was poor for copper ($R^2 < 0.1$) and decent for iron ($R^2 < 0.6$). For the copper specimen, the normalized mass difference was approx. 0.06 grams when the specimen was exposed to 100 mg/L malathion solution; this value is significantly larger than the normalized mass difference for copper specimen exposed only to DI (i.e. 0.06 > 0.000038). However, the normalized mass difference was ~ 1 0^{-5} when exposed to 25-75 mg/L malathion solution; these values are similar to the baseline measured with DI. For the iron specimen, the smallest (i.e. most negative) normalized mass difference was observed at 75 mg/L malathion and the largest (i.e. least negative) normalized mass difference was observed at 25 mg/L malathion. It is interesting to note that the normalized mass difference measured for the iron specimen exposed to DI was positive (i.e. 0.000013), which implied that malathion exposure may cause

negative normalized mass differences for iron specimen. The underlying chemistry associated with this issue should be explored further in future study. Overall, these results showed that normalized mass differences cannot be used to determine malathion adherence to these specimen. To the author's knowledge, this is the first time that negative normalized mass differences have been reported for pipe specimen subjected to desiccation.

Figure 13 shows the effect of immersion in malathion solution on specimen mass (24 hour, run 3). The normalized mass differences were mostly positive (excluding the specimen exposed to 100 mg/L) for copper specimen but all negative for iron specimen and the relationships between the normalized mass differences and the malathion concentrations were poor for both copper and iron ($R^2 < 0.6$ in both cases). For the copper specimen, the normalized mass difference was approx. 0.000077 g when the specimen was exposed to 75, 50, and 25 mg/L malathion solution; while the value for the normalized mass difference for the copper specimen exposed to 100 mg/L was negative at approx. -0.00001 g. The positive values were essentially twice that of the normalized mass difference for copper specimen exposed only to DI (i.e. 0.000077 > 0.000038). For the iron specimen, the smallest (i.e. most negative) normalized mass difference was observed at 100 mg/L malathion, while the largest (i.e. least negative) normalized mass differences were observed at 25, 50, and 75 mg/L malathion. It is interesting to note that the normalized mass difference measured for the iron specimen exposed to DI was positive (i.e. 0.000013), while those exposed to the malathion solution during this run clearly resulted in a negative normalized mass difference. This negative normalized mass difference for the exposed iron specimen is consistent with the results observed during run 2, providing further implication that malathion exposure may cause negative normalized mass differences for iron specimen. The underlying chemistry associated with this issue should be explored further in future study.

Overall, these results showed that normalized mass differences cannot be used to determine malathion adherence to these specimen. To the author's knowledge, this is the first time that negative normalized mass differences have been reported for pipe specimen subjected to desiccation.

Figure 14 shows the effect of immersion in malathion solution on specimen mass (24 hour, run 4). The normalized mass differences were positive for copper specimen at exposure concentrations of 50 and 25 mg/L and 0 at concentrations of 100 and 75 mg/L, but negative for iron specimen (0 at 100 mg/L exposure) and the relationships between the normalized mass differences and the malathion concentrations was poor for iron ($R^2 < 0.3$), but fairly decent for copper ($R^2 < 0.8$). For the copper specimen, the normalized mass difference was approx. 0.00007 g when the specimen was exposed to 50 and 25 mg/L malathion solution; this value is essentially twice that of the normalized mass difference for copper specimen exposed only to DI (i.e. 0.00007 > 0.000038). However, the normalized mass difference was ~ 0 when exposed to 100 and75 mg/L malathion solution. For the iron specimen, the normalized mass differences observed at 75, 50, and 25 mg/L malathion were all negative and essentially equal (~ 0.000017 g). Overall, these results showed that normalized mass differences cannot be used to determine malathion adherence to these specimen. To the author's knowledge, this is the first time that negative normalized mass differences have been reported for pipe specimen subjected to desiccation.

Figure 15 shows the effect of immersion in malathion solution on specimen mass (24 hour, run 5). The normalized mass differences were positive for both copper and iron specimen, with the exception of the iron specimen exposed to 100 mg/L malathion solution, and the relationships between the normalized mass differences and the malathion concentrations were

fairly decent for iron ($R^2 < 0.8$), and slightly less decent for copper ($R^2 < 0.6$). For the copper specimen, the normalized mass difference consistently decreased from 100 mg/L exposure to 50 mg/L exposure, yet, there was an observed increase from 50 mg/L exposure to 25 mg/L exposure. This behavior generated a decent correlation between that of the normalized mass difference for the copper specimen and the malathion concentrations. The average normalized mass difference for the exposed copper specimen was ~ 0.000033 g, which is essentially the same as that of the normalized mass difference for copper specimen exposed only to DI (i.e. $0.000033 \approx 0.000038$). However, the average normalized mass difference was ~ 0.000051 g for the iron specimen, which is essentially four times that of the normalized mass difference for iron specimen exposed to DI only (0.000013 g). Overall, these results showed that normalized mass differences cannot be used to determine malathion adherence to these specimen. To the author's knowledge, this is the first time that negative normalized mass differences have been reported for pipe specimen subjected to desiccation.

Figure 16 shows the effect of immersion in malathion solution on specimen mass (8 hour, run 2). The normalized mass differences were positive for both copper and iron specimen, with the exception of the iron specimen exposed to 25 mg/L malathion solution, and the relationships between the normalized mass differences and the malathion concentrations were significant for both copper and iron ($R^2 \sim 0.9$ in both cases). For the copper specimens, the normalized mass difference consistently increased from 0.000018 g to 0.000023 g when the specimen was exposed to the malathion solution; this range of values is clearly smaller than the normalized mass difference for copper specimens exposed only to DI (i.e. 0.000038). For the iron specimen, the smallest (i.e. most negative) normalized mass difference was observed at 25 mg/L malathion and the largest normalized mass difference was observed at 100 mg/L malathion. The trends

observed for normalized mass differences for the malathion solution exposure of both specimen types is consistent with that which would be expected in order to determine a theoretical partitioning coefficient. Overall, these results showed that normalized mass differences (for this specific run) have the possibility of being used to determine malathion adherence to these specimen.

Figure 17 shows the effect of immersion in malathion solution on specimen mass (4 hour, run 2). The normalized mass differences were negative for both copper and iron specimen and the relationships between the normalized mass differences and the malathion concentrations was decent for copper ($R^2 < 0.7$), but very poor for iron ($R^2 < 0.04$). For the copper specimen, the normalized mass difference experienced a consistent decrease (negatively) from 0.000038 g at a malathion solution exposure of 100 mg/L to 0.000013 g at a malathion solution exposure of 25 mg/L. For the iron specimen, the normalized mass difference was fairly consistent at a (negative) range of 0.000018 g to 0.000017 g. It is interesting to note that the normalized mass difference measured for both copper and iron specimen exposed to DI was positive (i.e. 0.000038 and 0.000013 respectively), which would imply that malathion exposure may cause negative normalized mass differences for both copper and iron specimen. The underlying chemistry associated with this issue should be explored further in future study. Overall, these results showed that normalized mass differences cannot be used to determine malathion adherence to these specimen. To the author's knowledge, this is the first time that negative normalized mass differences have been reported for pipe specimen subjected to desiccation.

Figure 18 shows the effect of immersion in malathion solution on specimen mass (4 hour, run 3). The normalized mass differences were negative for both copper and iron specimen and the relationship between the normalized mass differences and the malathion concentrations was

significant for iron ($R^2 < 0.9$), and very poor for copper ($R^2 < 0.06$). For the copper specimen, the normalized mass difference was fairly (negative) consistent ranging from 0.000025 g at a malathion solution exposure of 100 mg/L to 0.000019 g at a malathion solution exposure of 25 mg/L; this range is inconsistent in comparison to the normalized mass difference for copper specimen exposed only to DI ($\sim$ 0.000038 g). For the iron specimen, the smallest (i.e. most negative) normalized mass difference was observed at 25 mg/L malathion and the largest (i.e. least negative) normalized mass difference was observed at 100 mg/L malathion. It is interesting to note that the normalized mass difference measured for both copper and iron specimen exposed to DI was positive (i.e. 0.000038 and 0.000013 respectively), which would imply that malathion exposure may cause negative normalized mass differences for both copper and iron specimen. The underlying chemistry associated with this issue should be explored further in future study. Overall, these results showed that normalized mass differences cannot be used to determine malathion adherence to these specimens. To the author's knowledge, this is the first time that negative normalized mass differences have been reported for pipe specimens subjected to desiccation.

Figure 19 shows the effect of immersion in malathion solution on specimen mass (4 hour, run 4). The normalized mass differences were negative for both the copper and iron specimen, with the exception of the iron specimen exposed to the 75 mg/L malathion solution. The relationships between the normalized mass differences and the malathion concentrations were poor for both copper and iron ($R^2 < 0.4$ in both cases). For the copper specimen, the normalized mass difference was fairly (negative) consistent ranging from 0.000017 g at a malathion solution exposure of 100 mg/L to 0.00002 g at a malathion solution exposure of 25 mg/L; this range is inconsistent in comparison to the normalized mass difference for copper specimen exposed only

to DI (~ 0.000038 g). For the iron specimen, the smallest (i.e. most negative) normalized mass difference was observed at 50 mg/L malathion and the largest (i.e. positive) normalized mass difference was observed at 75 mg/L malathion. It is interesting to note that the normalized mass difference measured for both copper and iron specimen exposed to DI was positive (i.e. 0.000038 and 0.000013 respectively), which would imply that malathion exposure may cause negative normalized mass differences for both copper and iron specimen. The underlying chemistry associated with this issue should be explored further in future study. Overall, these results showed that normalized mass differences cannot be used to determine malathion adherence to these specimen. To the author's knowledge, this is the first time that negative normalized mass differences have been reported for pipe specimen subjected to desiccation.

Figure 20 shows the effect of immersion in malathion solution on specimen mass (4 hour, run 5). The normalized mass differences were negative for both the copper and iron specimen. The relationships between the normalized mass differences and the malathion concentrations was decent for the copper ($R^2 < 0.6$) and poor for the iron ($R^2 < 0.001$). For the copper specimen, the normalized mass difference experienced a consistent decrease (negatively) from 0.000063 g at a malathion solution exposure of 100 mg/L to 0.000015 g at a malathion solution exposure of 25 mg/L; this range is inconsistent in comparison to the normalized mass difference for copper specimen exposed only to DI (~ 0.000038 g). For the iron specimen, the smallest (i.e. most negative) normalized mass difference was observed at 75 mg/L malathion and the largest (i.e. least negative) normalized mass difference was observed at 25 mg/L malathion. It is interesting to note that the normalized mass difference measured for both copper and iron specimen exposed to DI was positive (i.e. 0.000038 and 0.000013 respectively), which would imply that malathion exposure may cause negative normalized mass differences for both copper and iron specimen.

The underlying chemistry associated with this issue should be explored further in future study. Overall, these results showed that normalized mass differences cannot be used to determine malathion adherence to these specimen. To the author's knowledge, this is the first time that negative normalized mass differences have been reported for pipe specimen subjected to desiccation.

Figure 21 shows the effect of immersion in malathion solution on specimen mass (8 hour, run 3). The normalized mass differences were positive for copper specimen exposed to malathion solution at 100 and 50 mg/L, and negative for copper specimen exposed to malathion solution at 75 and 25 mg/L, while the normalized mass differences were all negative for iron specimen. The relationships between the normalized mass differences and the malathion concentrations were decent for both copper and iron ($R^2 < 0.7$ in both cases). For the copper specimen, the normalized mass difference was 0.00024 g when the specimen was exposed to 100 mg/L malathion solution and 0.000031 g when the specimen was exposed to 50 mg/L malathion solution; however, the normalized mass difference values were negative (0.00001 and 0.000026) when the specimen was exposed to 75 and 25 mg/L malathion solution respectively. Therefore, the normalized mass difference values for the 100 and 50 mg/L exposed specimen were consistent with that of the normalized mass difference values for copper specimen exposed only to DI ($\sim$ 0.000038 g), while the values for the copper specimen exposed to 75 and 25 mg/L malathion solutions were not. For the iron specimen, the smallest (i.e. most negative) normalized mass difference was observed at 100 mg/L malathion and the largest (i.e. least negative) normalized mass difference was observed at 75 mg/L malathion. It is interesting to note that the normalized mass difference measured for both copper and iron specimen exposed to DI was positive (i.e. 0.000038 and 0.000013 respectively), which would imply that malathion exposure

may cause negative normalized mass differences for both copper and iron specimen. Overall, these results showed that normalized mass differences cannot be used to determine malathion adherence to these specimen. To the author's knowledge, this is the first time that negative normalized mass differences have been reported for pipe specimen subjected to desiccation.

Figure 22 shows the effect of immersion in malathion solution on specimen mass (8 hour, run 4). The normalized mass differences were negative for both the copper and iron specimen, with the exception of the copper specimen exposed to the 75 mg/L malathion solution, and the relationships between the normalized mass differences and the malathion concentrations were poor for both copper and iron ($R^2 < 0.2$ in both cases). For the copper specimen, the normalized mass difference experienced a consistent decrease (negatively) from 0.000012 g at a malathion solution exposure of 100 mg/L to 0.0000031 g at a malathion solution exposure of 25 mg/L; this range is inconsistent in comparison to the normalized mass difference for copper specimen exposed only to DI (~ 0.000038 g). However, the normalized mass difference was 0.0000042 g when exposed to 75 mg/L malathion solution, which is more consistent with the baseline measured with DI. For the iron specimen, the smallest (i.e. most negative) normalized mass difference was observed at 25 mg/L malathion and the largest (i.e. least negative) normalized mass difference was observed at 50 mg/L malathion. It is interesting to note that the normalized mass difference measured for both copper and iron specimen exposed to DI was positive (i.e. 0.000038 and 0.000013 respectively), which would imply that malathion exposure may cause negative normalized mass differences for both copper and iron specimen. The underlying chemistry associated with this issue should be explored further in future study. Overall, these results showed that normalized mass differences cannot be used to determine malathion

adherence to these specimen. To the author's knowledge, this is the first time that negative normalized mass differences have been reported for pipe specimen subjected to desiccation.

Figure 23 shows the effect of immersion in malathion solution on specimen mass (8 hour, run 5). The normalized mass differences were negative for both the copper and iron specimen, and the relationships between the normalized mass differences and the malathion concentrations was decent for iron ($R^2 < 0.6$) and very poor for copper ($R^2 < 0.1$). For the copper specimen, the normalized mass difference was fairly (negative) consistent ranging from 0.0000235 g at a malathion solution exposure of 100 mg/L to 0.0000239 g at a malathion solution exposure of 25 mg/L; this range is inconsistent in comparison to the normalized mass difference for copper specimen exposed only to DI ($\sim$ 0.000038 g). For the iron specimen, the smallest (i.e. most negative) normalized mass difference was observed at 25 mg/L malathion and the largest (i.e. least negative) normalized mass difference was observed at 100 mg/L malathion. It is interesting to note that the normalized mass difference measured for both copper and iron specimen exposed to DI was positive (i.e. 0.000038 and 0.000013 respectively), which would imply that malathion exposure may cause negative normalized mass differences for both copper and iron specimen. The underlying chemistry associated with this issue should be explored further in future study. Overall, these results showed that normalized mass differences cannot be used to determine malathion adherence to these specimen. To the author's knowledge, this is the first time that negative normalized mass differences have been reported for pipe specimen subjected to desiccation.

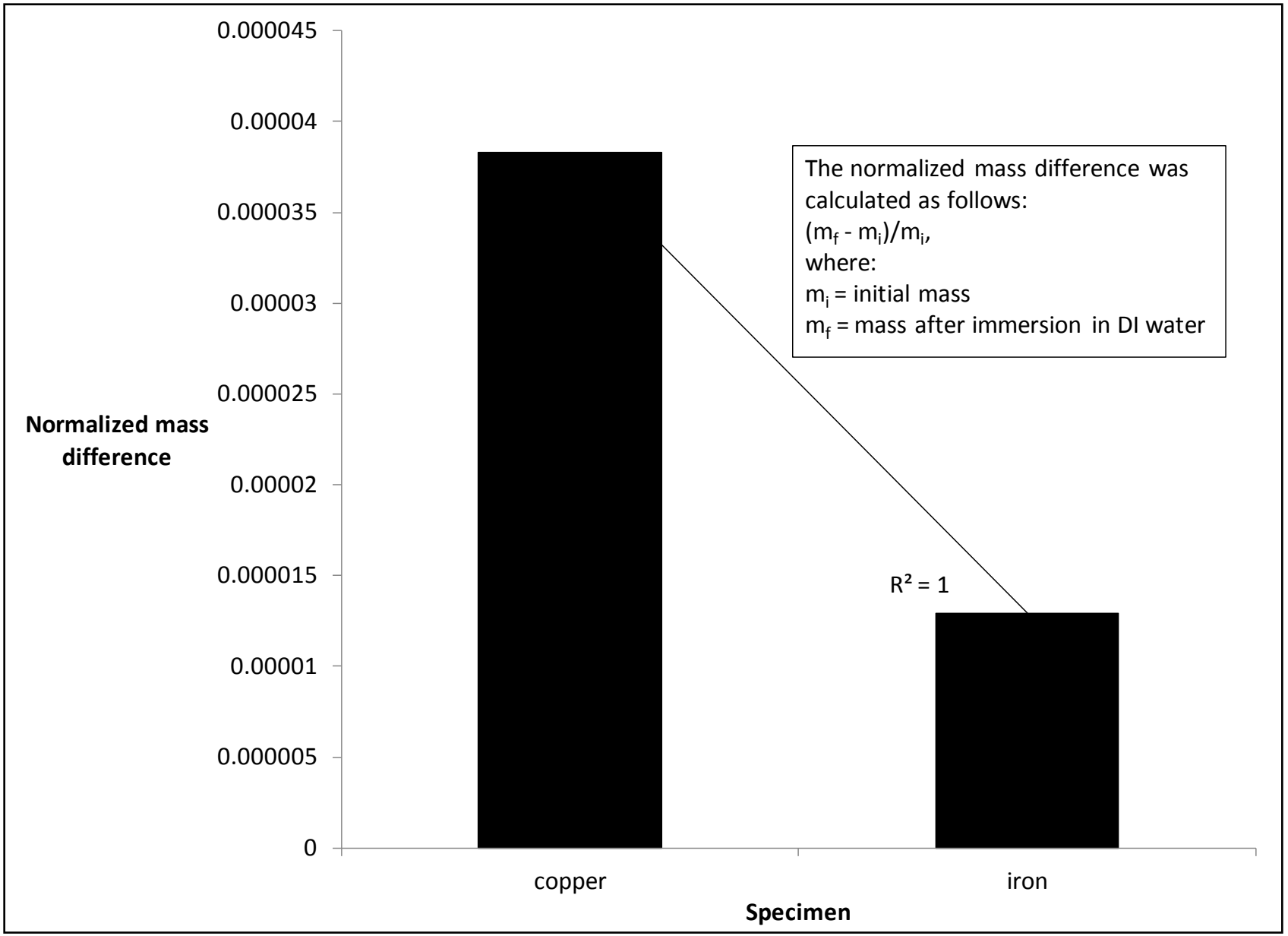

Figure 11. The Effect of Immersion in DI Water on Specimen Mass

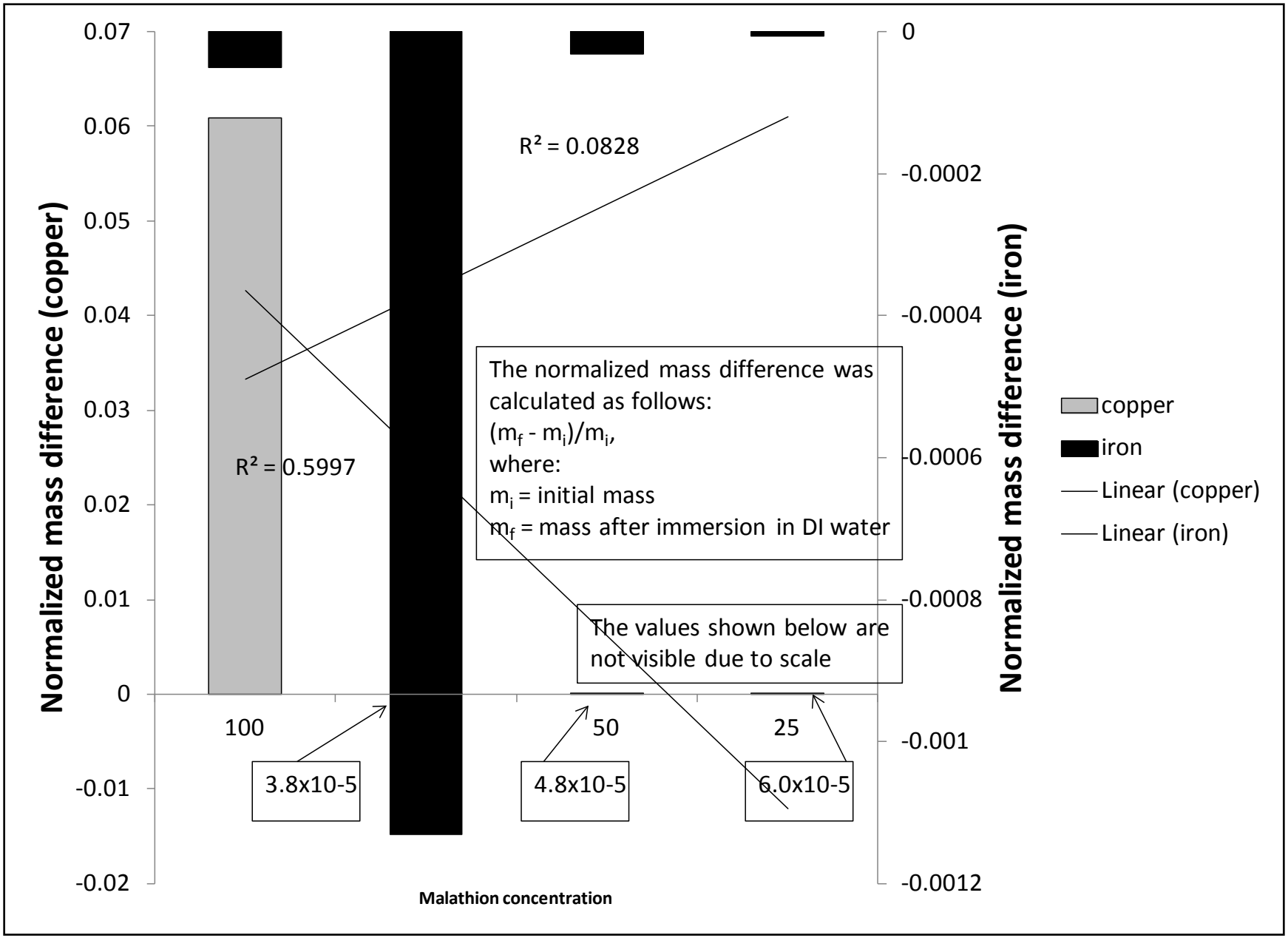

Figure 12. The Effect of Immersion in Malathion Solution on Specimen Mass (24 Hour, run 2)

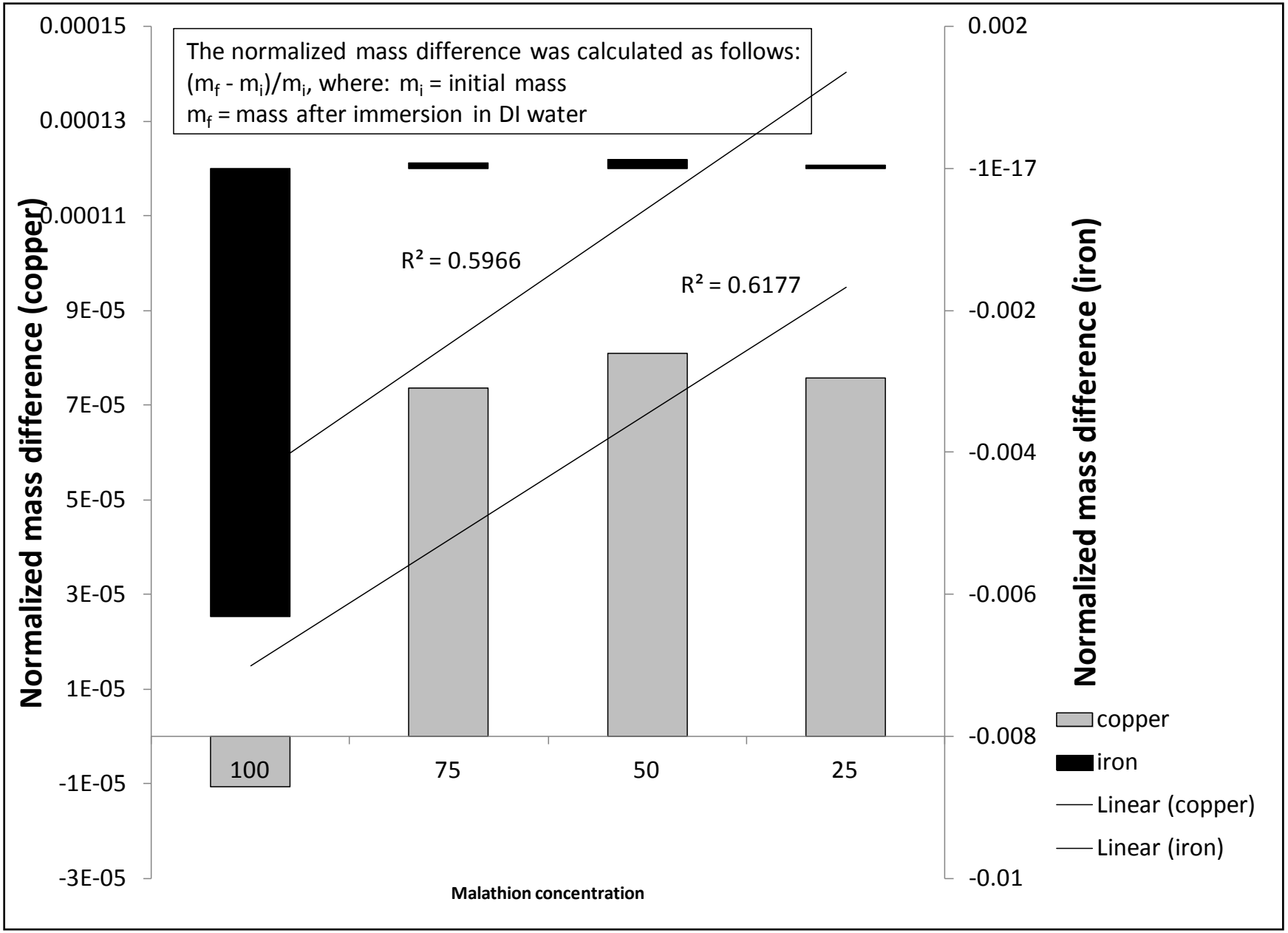

Figure 13**.** The Effect of Immersion in Malathion Solution on Specimen Mass (24 Hour, run 3)

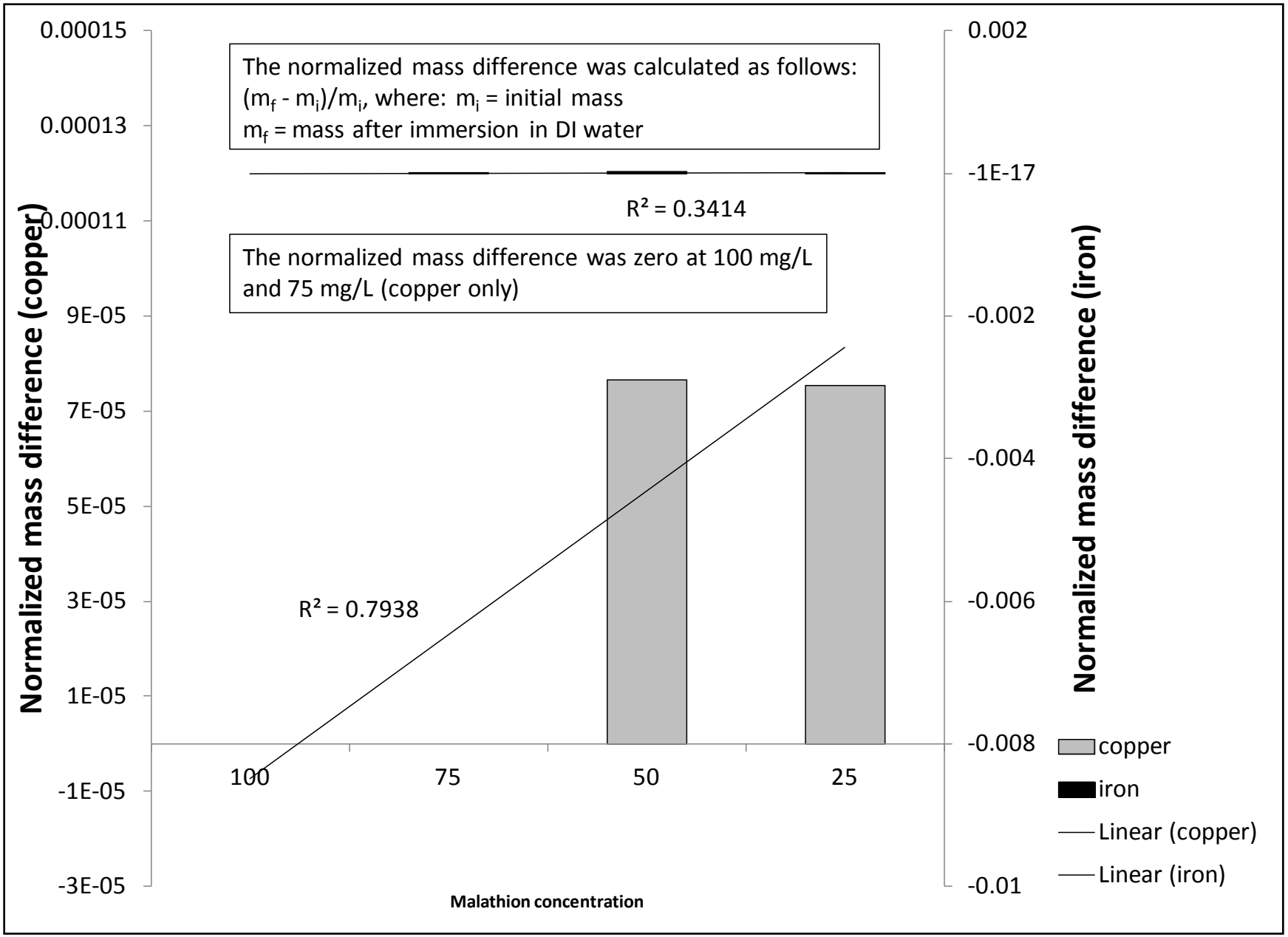

Figure 14. The Effect of Immersion in Malathion Solution on Specimen Mass (24 Hour, run 4)

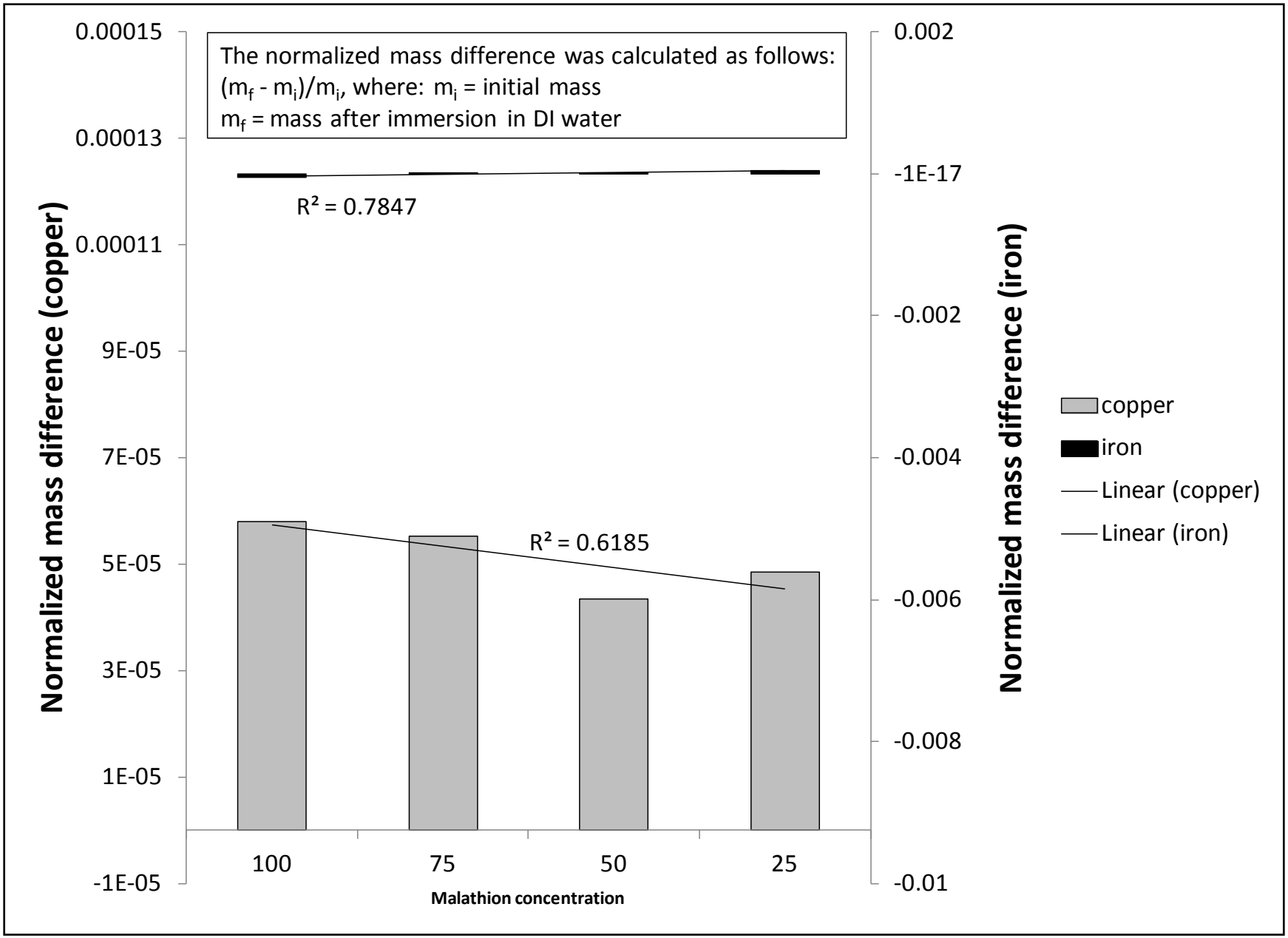

Figure 15. The Effect of Immersion in Malathion Solution on Specimen Mass (24 Hour, run 5)

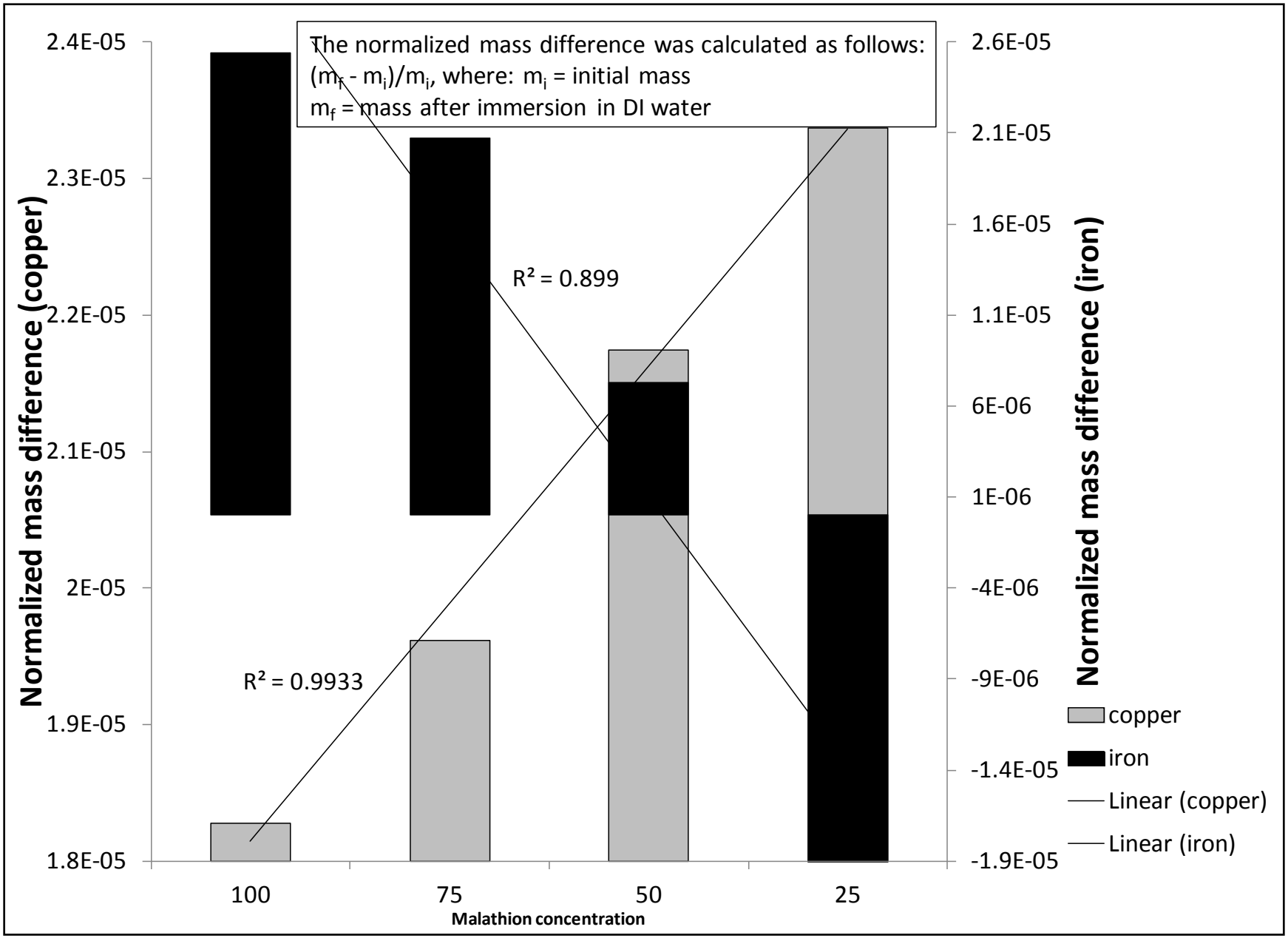

Figure 16. The Effect of Immersion in Malathion Solution on Specimen Mass (8 Hour, run 2)

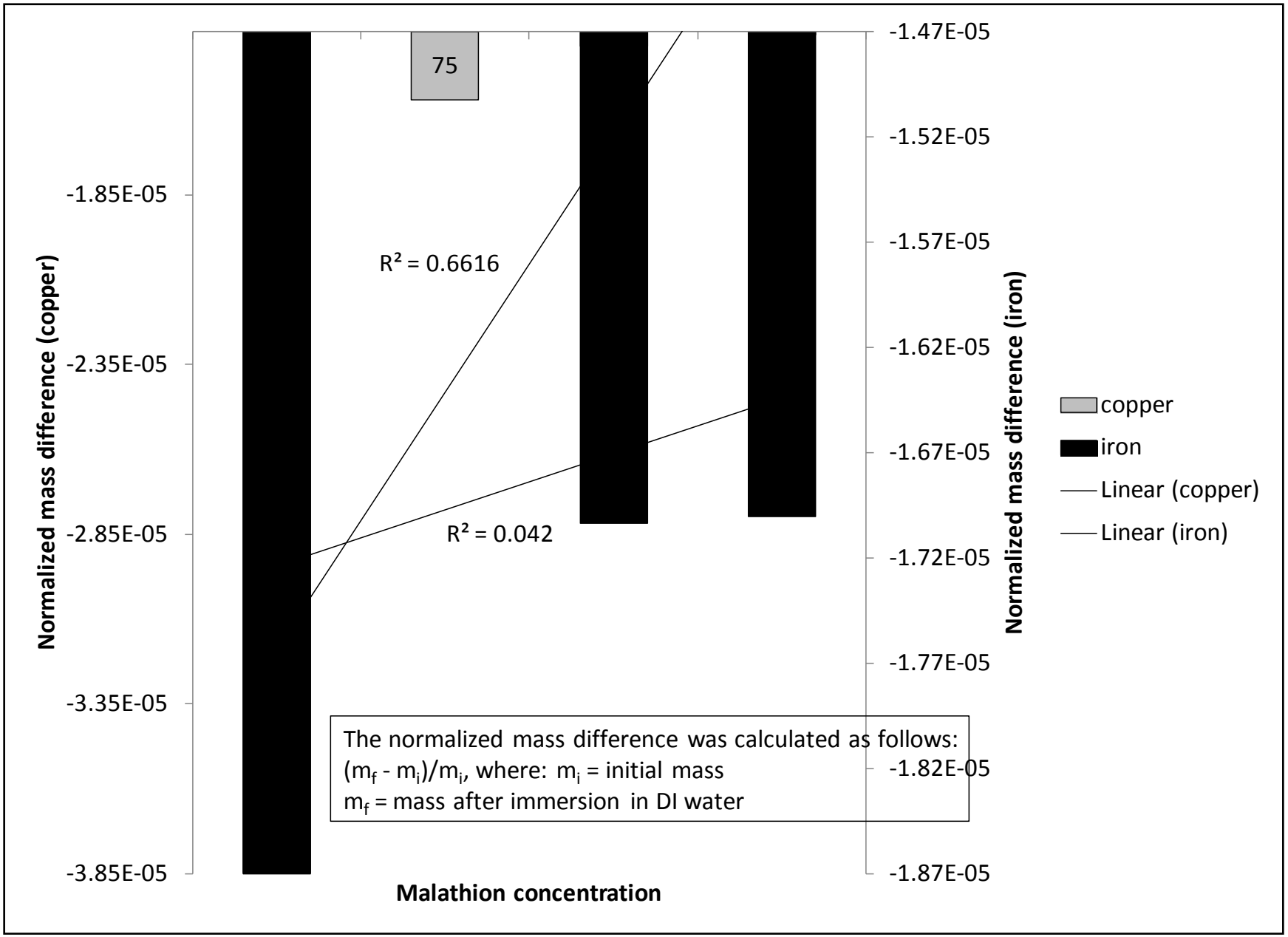

Figure 17. The Effect of Immersion in Malathion Solution on Specimen Mass (4 Hour, run 2)

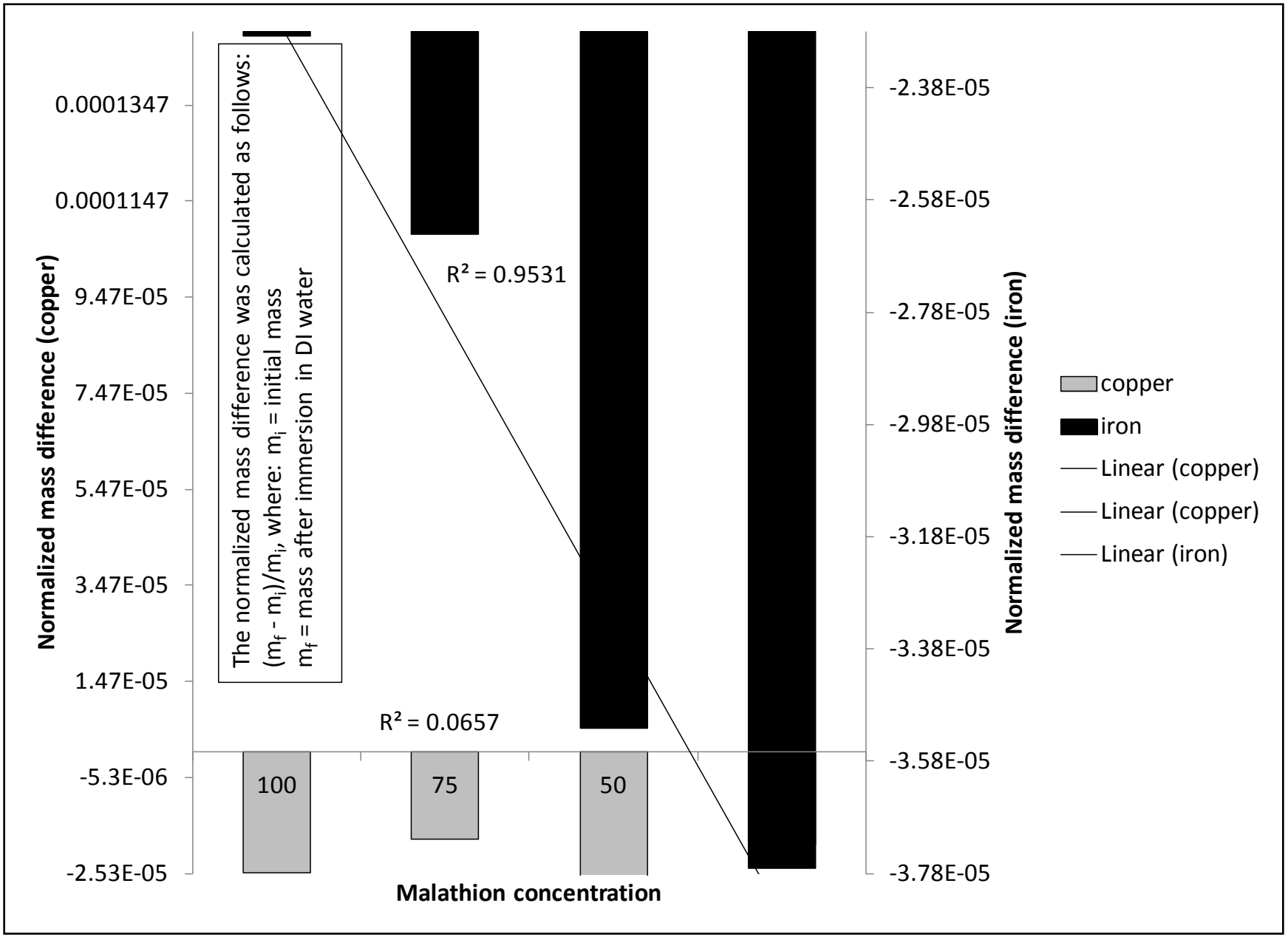

Figure 18. The Effect of Immersion in Malathion Solution on Specimen Mass (4 Hour, run 3)

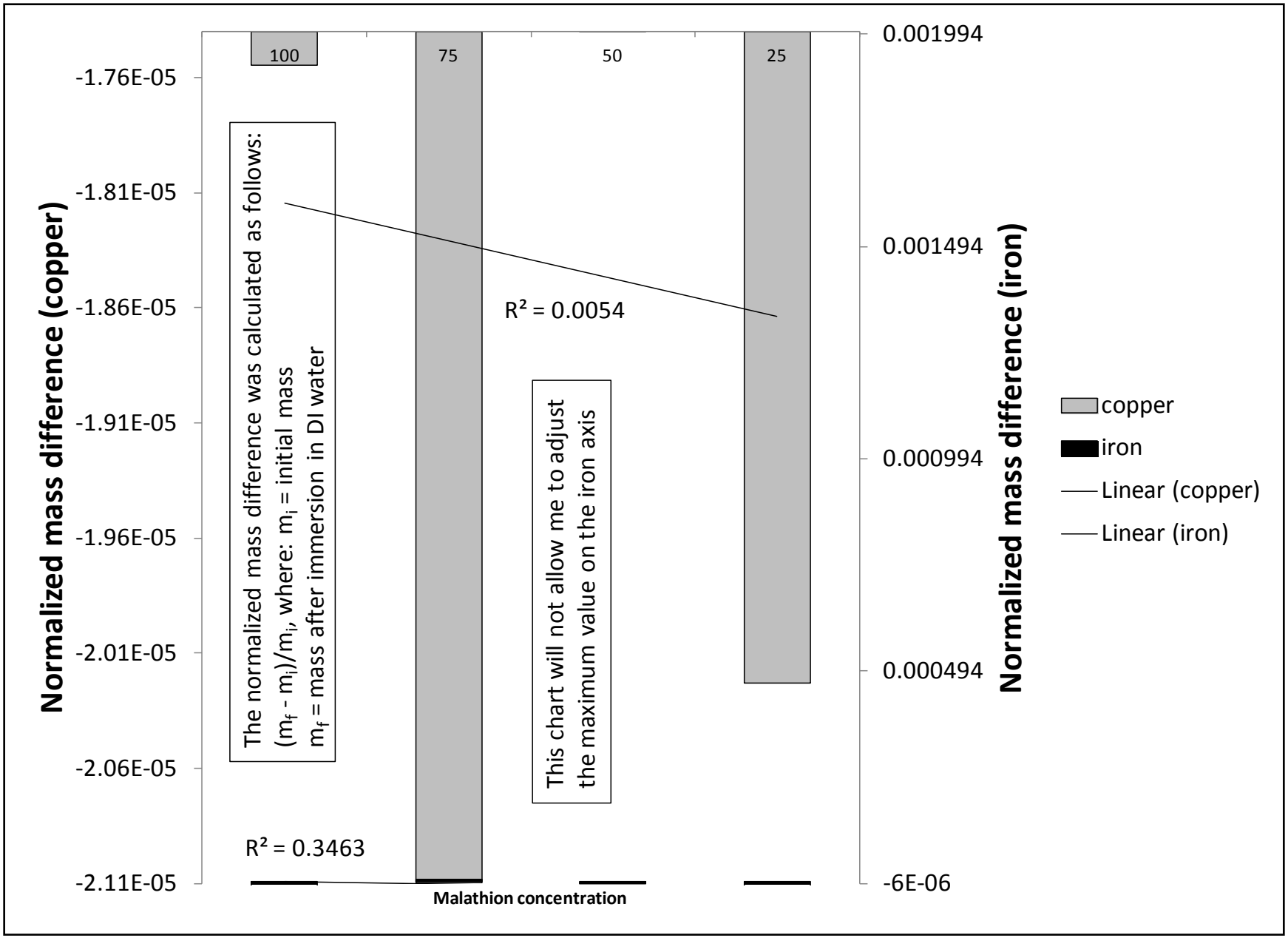

Figure 19. The Effect of Immersion in Malathion Solution on Specimen Mass (4 Hour, run 4)

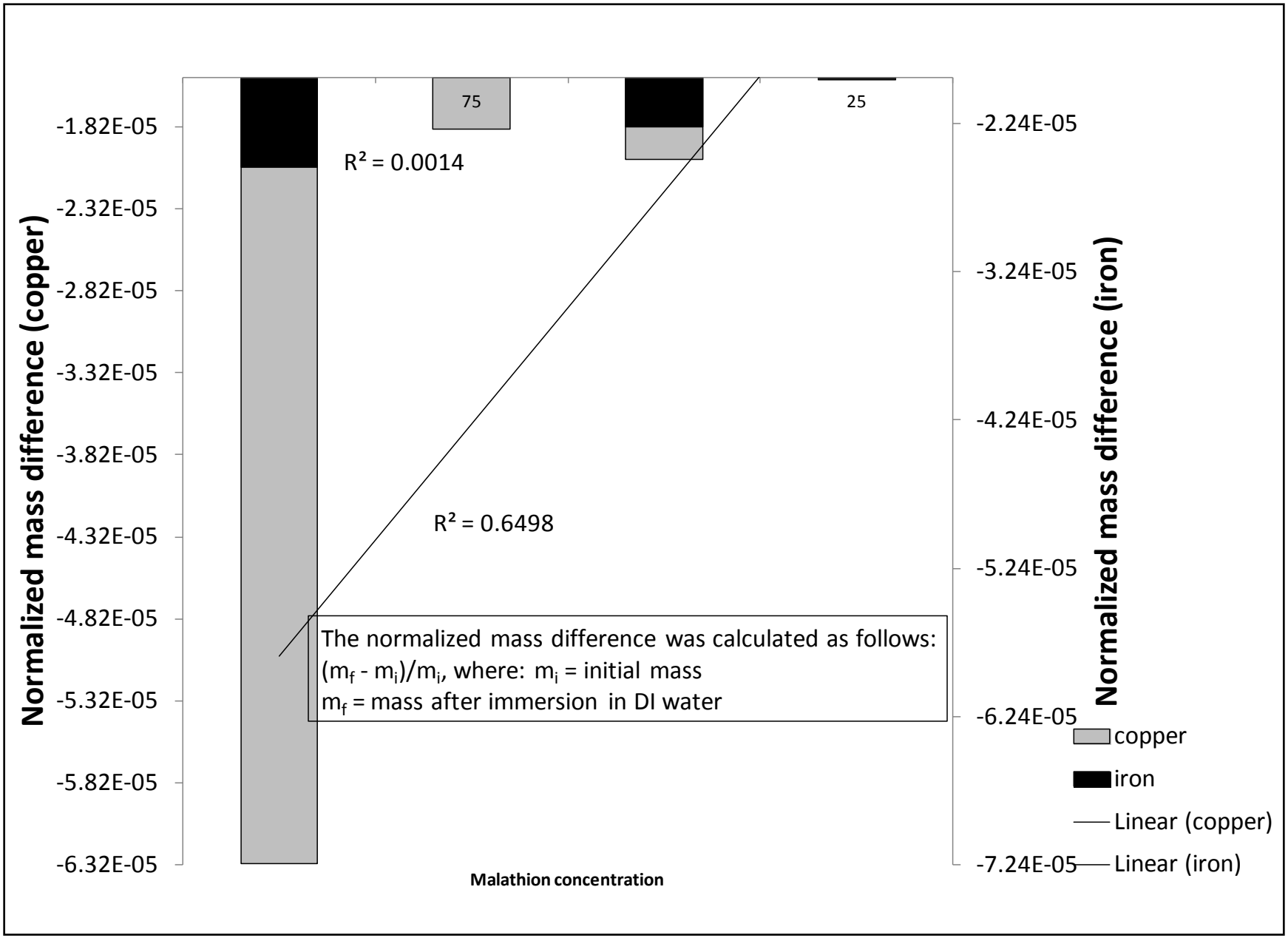

Figure 20. The Effect of Immersion in Malathion Solution on Specimen Mass (4 Hour, run 5)

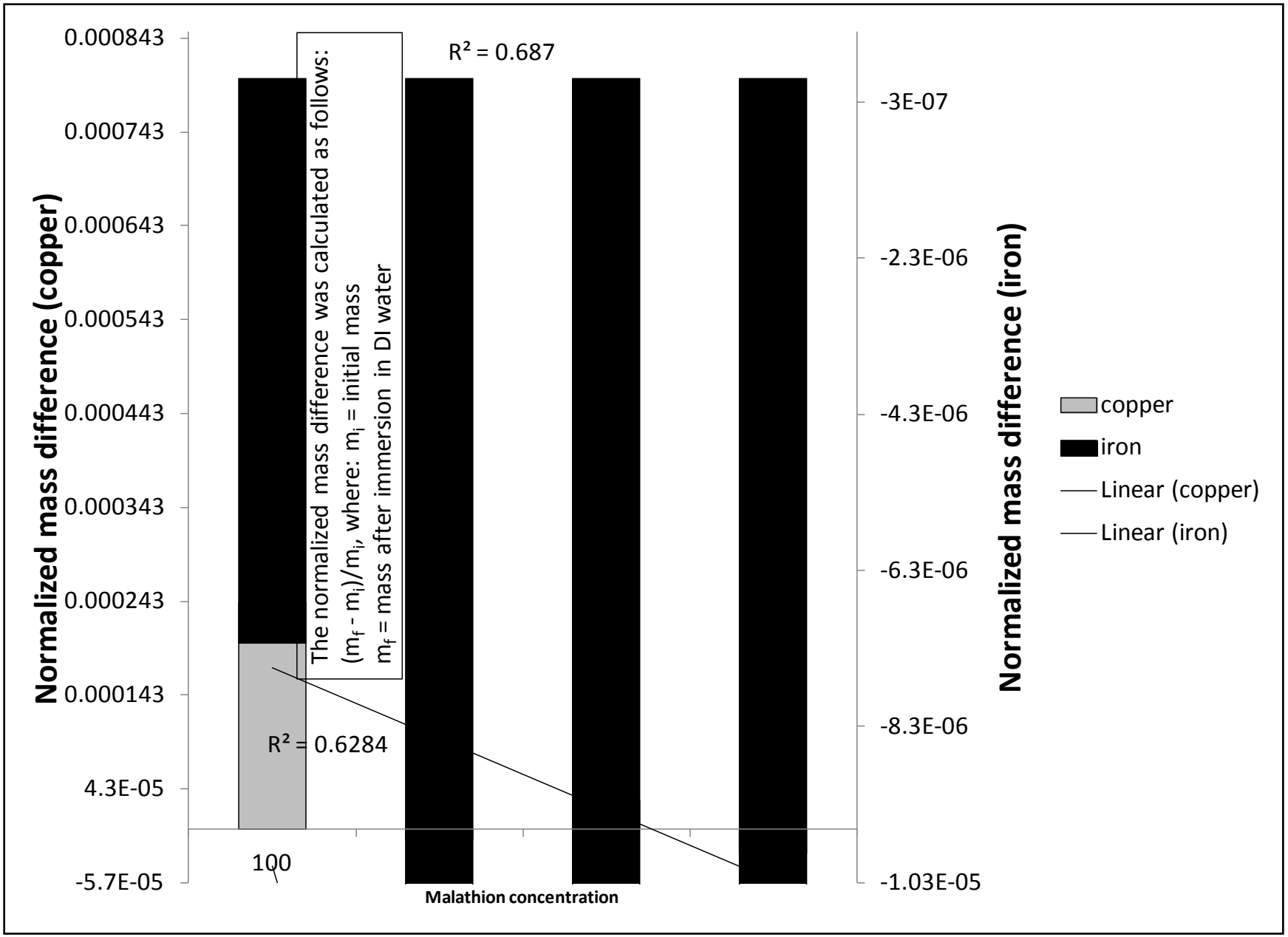

Figure 21. The Effect of Immersion in Malathion Solution on Specimen Mass (8 Hour, run 3)

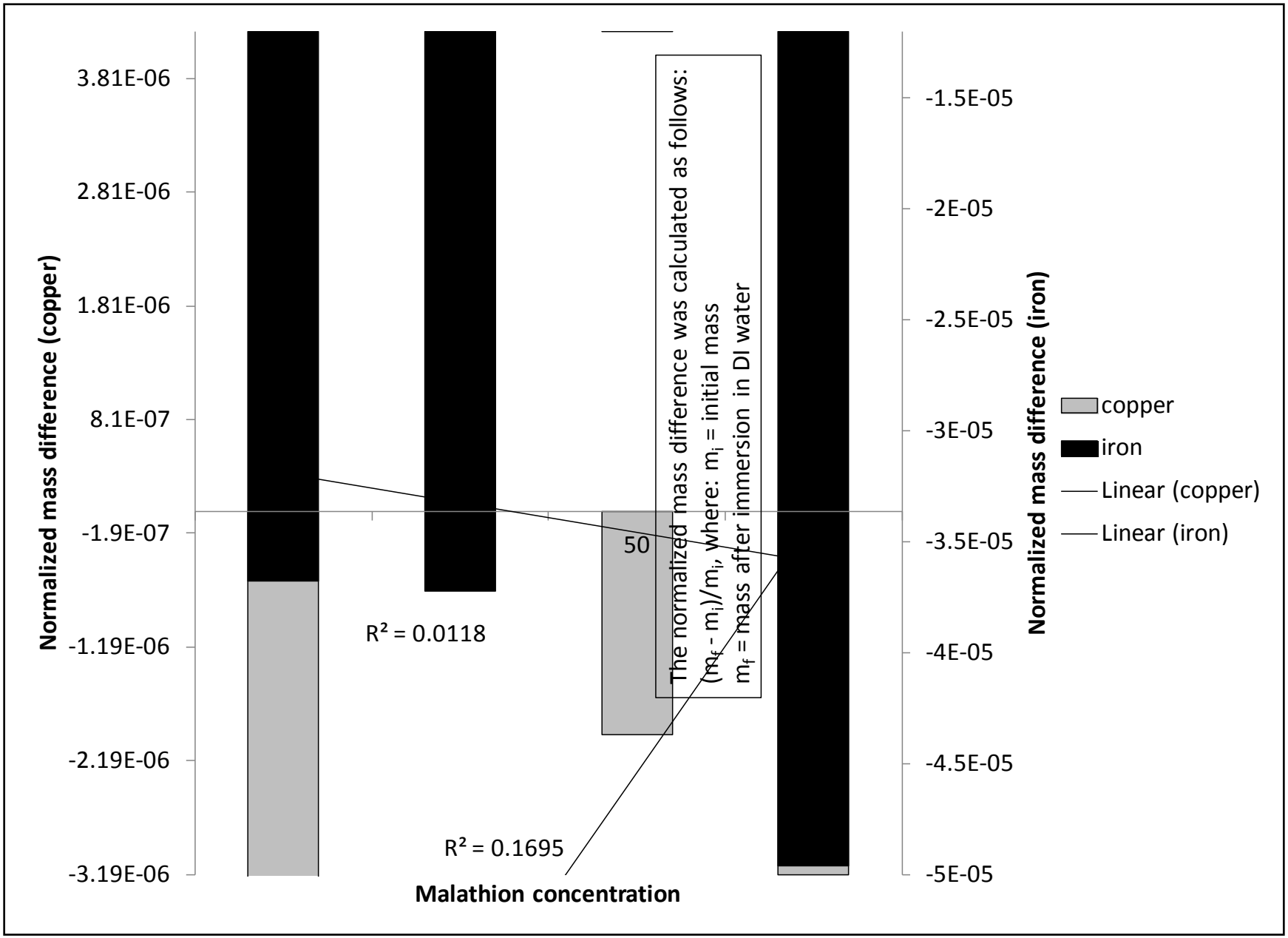

Figure 22. The Effect of Immersion in Malathion Solution on Specimen Mass (8 Hour, run 4)

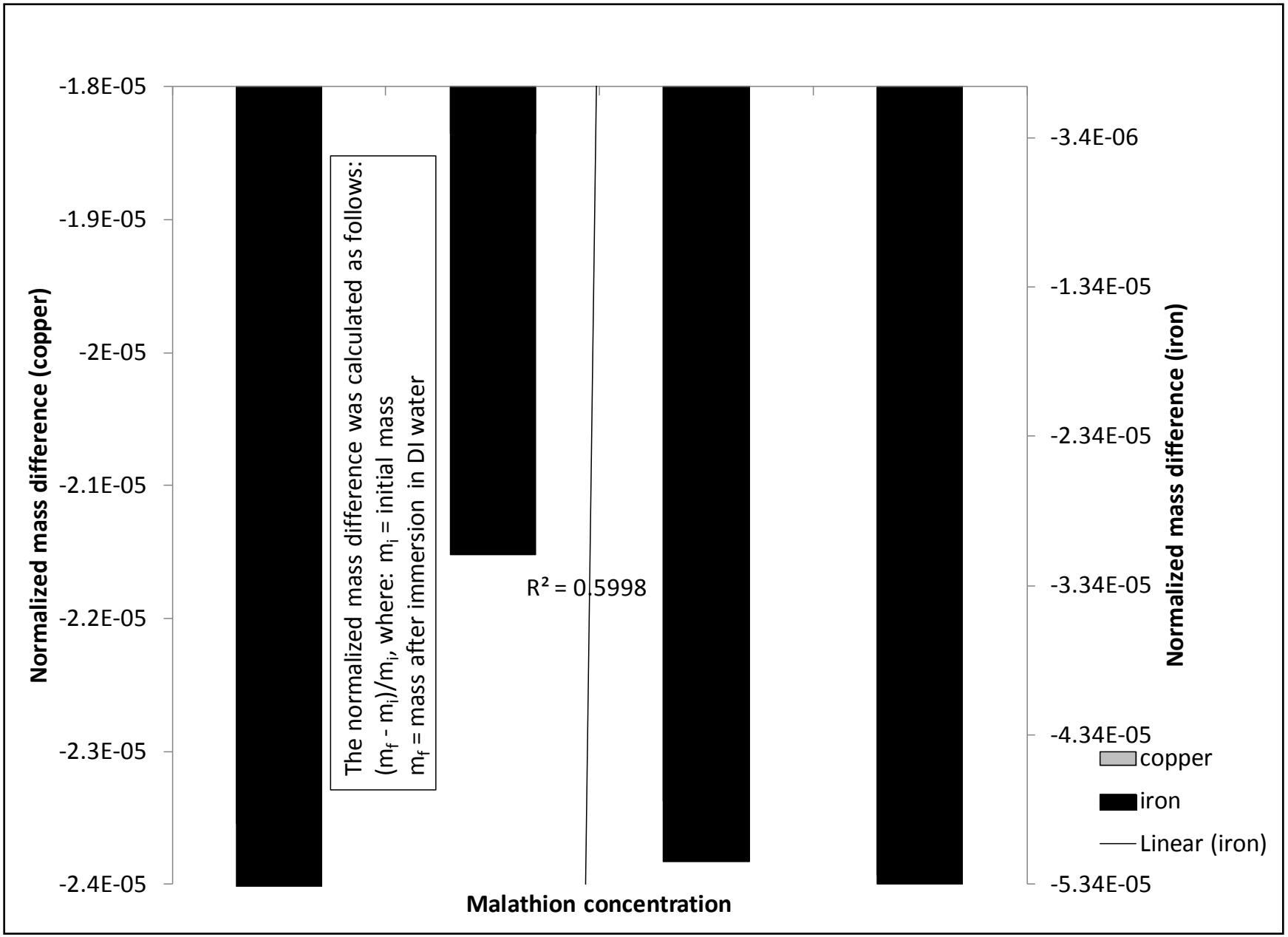

Figure 23. The Effect of Immersion in Malathion Solution on Specimen Mass (8 Hour, run 5)

5.2 Assessment

The results show numerous examples of increases in mass during desiccation and a critique of the possible mechanisms responsible for the measured increase in mass must be explored. Condensation of water vapor can be ruled out because of the temperature (298 K) and pressure (1 atm) of the experiment. Crystallization of liquid water may also be ruled out because the density of solid water is lower than that of liquid. Phase transitions associated with organic impurities can also be ruled out because of the experimental conditions [44]. Phase transitions do not appear to explain an increase in mass during desiccation.

Redox reactions involving copper and iron are known to occur at standard temperature and pressure. Corrosion produces soluble Fe^{+2} or Cu^{+2} , which can in turn react in water with molecular oxygen to form metal oxide compounds. $Fe(OH)^3$ is sparingly soluble in waters with pH values above 6 (K_{sp} = 10 - 38), while $Fe(OH)^2$ is partially soluble (K_{sp} = 10 - 14.5) [43]. $Cu(OH)^2$ is also sparingly soluble (K_{sp} = 10 - 20) [43]. Corrosion also produces hydroxide ions at the cathodic end of the galvanic cell, which can react with bicarbonate and calcium to form calcium carbonate, which is only partially soluble (K_{sp} = 10 - 8.3) [43]. $Fe(OH)^3$, $Fe(OH)^2$, $Cu(OH)^2$, and $CaCO^3$ are corrosion products with the potential to increase the mass of pipe specimens during desiccation.

The analysis of the Mass Loss vs. Time graphs suggest that an average overall $R^2 < 0.6$ could be applied to the relationship between that of the copper and iron specimen mass loss and the malathion/water solution concentrations. The R^2 value is interpreted as a measure of the correlation between two variables (independent and dependent) [45]. An R^2 value of < 0.6 would suggest some correlation between the two variables of concern (mass loss and solution

concentration), but the level of correlation would be much less than direct. This is important to note as direct correlation is a characteristic that would be required in order to adequate use the mass loss relationship to determine the presence of the contaminant malathion on the surface of the copper and/or iron specimen.

5.3 The Effect of Malathion Exposure on XPS Spectra for Copper and Iron Specimen

5.3.1 XPS Library

As previously stated, in order to conduct a sufficient interpretation of the XPS spectra that result from the XPS analysis, it is imperative that an adequate XPS spectral library is available for comparison purposes. In addition to the library of spectral lines, it is also imperative that knowledge of the binding energies associated with the elements or compounds expected on observation is available as well. The following tables show the binding energy values for the elements and compounds that are most likely to be present on the surface of the copper (Cu) and iron (Fe) coupon samples. These values have been taken from those available in the literature and used for the purpose of generating the XPS library of accepted values upon which the results of this study will be referenced and validated. Table 1 shows the binding energy values for copper and copper oxide compounds. Table 2 shows the binding energy values for iron and iron compounds. Table 3 shows binding energy values for carbon and carbon compounds. Table 4 shows the binding energy values for sulfur and sulfur compounds. Table 5 shows the binding energy values for oxygen and oxygen compounds. And finaly, Table 6 shows binding energy values for two phosphorus metal structures.

Table 1. Binding Energy Values for Copper (eV) **[80]**

Cu metal	933
Cu (I) oxide	933
Cu (II) oxide	~933.5
Cu (II) carbonate dihydroxide	934.7

Table 2. Binding Energy Values for Iron (eV) **[77]**

Fe metal	706.7
FeO	709.6
Fe_2O_3	710.8
$FeCl_2$	710.4

Table 3. Binding Energy Values for Carbon (eV) **[78]**

C-C	284.8
C-O-C	~286
O-C=O	~288.5

Table 4. Binding Energy Values for Sulfur (eV) **[80]**

Metal sulfide	~161.5
Thiol bound to gold, Au-S	162.5
Thiol, R-SH	~164
$Na_2(SO_3)_2$	166.5
Metal sulfate	~169

Table 5. Binding Energy Values for Oxygen (eV) **[79]**

Metal oxides	529–530
Metal carbonates	531.5–523
Al_2O_3 (alumina)	531.1
SiO_2	532.9
Organic C-O	531.5–53
Organic C=O	~533
O-F_x	~535

Table 6. Binding Energy Values for Phosphorus (eV) **[80]**

Metal phosphode	~128.5
Metal phosphate	~133

Additionally, as previously stated, it is also necessary to have access to an XPS spectra library for the elements and/or compounds of concern for comparison purposes as well. The following graphs were obtained from an XPS library of spectral images for the elements and/or compounds of concern. These spectra have been taken from those available in the literature and used for the purpose of generating the XPS library of accepted spectra upon which the results of this study will be referenced and validated. It is important to note that the presented spectra show an overlay of the results of the curve fitting that was necessary to adjust the graphs because of the chemical shifts that took place during XPS analysis. These chemical shifts are of extreme importance as they are the result of a shift in the binding energy of a particular element due to its chemical interaction with other elements to form specific compounds. The peaks observed on the graphs will represent not only the base elemental structure, but any compound structures that have formed on the surface that has been analyzed. Figure 24 shows the XPS spectrum for copper. Figure 25 shows the XPS spectrum for iron and a couple of iron oxide compounds. Figure 26 shows the XPS spectra for carbon and a couple of carbon compounds. Figure 27 shows the XPS spectrum for sulfur. Figure 28 shows the XPS spectrum for oxygen and a corbonate compound. And finally, Figure 29 shows the XPS spectrum for phosphorus. It is necessary to understand that binding energy ranges for each element are just as significant as the shape and location of the characteristic peaks. The elements of concern for this study do not have binding energy peaks that are present in overlapping ranges. Therefore, identification of the charateristic peaks and their relative binding energy values for verification purposes is less complex here than it could be for a study involving elements that are much closer in binding energy values, where curve fitting would be required in order to properly identify each element.

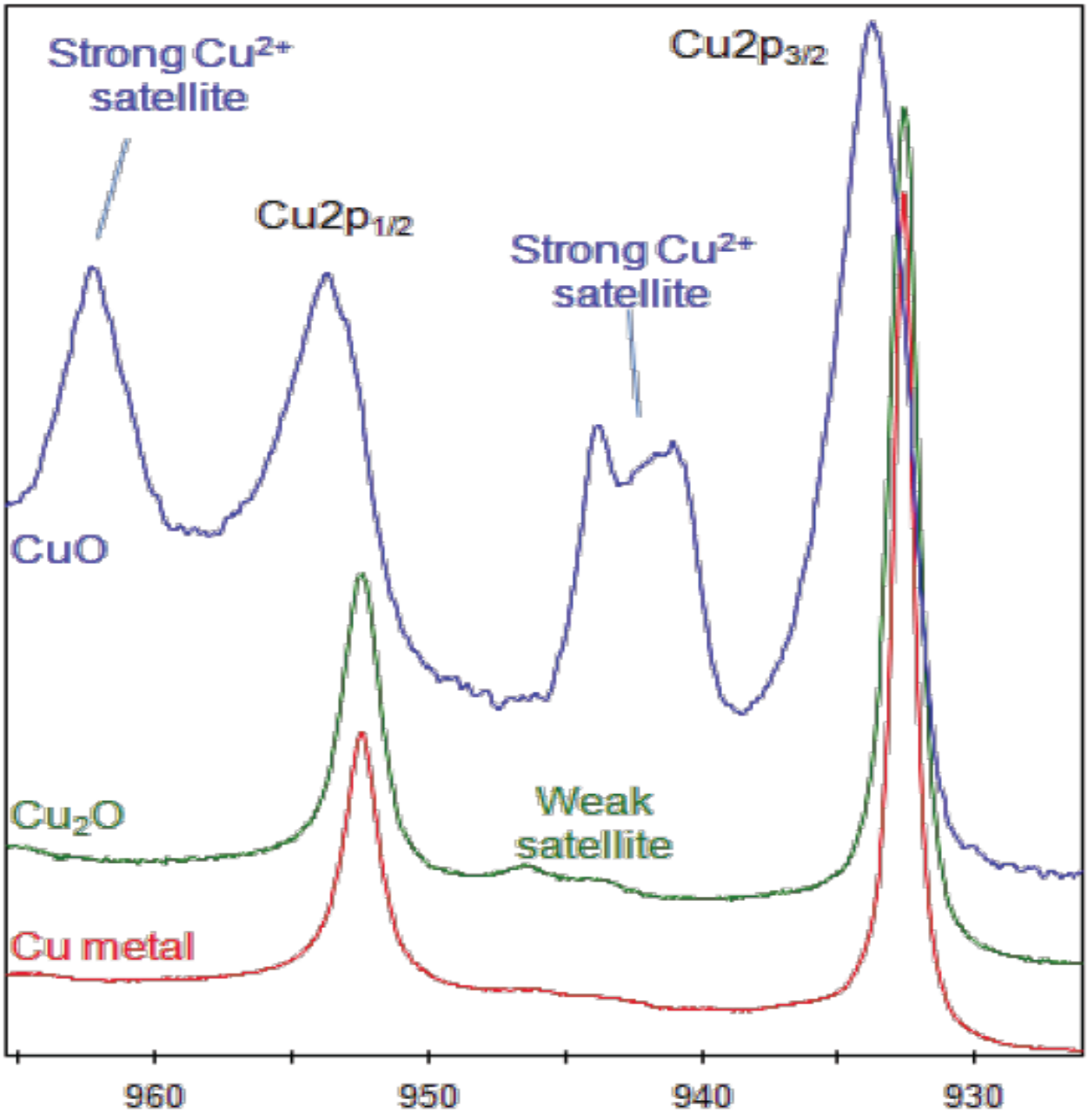

Figure 24. XPS Spectrum for Copper from Library **[80]**

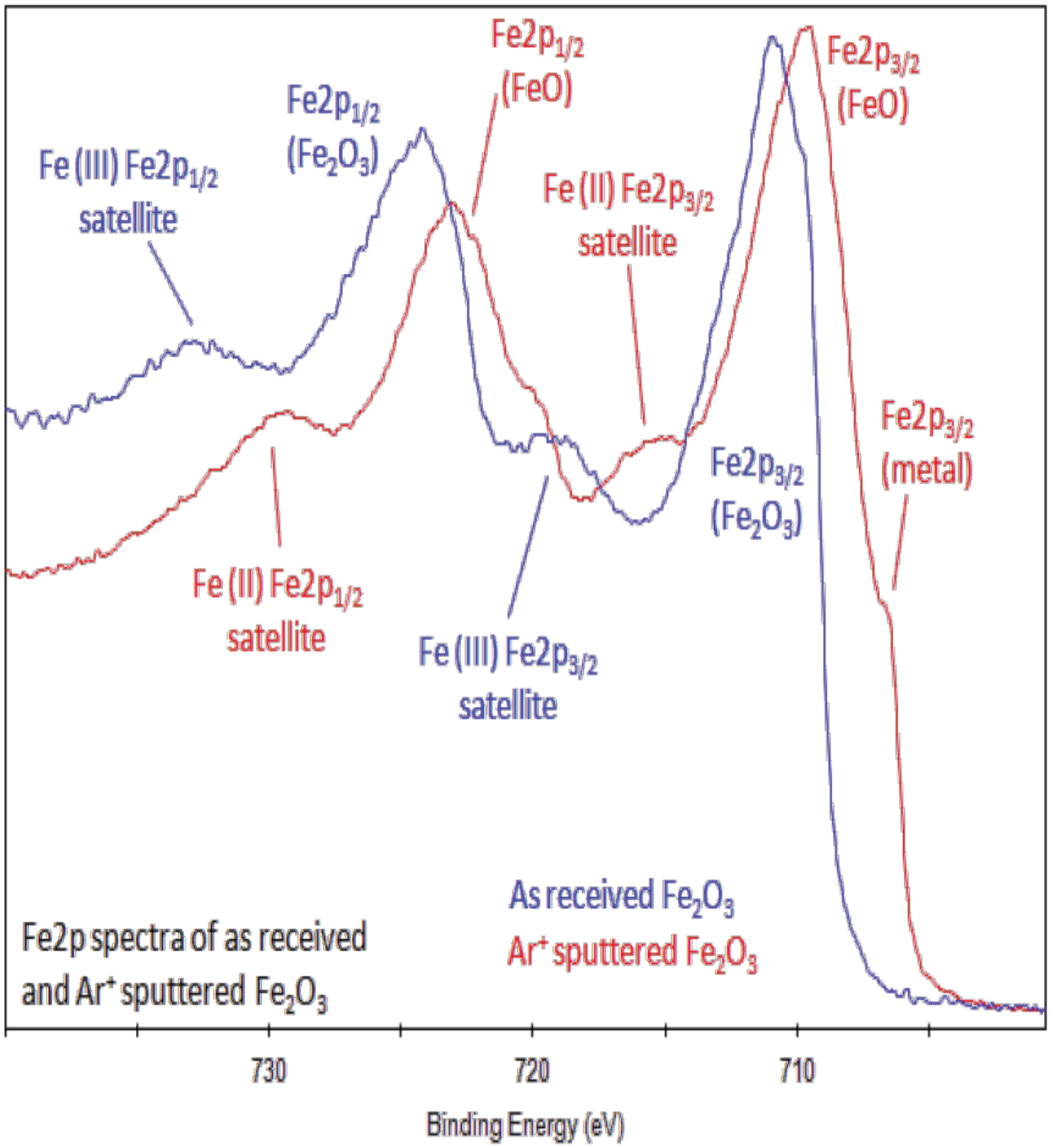

Figure 25. XPS Spectrum for Iron from Library **[77]**

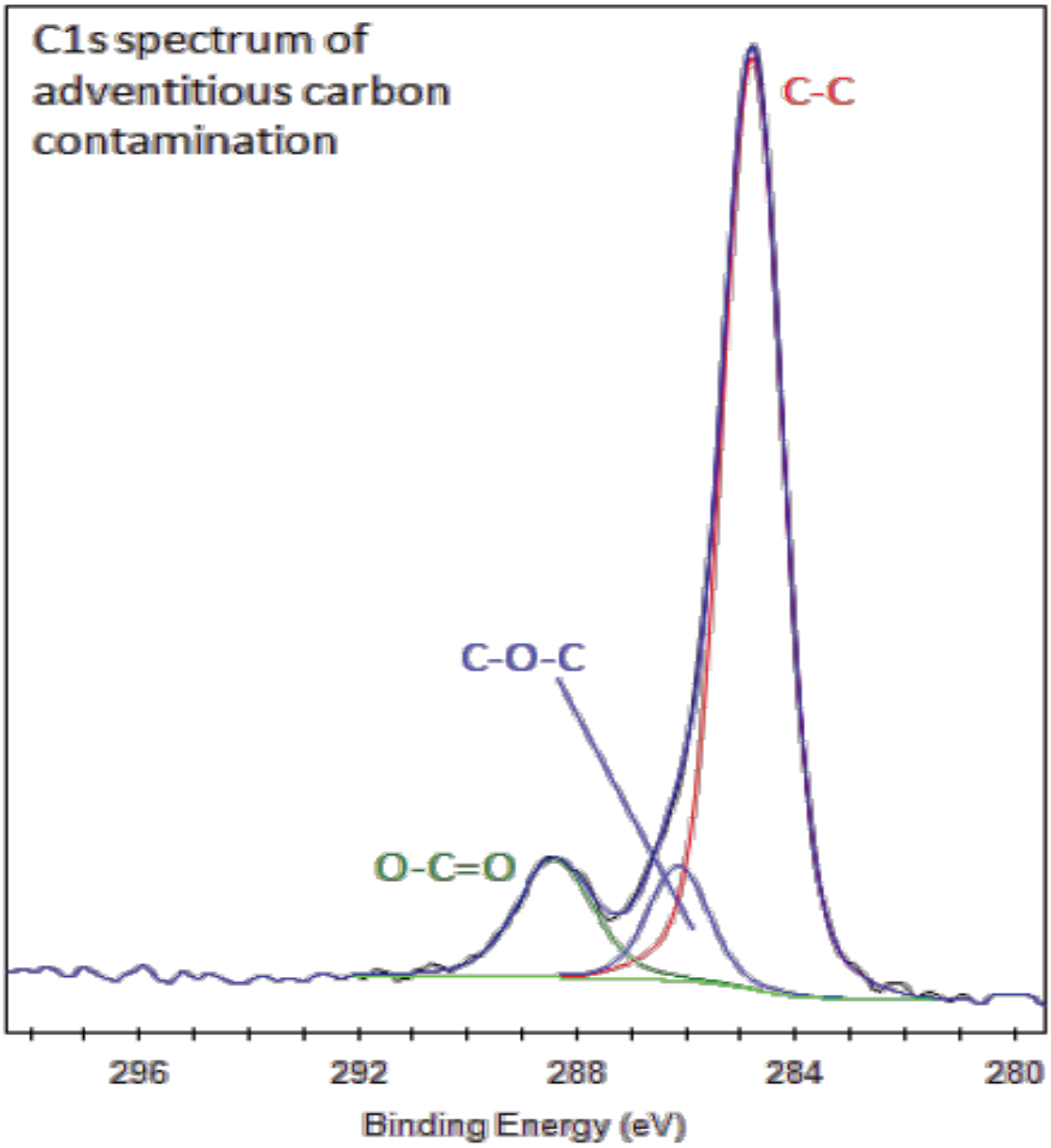

Figure 26. XPS Spectrum for Carbon from Library **[78]**

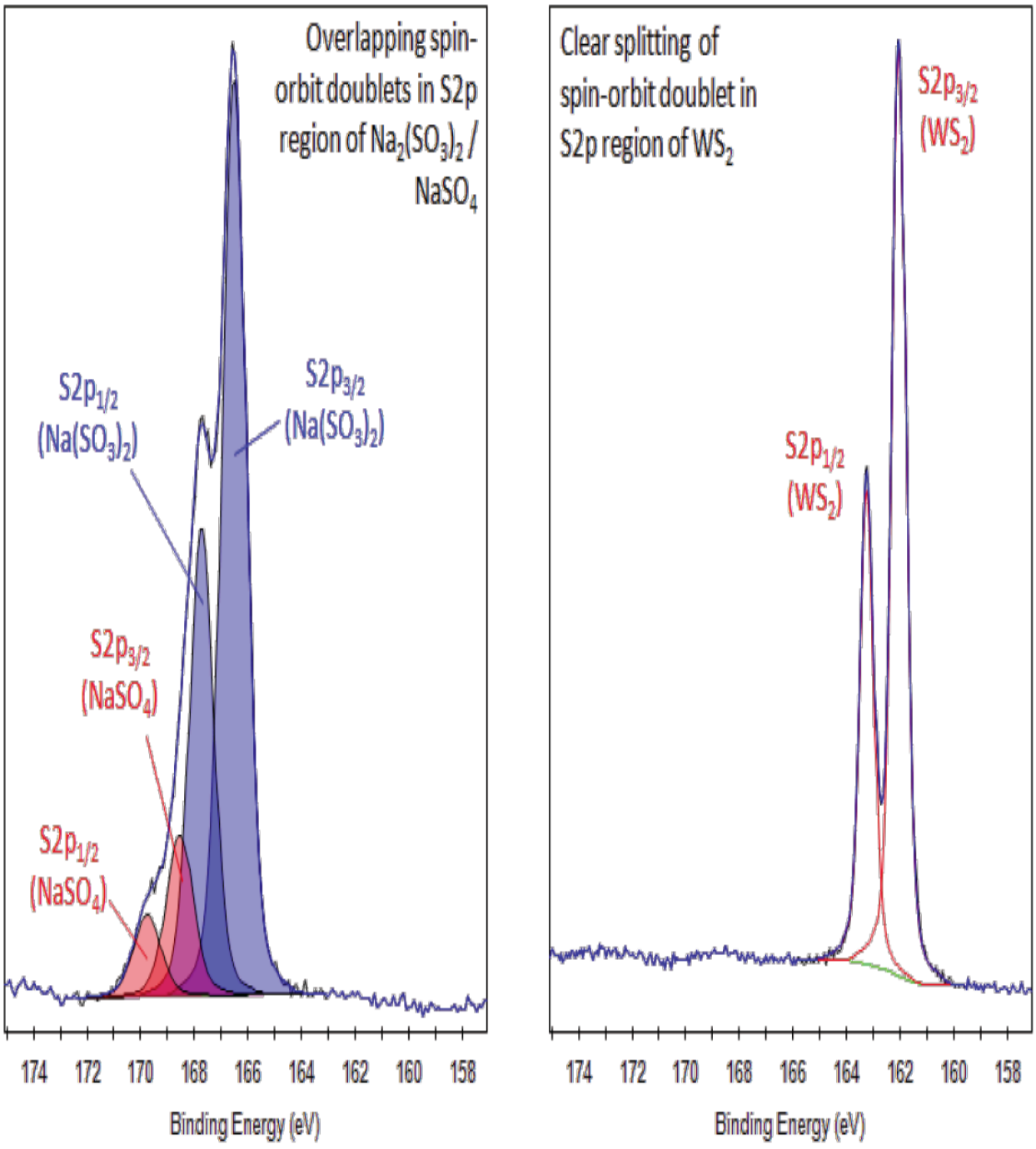

Figure 27. XPS Spectrum for Sulfur from Library **[80]**

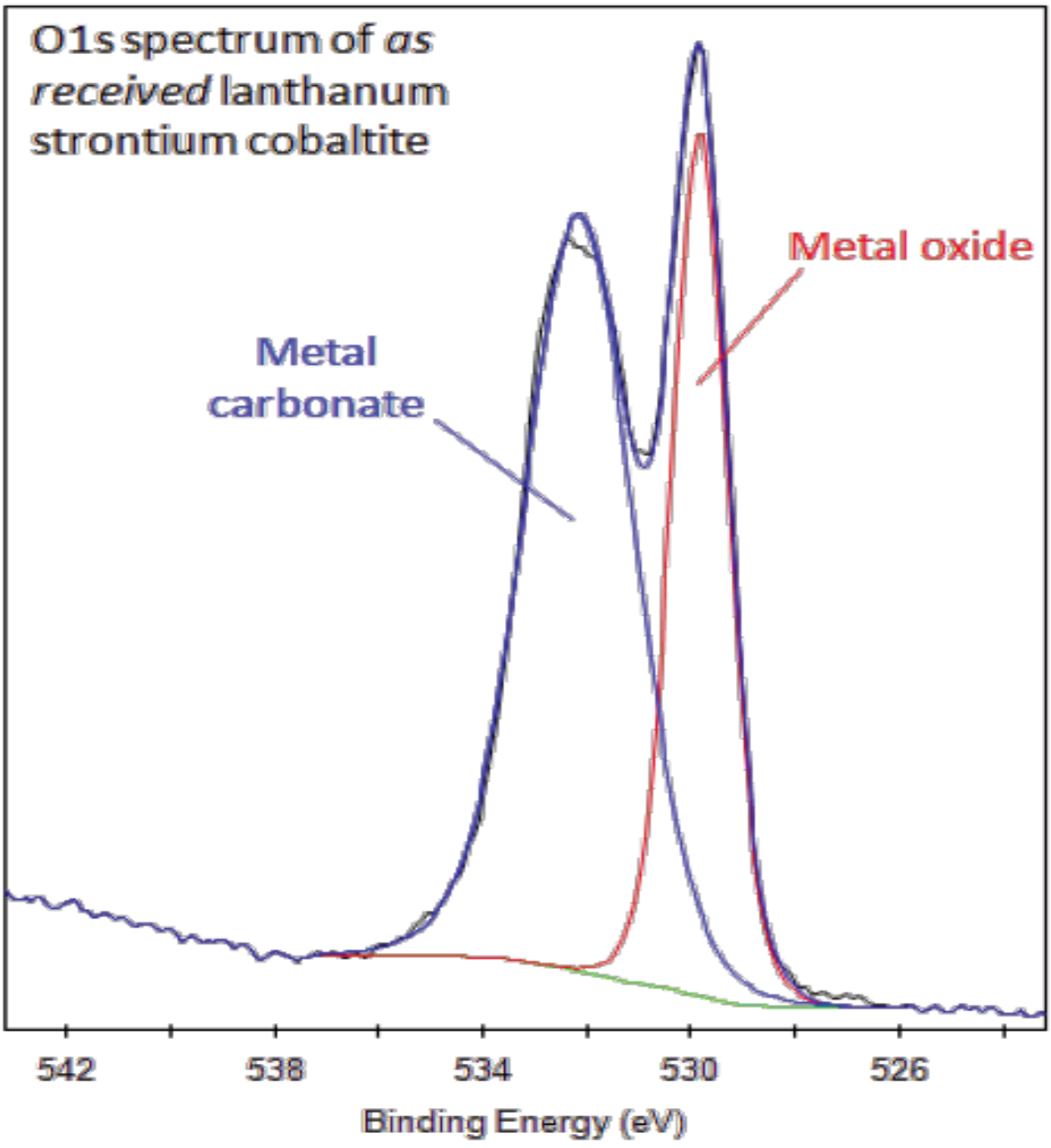

Figure 28. XPS Spectrum for Oxygen from Library **[79]**

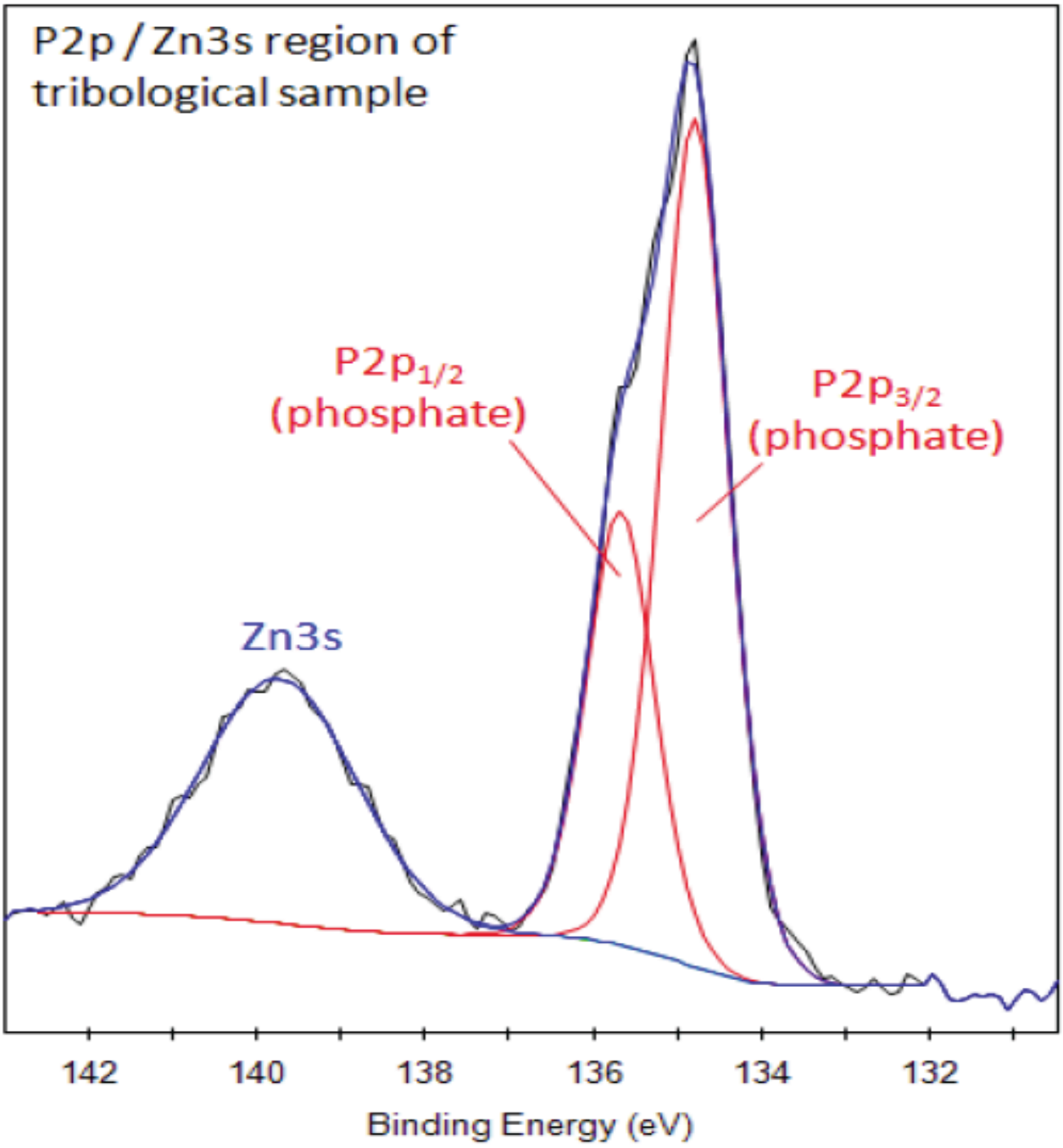

Figure 29. XPS Spectrum for Phosphorus from Library **[80]**

5.3.2 XPS Experimental Data

Figure 30 shows the resulting XPS spectrum from the analysis of a copper specimen that was submerged in deionized water for a period of 24 hours. In order to properly interpret an XPS spectrum graph, the resulting spectrum graph must be compared to that available from the XPS spectrum library. Figure shows the XPS spectrum for Copper (Cu) from an XPS library. A comparison of these two graphs highlights two common peaks, one at ~ 953 eV for $Cu2p_{1/2}$ and ~ 933 eV for $Cu2p_{3/2}$. The agreement between that of the copper specimen XPS spectrum and the copper spectrum for the XPS library serves as validation of the element(s) that were present on the surface of the copper specimen [46]. The results are consistent with what was expected as a result of an XPS analysis of an unexposed copper sample.

Figure 31 shows the resulting XPS spectrum from the analysis of an iron specimen that was submerged in deionized water for a period of 24 hours. In order to properly interpret an XPS spectrum graph, the resulting spectrum graph must be compared to that available from the XPS spectrum library. Figure shows the XPS spectrum for Iron (Fe) from an XPS library. A comparison of these two graphs highlights two common peaks, one at ~ 713 eV for $Fe2p_{1/2}$ and ~ 724 eV for $Fe2p_{3/2}$. The agreement between that of the copper specimen XPS spectrum and the copper spectrum for the XPS library serves as validation of the element(s) that were present on the surface of the iron specimen [46]. The results are consistent with what was expected as a result of an XPS analysis of an unexposed iron sample.

Figure 32 shows the resulting XPS spectrum from the analysis of a copper specimen that was exposed to a 100 mg/L malathion solution for a period of 24 hours. In order to properly interpret an XPS spectrum graph, the resulting spectrum graph must be compared to that available from an XPS spectrum library. In this instance, the comparison must include several

XPS spectra from an XPS library in order to account for the presence of numerous distinctive peaks. Figures 27, 28, 29, 30, 31, and 32 show the XPS spectra for Copper (Cu), Iron (Fe), Carbon (C), Sulfur (S), Oxygen (O), and Phosphorus(P) respectively, from an XPS library. These individual spectra must be compared with that of the individual spectra obtained during the XPS analysis of the exposed copper specimen. The survey spectrum displayed above covers a range of 0 – 1000 eV, which covers the spectrum range for all of the elements that are expected to be present on the surface of the exposed copper specimen. However, it is difficult at best to clearly identify all distinctive peaks displayed on a survey spectrum. This makes it necessary to obtain XPS spectra of specific electron volt (eV) ranges in an effort to more clearly identify the distinctive peaks for specific elements and/or compounds that are present. This does not remove the capability of analyzing the general shape of the survey spectra and stating the observations. For the survey spectra displayed above, there are five distinctive peaks that can be observed at ~ 75 eV, 280 eV, 530 eV, 930 eV, and 950 eV. These binding energy values; along with those provided in Tables, suggests the presence of carbon, oxygen, phosphorus, and copper [46]. This observation is consistent with what would be expected for the given analysis scenario.

Figure 33 shows the resulting XPS spectrum from the analysis of an iron specimen that was exposed to a 100 mg/L malathion solution for a period of 24 hours. This spectrum requires an analysis consistent with that of which was conducted on the survey spectrum representing the exposed copper specimen. The above spectrum displays the same binding energy spectra as that of the survey spectrum for the exposed copper specimen, but with a couple of distinct differences. Data analysis software was used to more accurately define the binding energy peaks displayed on the survey spectrum. The most distinct differences between this survey spectrum and that of the survey spectrum for the exposed copper specimen; as highlighted by the data

analysis software, is that of the presence of both copper and iron on the surface of the exposed iron specimen. The suggested presence of copper on the surface of the exposed iron specimen will be discussed later within the assessment section. The suggested presence of that of carbon, oxygen, phosphorus, and iron on the surface of the exposed iron specimen is consistent with that of what would be expected for the given analysis scenario.

Figure 34 displays the XPS spectrum for the exposed copper specimen taken in the binding energy range of 918 – 966 eV. The more specific binding energy range provides the capability of much more accurately identifying any distinct binding energy peaks present within the chosen range. The binding energy range shown here highlights the presence of two distinctive peaks located at ~ 953 eV and 933 eV. These values are consistent with those found in the literature that would suggest the presence of copper [46]. This is also consistent with that of what would be expected for the given analysis scenario. It should be noted that the lack of distinct clarity in the graph was assumed to be the result of background noise interference within the detector. Yet, despite the limitation placed on clarity by this detector background noise, the ability to identify the two binding energy peaks of concern was not compromised.

Figure 35 displays the XPS spectrum for the exposed iron specimen taken in the binding energy range of 918 – 966 eV. The more specific binding energy range provides the capability of much more accurately identifying any distinct binding energy peaks present within the chosen range. The binding energy range shown here highlights the presence of two distinctive peaks located at ~ 953 eV and 933 eV. These values are consistent with those found in the literature that would suggest the presence of copper [46]. This is not consistent with that of what would be expected for the given analysis scenario, and it will be discussed further in the conclusion section.

Figure 36 displays the XPS spectrum for the exposed iron specimen taken in the binding energy range of 696 - 746e V. The more specific binding energy range provides the capability of much more accurately identifying any distinct binding energy peaks present within the chosen range. The binding energy range shown here highlights the presence of two distinctive peaks located at ~ 726 eV and 711 eV. These values are consistent with those found in the literature that would suggest the presence of iron [46]. This is also consistent with that of what would be expected for the given analysis scenario.

Figure 37 displays the XPS spectrum for the exposed copper specimen taken in the binding energy range of 270 – 299 eV. The more specific binding energy range provides the capability of much more accurately identifying any distinct binding energy peaks present within the chosen range. The binding energy range shown here highlights the presence of a distinctive peak located at ~ 286 eV. This value is consistent with that found in the literature that would suggest the presence of carbon on the surface of the copper specimen [46]. This is also consistent with that of what would be expected for the given analysis scenario.

Figure 38 displays the XPS spectrum for the exposed iron specimen taken in the binding energy range of 271 – 299 eV. The more specific binding energy range provides the capability of much more accurately identifying any distinct binding energy peaks present within the chosen range. The binding energy range shown here highlights the presence of a distinctive peak located at ~ 286 eV. This value is consistent with that found in the literature that would suggest the presence of carbon on the surface of the iron specimen [46]. This is also consistent with that of what would be expected for the given analysis scenario.

Figure 40 displays the XPS spectrum for the exposed copper specimen taken in the binding energy range of 523 – 551 eV. The more specific binding energy range provides the

capability of much more accurately identifying any distinct binding energy peaks present within the chosen range. The binding energy range shown here highlights the presence of a distinctive peak located at ~ 533 eV. This value is consistent with that found in the literature that would suggest the presence of oxygen on the surface of the copper specimen [46]. This is also consistent with that of what would be expected for the given analysis scenario.

Figure 41 displays the XPS spectrum for the exposed iron specimen taken in the binding energy range of 521 – 545 eV. The more specific binding energy range provides the capability of much more accurately identifying any distinct binding energy peaks present within the chosen range. The binding energy range shown here highlights the presence of a distinctive peak located at ~ 532 eV. This value is consistent with that found in the literature that would suggest the presence of oxygen on the surface of the iron specimen [46]. This is also consistent with that of what would be expected for the given analysis scenario.

Figure 42 displays the XPS spectrum for the exposed copper specimen taken in the binding energy range of 219 – 242 eV. The more specific binding energy range is intended to provide the capability of much more accurately identifying any distinct binding energy peaks present within the chosen range. However, the binding energy range shown here highlights the presence of numerous distinctive peaks located within the range. The presence of these numerous peaks make it difficult to isolation of one or more distinctive peaks, but a distinctive peak located at ~ 227 eV can be identified. The XPS analysis suggests the presence on sulfur, despite the discrepancy between the binding energy value of the observed peak and that of what can be found in the literature for sulfur. This discrepancy could be the result of a chemical shift in the binding energies that can occur as a consequence of the presence of ionically or covalently bonded compounds on the surface of the exposed copper specimen [47]. This behavior may be

consistent with that of what should be expected, but that determination can only be made after more extensive chemical analysis of the experimental scenario, as well as curve fitting of the XPS spectra.

Figure 43 displays the XPS spectrum for the exposed iron specimen taken in the binding energy range of 153 – 179 eV. The more specific binding energy range provides the capability of much more accurately identifying any distinct binding energy peaks present within the chosen range. The binding energy range shown here highlights the presence of two distinctive peaks located at ~ 164 eV and 149 eV ($S2p_{3/2}$ and S2s). These values are consistent with those found in the literature that would suggest the presence of sulfur on the surface of the iron specimen [46]. This is also consistent with that of what would be expected for the given analysis scenario.

Figure 44 displays the XPS spectrum for the exposed copper specimen taken in the binding energy range of 179 - 200eV. The more specific binding energy range provides the capability of much more accurately identifying any distinct binding energy peaks present within the chosen range. The binding energy range shown here highlights the presence of numerous distinctive peaks. These binding energy peaks do not exist at binding energy values that are consistent with those found in the literature that would suggest the presence of phosphorus, however, the peaks are consistent with those found in the literature that would suggest the presence of phosphorus on the surface of the copper specimen that has experienced a chemical shift [46]. This chemical shift would need to be validated via curve fitting, but the suggested presence of phosphorus on the surface of the copper specimen is consistent with that of what would be expected for the given analysis scenario.

Figure 45 displays the XPS spectrum for the exposed iron specimen taken in the binding energy range of 179 - 200eV. The more specific binding energy range provides the capability of

much more accurately identifying any distinct binding energy peaks present within the chosen range. The binding energy range shown here highlights the presence of numerous distinctive peaks. These binding energy peaks do not exist at binding energy values that are consistent with those found in the literature that would suggest the presence of phosphorus, however, the peaks are consistent not only with those found in the literature that would suggest the presence of phosphorus on the surface of the copper specimen that has experienced a chemical shift, but also with the binding energy peaks identified on the previous graph displaying the same eV range for an exposed copper specimen [46]. The consistency between both graphs along with the XPS spectra data found in the literature for phosphorus make a strong case for the suggested presence of this element on the surface of both the iron and the copper specimen. This is also consistent with that of what would be expected for the given analysis scenario.

5.4 Assessment

The suggested presence of the elements carbon (C), oxygen (O), sulfur (S), and phosphorus (P) on the surface the specimen is consistent with what one would expect for a scenario where an organophosphorus compound such as malathion has been detected on the surface of a metal by XPS analysis. It is important to note that the results are merely suggestive and that evidence of this detection can only be obtained through further analyses and the application of XPS spectrum curve fitting techniques to verify the suggested chemical shifts.

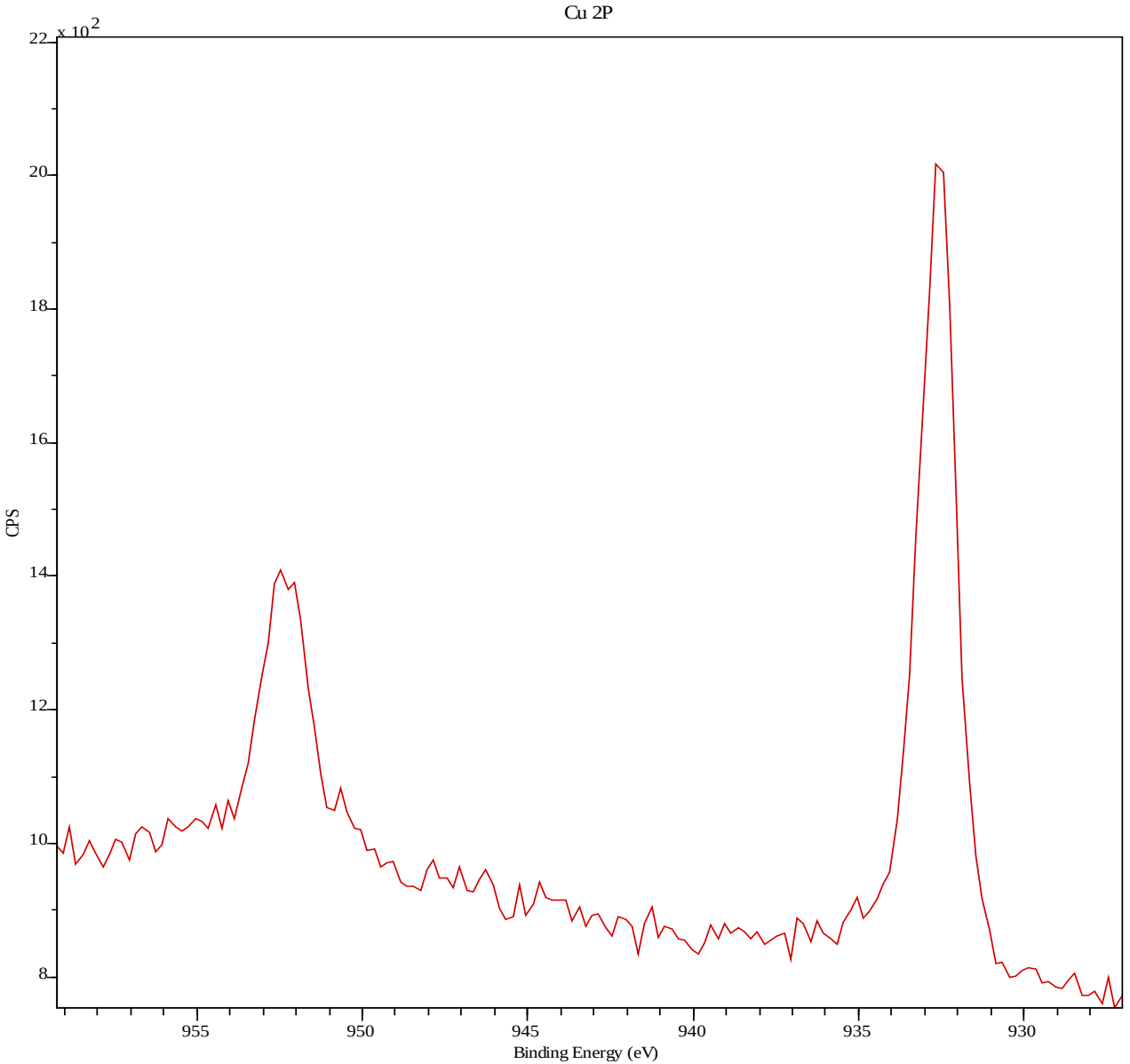

Figure 30. XPS Spectrum for Unexposed Copper Specimen

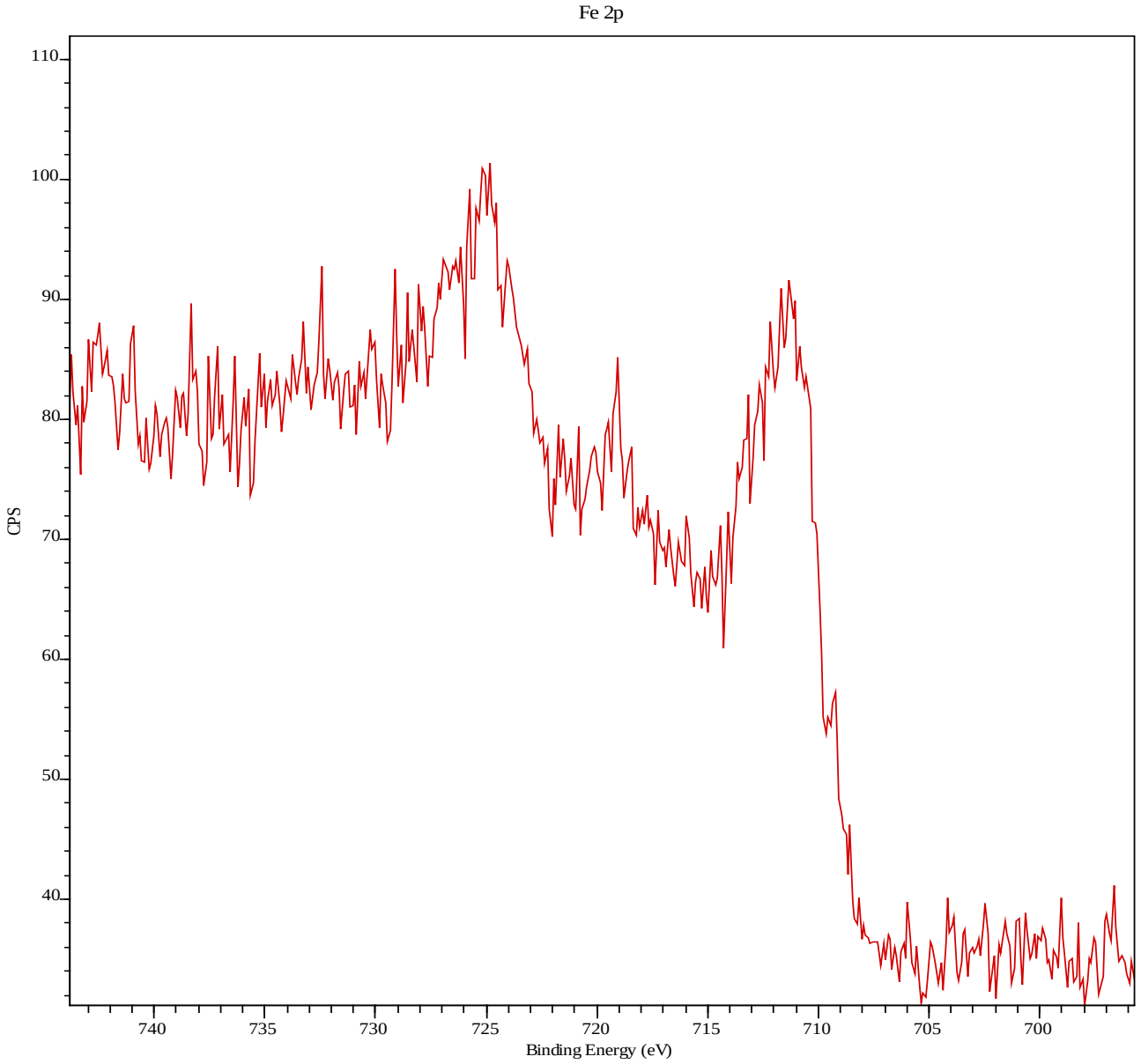

Figure 31. XPS Spectrum for Unexposed Iron Specimen

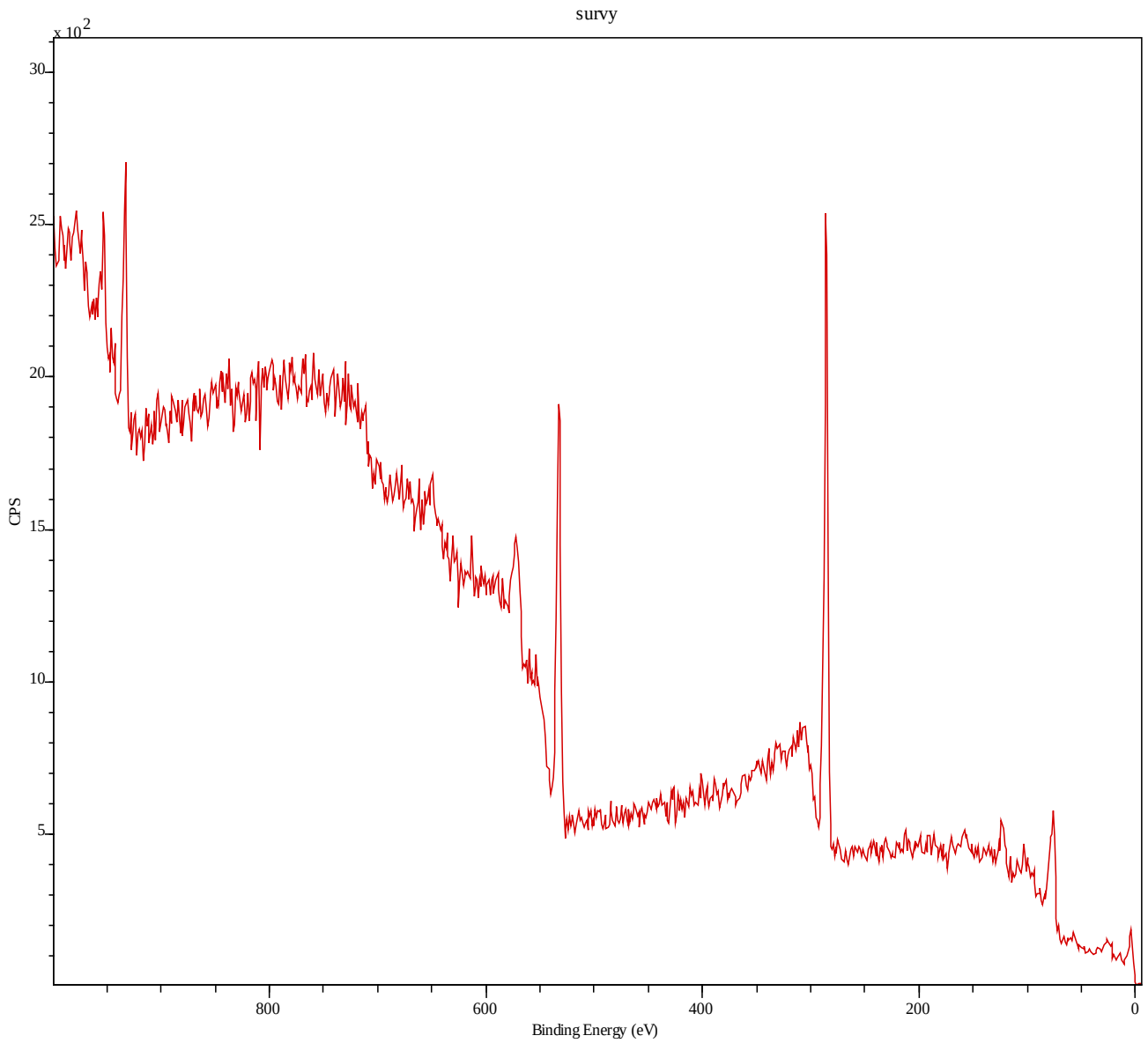

Figure 33. XPS Survey Spectrum for Copper Specimen Exposed to 100 mg/L Malathion

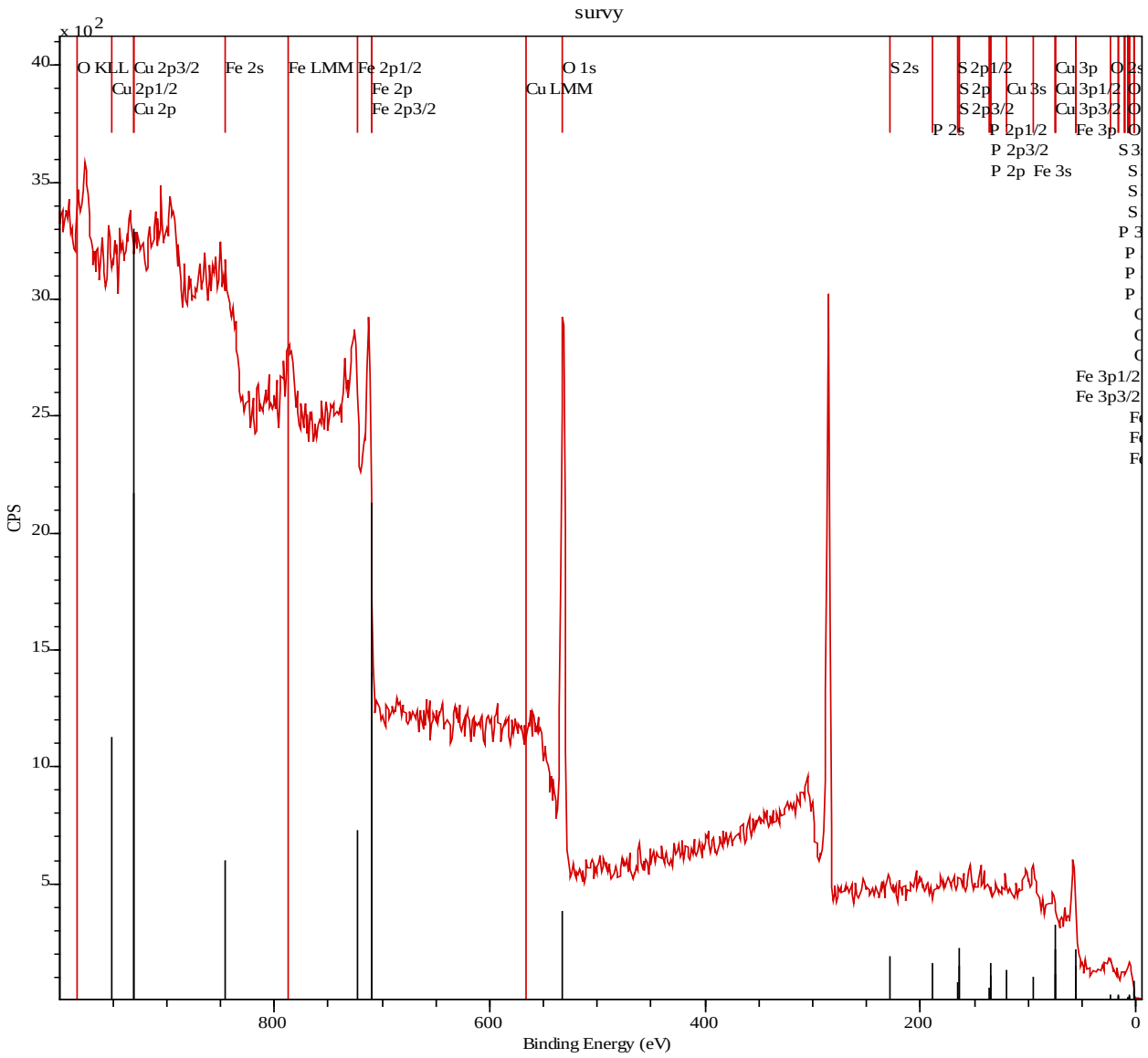

Figure 34. XPS Survey Spectrum for Iron Exposed to 100 mg/L Malathion

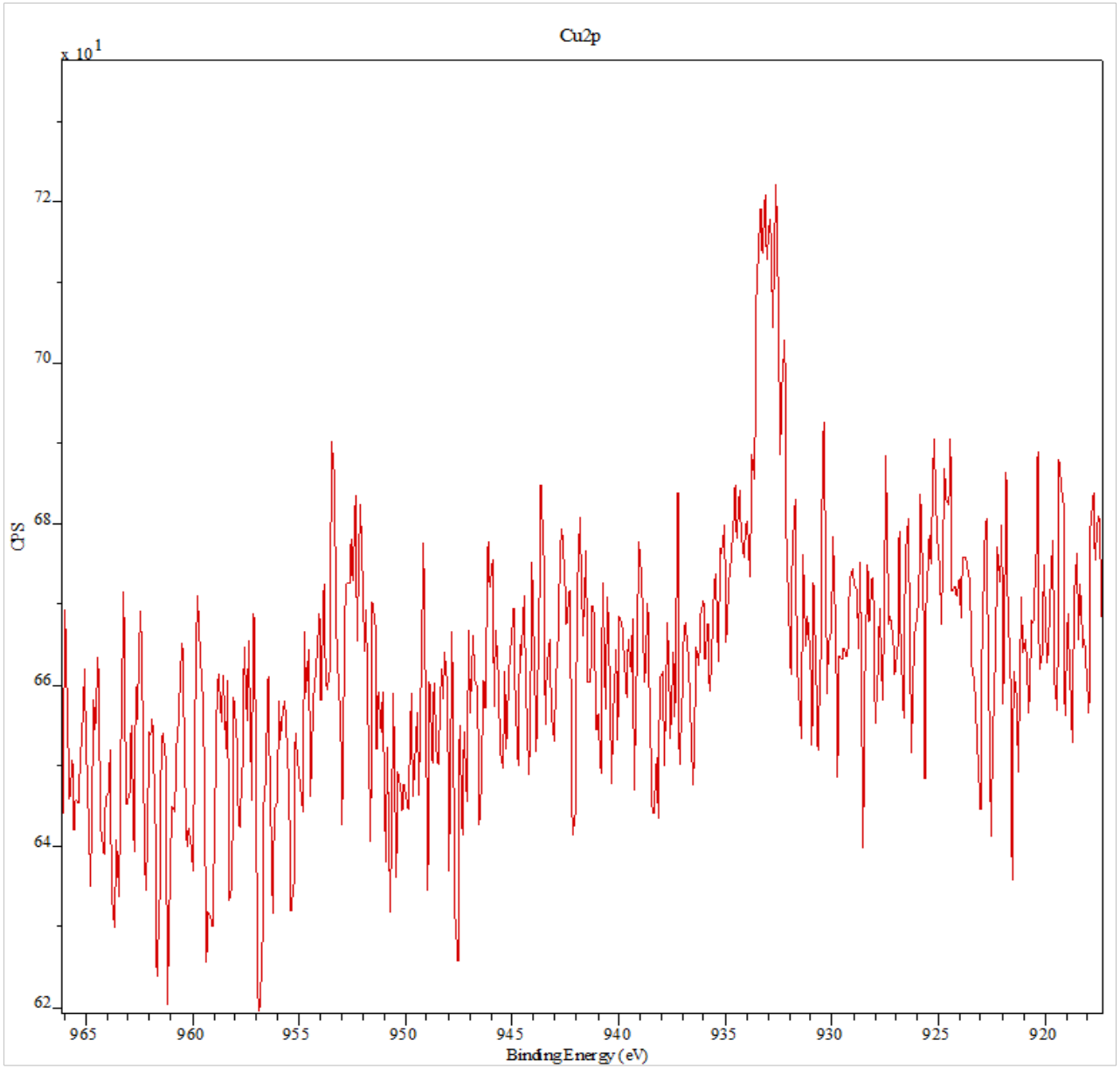

Figure 35. XPS Spectrum for Exposed Copper (918 – 966 eV range)

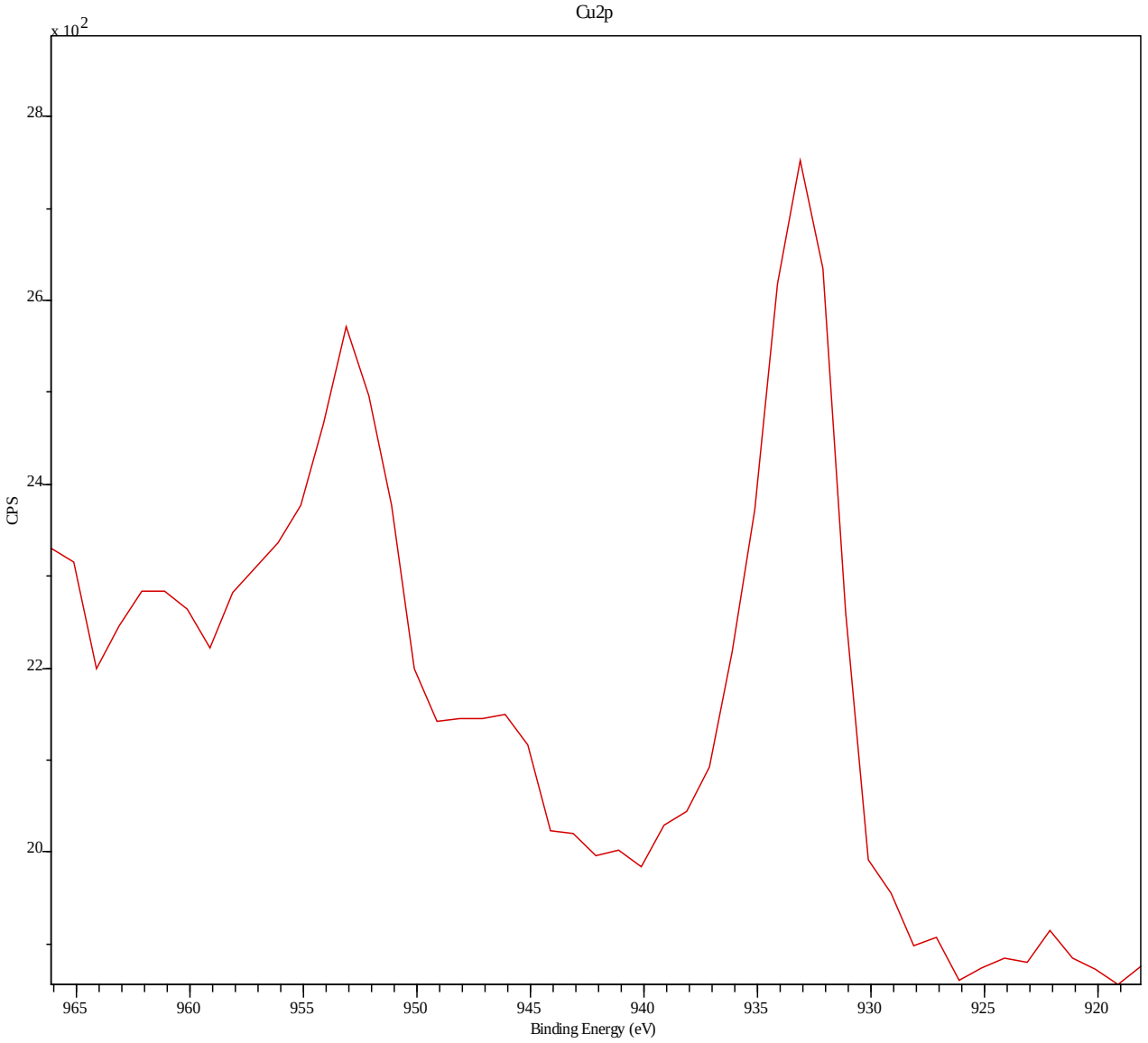

Figure 36. XPS Spectrum for Exposed Iron (918 – 966 eV range)

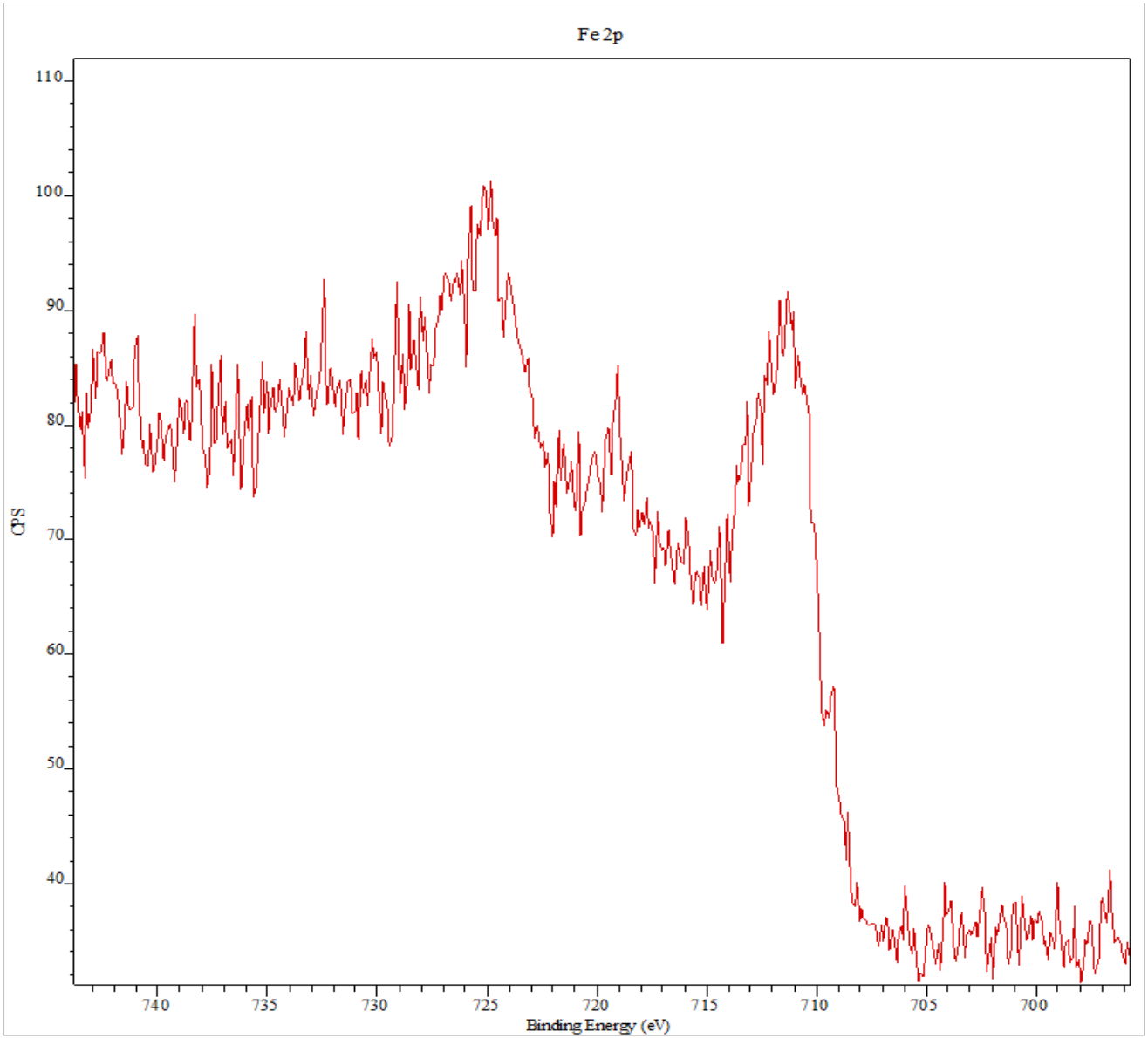

Figure 37. XPS Spectrum for Exposed Iron (696 – 743 eV range)

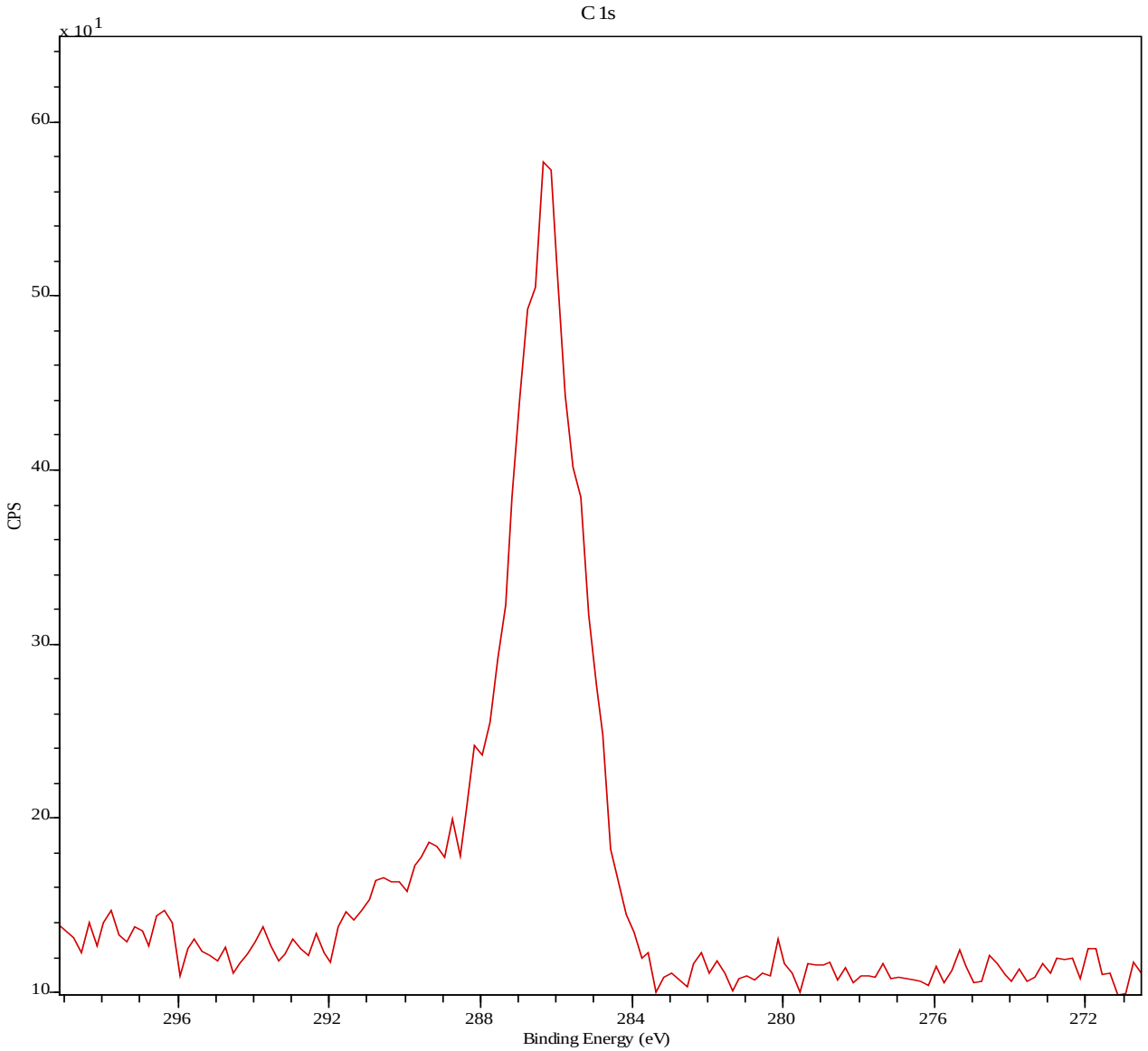

Figure 38. XPS Spectrum for Exposed Copper (271 – 299 eV range)

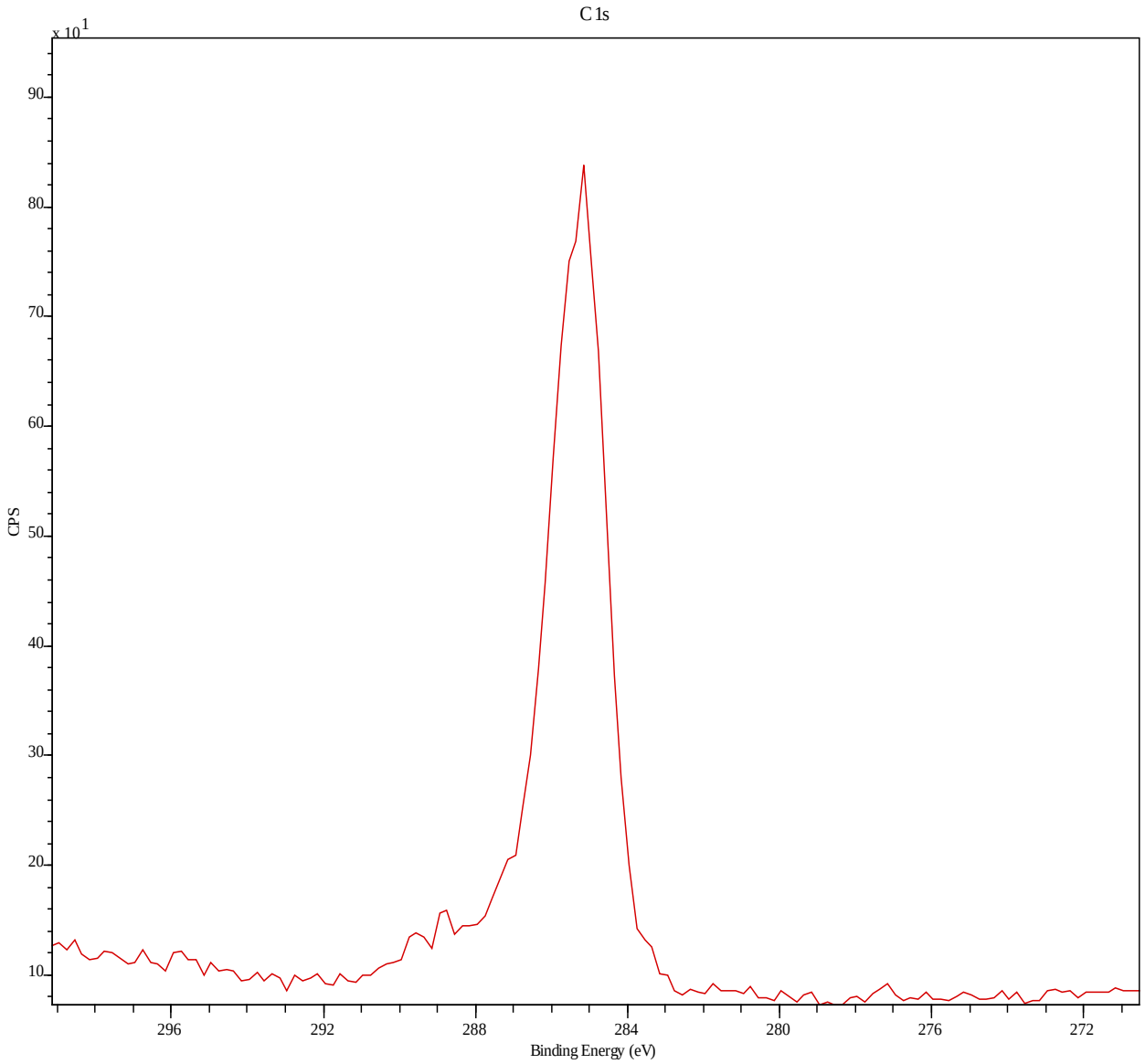

Figure 39. XPS Spectrum for Exposed Iron (271 – 299 eV range)

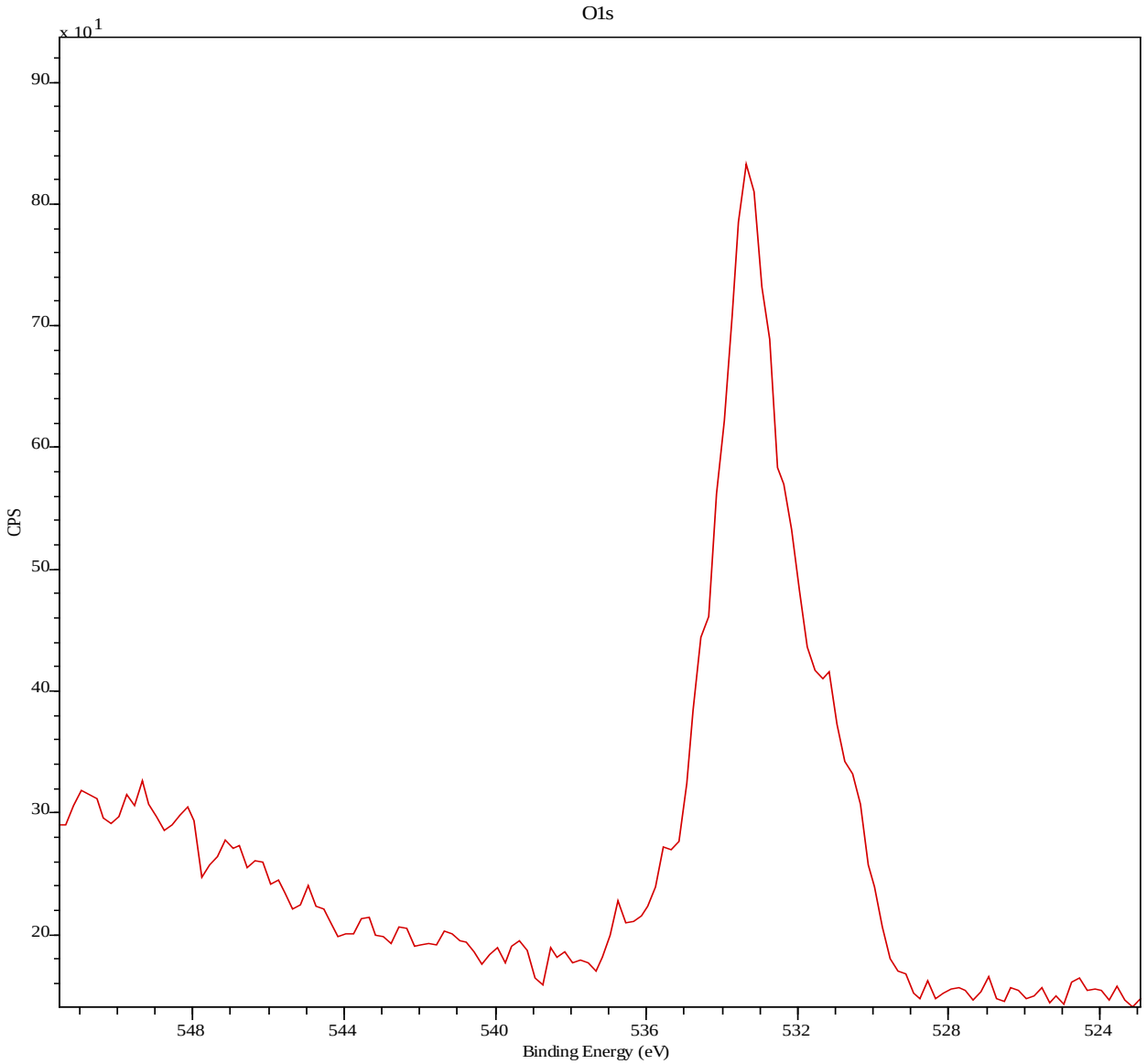

Figure 40. XPS Spectrum for Exposed Copper (523 – 551 eV range)

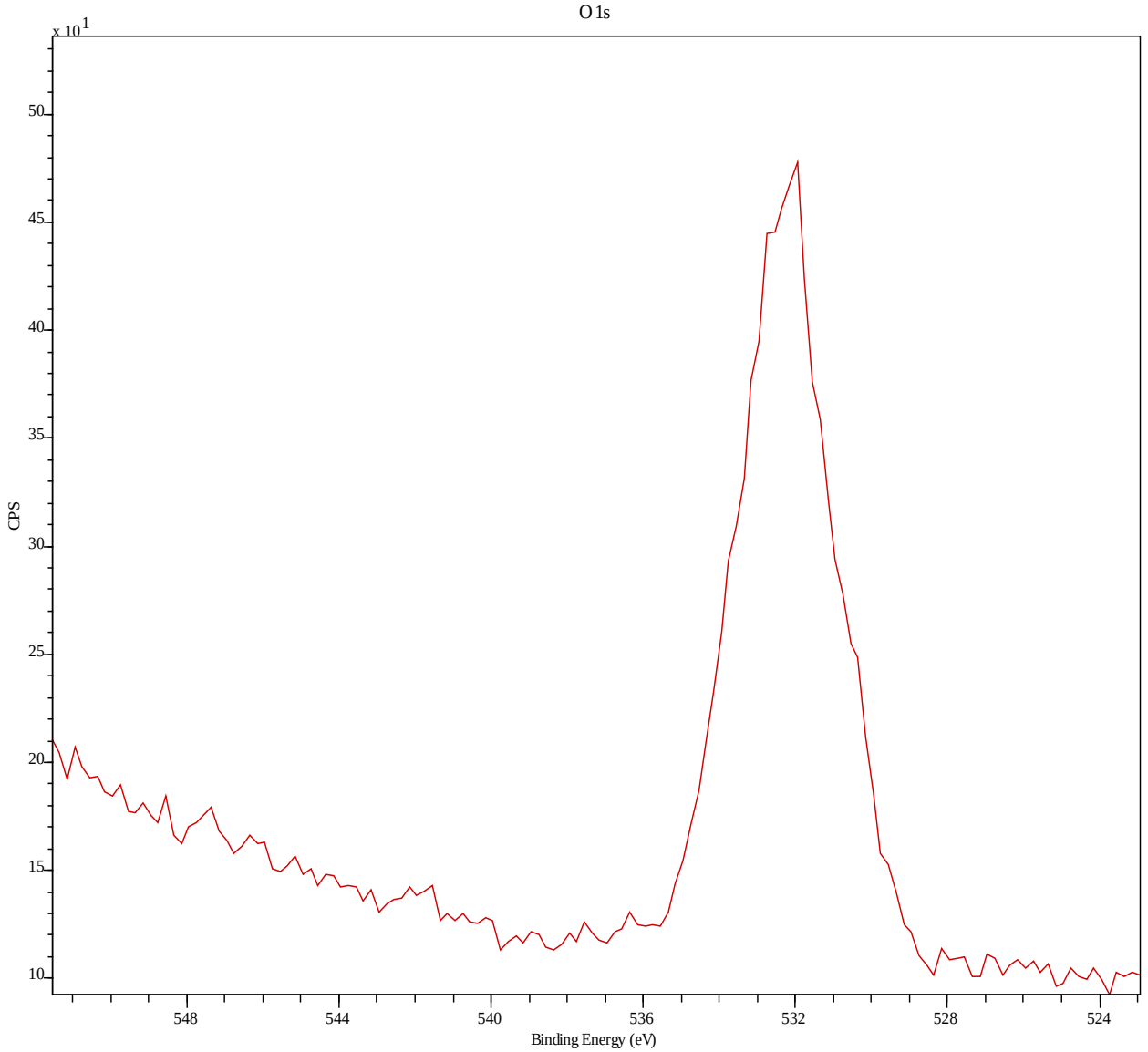

Figure 41. XPS Spectrum for Exposed Iron (523 – 551 eV range)

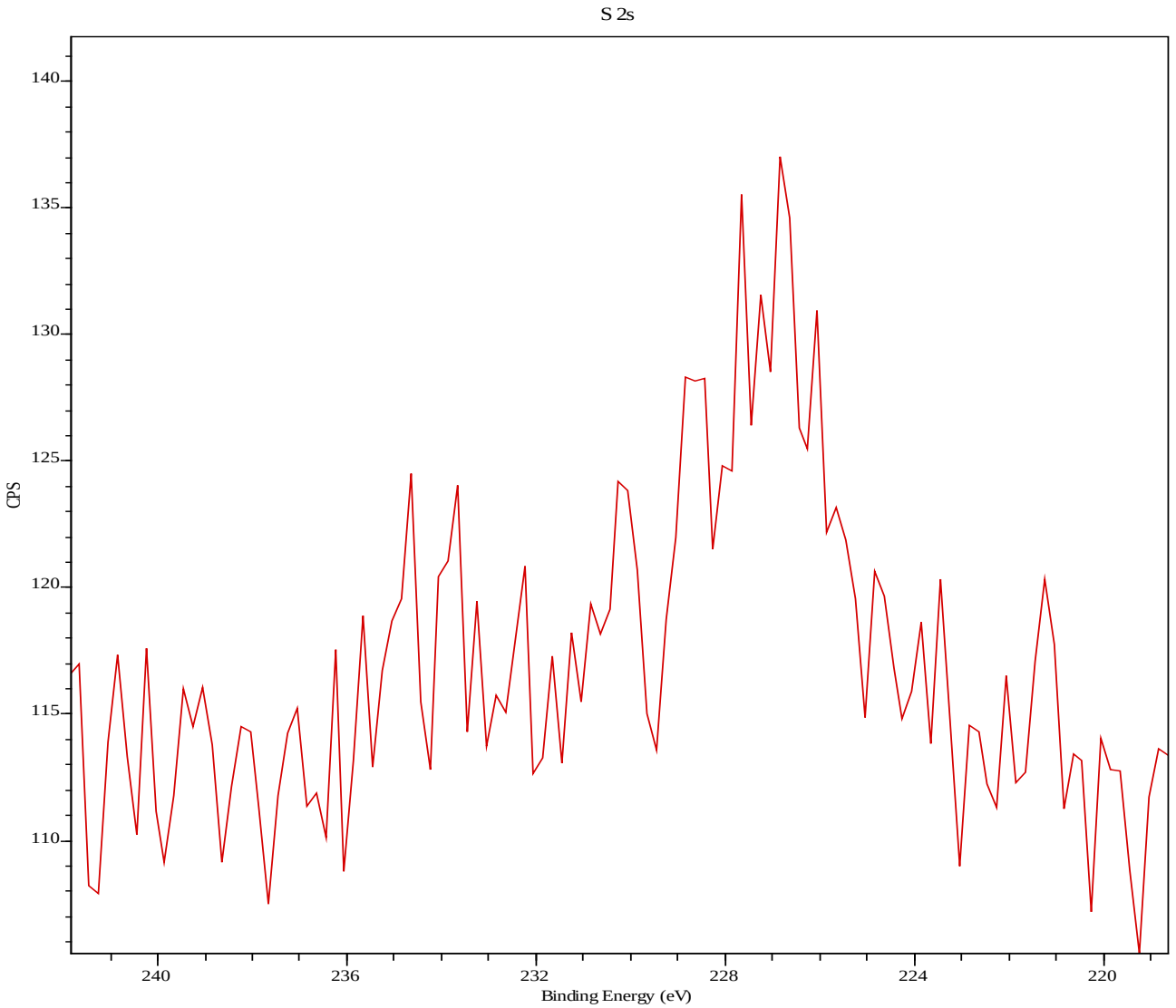

Figure 42. XPS Spectrum for Exposed Copper (221 – 241 eV range)

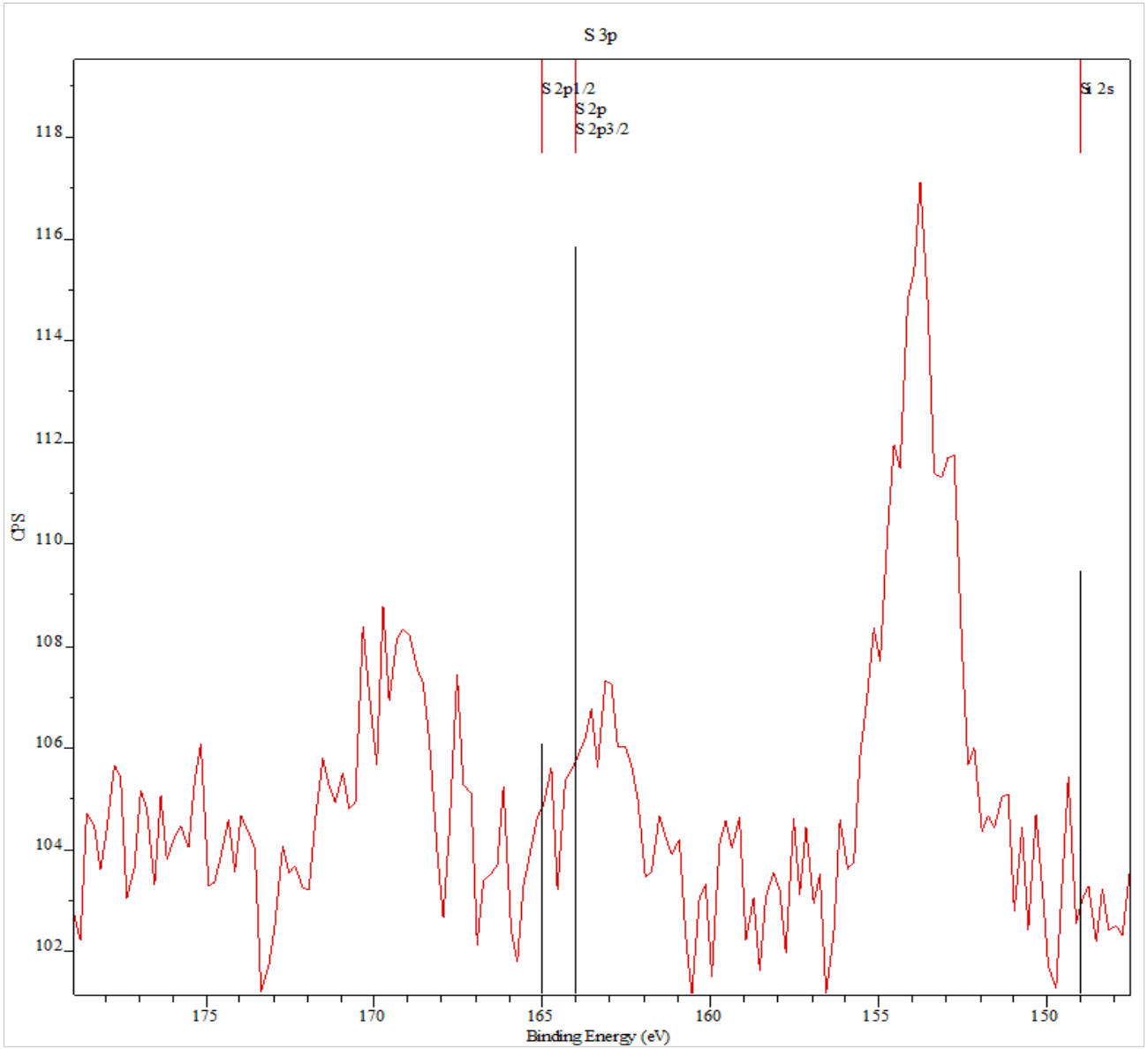

Figure 43. XPS Spectrum for Exposed Iron (148 – 178 eV range)

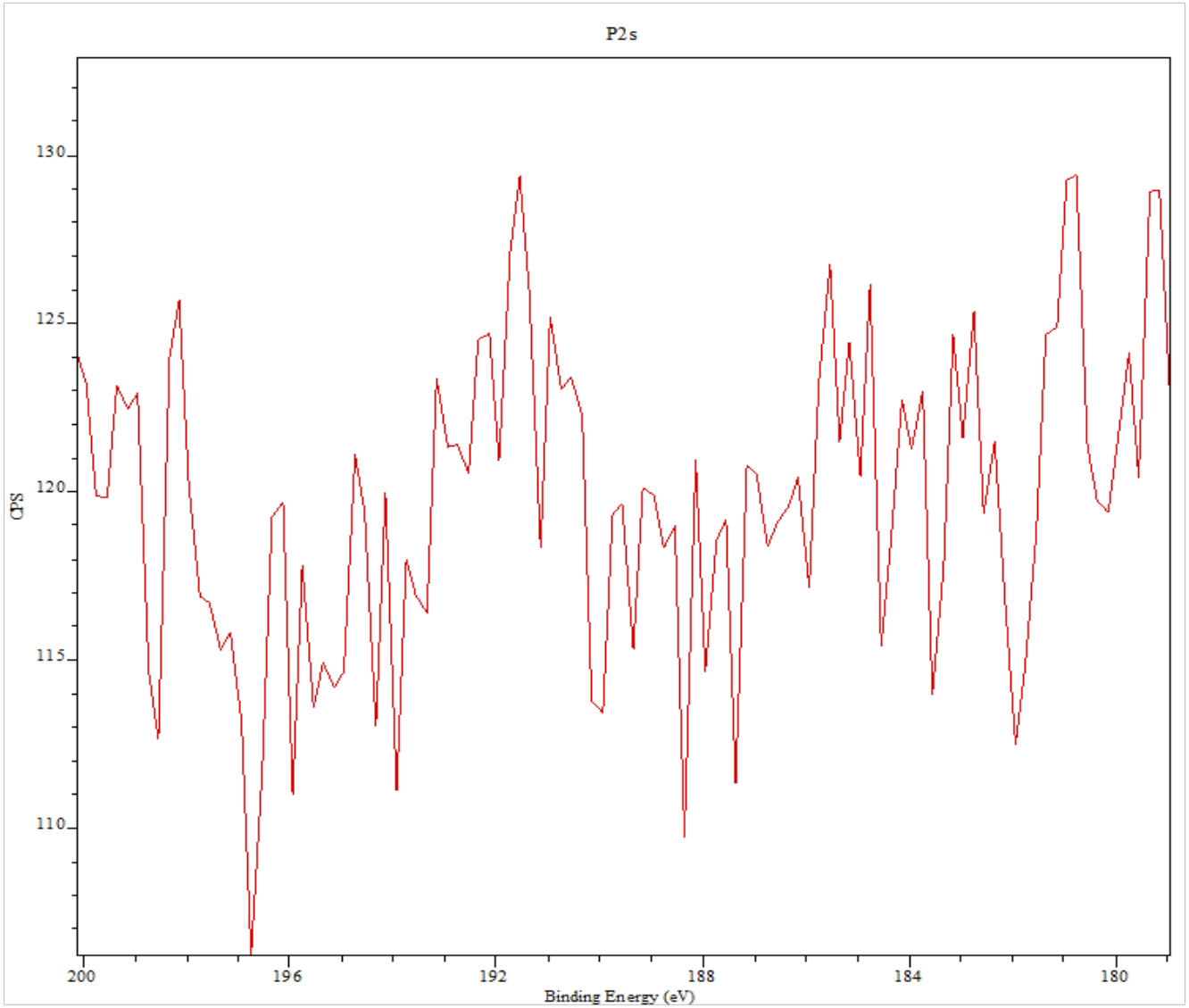

Figure 44. XPS Spectrum for Exposed Copper (179 – 200 eV range)

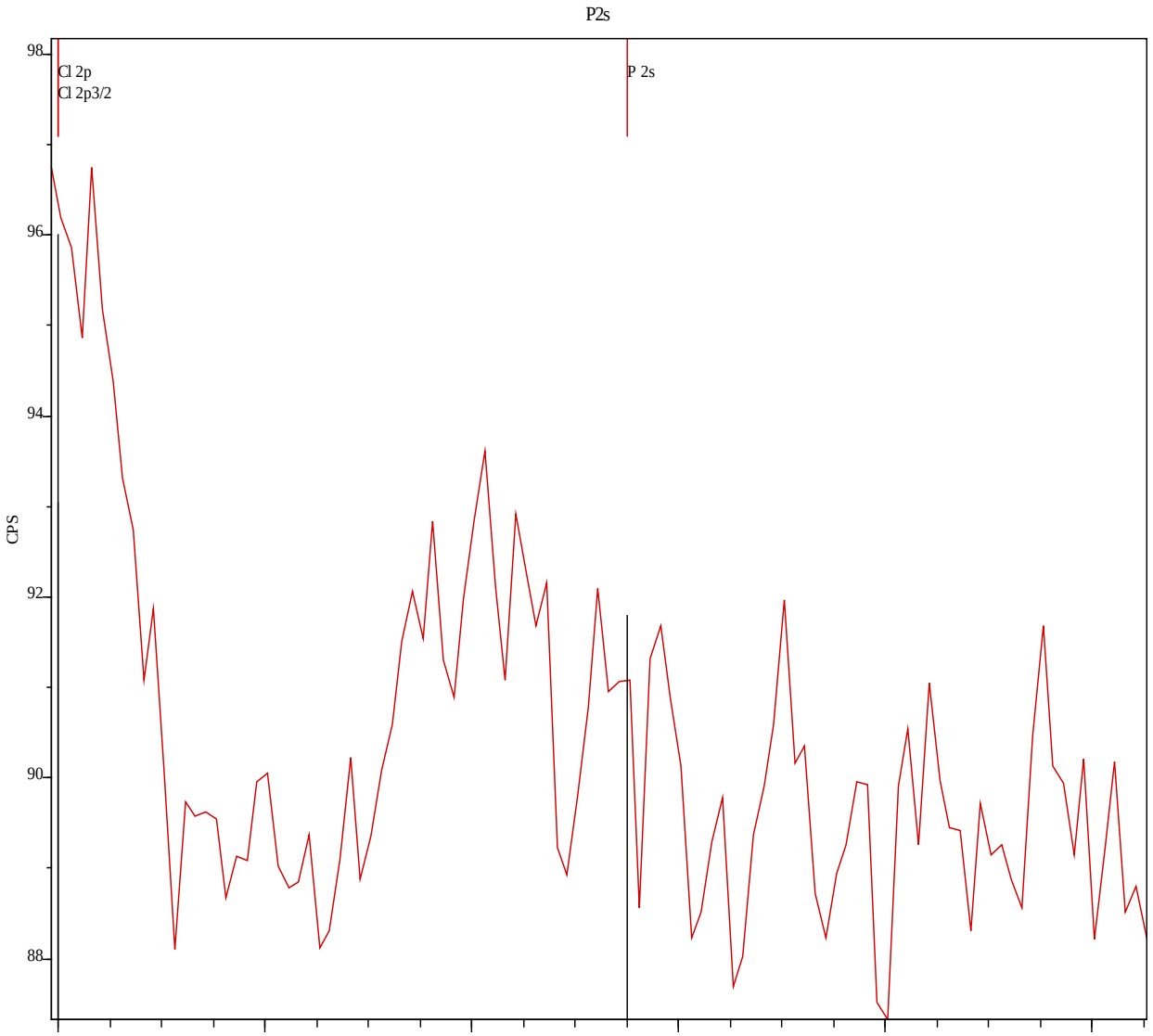

Figure 45. XPS Spectrum for Exposed Iron (179 – 200 eV range)

VI. Conclusion

6.1 Final Thoughts

The conclusions from this study are:

- Nonlinear mass loss profiles occurred during the desiccation of copper and iron specimens. Mass loss range was approx. 0.01-0.02% for copper and iron specimen. Significant mass increases were measured and are likely due to oxidation/reduction reactions involving oxygen.
- Normalized mass differences observed after desiccation cannot be used to determine malathion adherence to these specimen. Negative normalized mass differences were observed for iron because of the loss of iron flakes during exposure to malathion.
- XPS spectra can be used to detect the presence of phosphorus-containing compounds present on the surface of copper and iron specimen.

6.2 Limitations

Possible errors:

- The presence of copper on the surface of the iron specimen is most likely a result of using the same sand paper pad to clean both metals during the isotherm experiment.
- The possibility of an increase in the weight of the copper coupon as a result of oxidation/reduction reactions.
- The possibility of a decrease in the weight of the iron coupon as a result of oxidation/reduction reactions.

- The possible increase in weight of both the iron and copper coupons as a result of water crystallization after the desiccation period, just prior to the final weighing of the specimen.

6.3 Future Research

The following topics are recommended for future research:

- The effect of malathion exposure on TGA-GC-MS profiles for copper and iron specimen.
- The effect of malathion exposure on TGA/FTIR profiles for concrete and PVC specimen.
- The effect of malathion exposure on normalized mass differences for copper and iron specimen containing bio films and inorganic deposits.

VII. Bibliography

[1] "Weapons of Mass Decstruction (Chem/Bio)," [Online]. Available: http://www.thewednesdayreport.com/twr/vx.htm. [Accessed 2015].

[2] U. E. P. Agency, "Homeland Security Research," [Online]. Available: http://www2.epa.gov/homeland-security-research/homeland-security-research-program-hsrp. [Accessed 14 January 2015].

[3] B. L. D. S. J.A. Gervais, "Malathion Technical Fact Sheet," National Pesticide Information Center, Oregon State University Extension Services, 2009.

[4] U. E. P. Agency, "Mosquito control/Malathion," [Online]. Available: http://www2.epa.gov/mosquitocontrol/malathion. [Accessed 11 January 2015].

[5] E. P. Agency, "Environmental Potection Agency," [Online]. Available: www.epa.gov. [Accessed 17 February 2015].

[6] L. WebMD, "Medscape," [Online]. Available: http://www.emedicine.medscape.com. [Accessed 2015].

[7] B. R. Schneider, "Chemical Weapon," [Online]. Available: http://www.britanica.com. [Accessed 2015].

[8] U. A. S. a. B. C. C. (SBCCOM), "Lethal Nerve Agent (VX)," [Online]. Available: http://www.ilip.com. [Accessed 2015].

[9] R. Sferopoulos, "A review of chemical warfare agent (CWA) etector technologies and commercial off-the-shelf items," Australian Government, Department of Defense, Defense Science and Technology Organization, 2009.

[10] "About RAND," [Online]. Available: http://www.rand.org/nsrd/about.html. [Accessed 2015].

[11] "The Brownfields and Land Revitalization Technology Support Center," 2009. [Online]. Available: http://www.brownfieldstsc.org/glossary. [Accessed 2015].

[12] "Adsorption," [Online]. Available: http://www.rpi.edu. [Accessed 2015].

[13] J. K. F. W. J. P. L. Ferrari, "Interaction of Cement Model Systems with Superplasticizers Investigatedby Atomic Force Microscopy, Zeta Potential, and Adsorption Measurements," *Colloid Interface Science,* pp. 15-24, 2010.

[14] "Adsorption," [Online]. Available: http://www.memidex.com. [Accessed 2015].

[15] M. M. Clark, Transport Modeling for Environmental Engineers and Scientists, 2nd Edition, John Wiley and Sons, Inc., 2009.

[16] "Volatilization," [Online]. Available: http://www.scienceinthebox.com. [Accessed 2015].

[17] D. Larsen, "Chemwiki: The Dynamic Chemistry E-textbook," [Online]. Available: http://www.chemwiki.ucdavis.edu. [Accessed 2015].

[18] "US National Library of Medicine," 10 October 1993. [Online]. Available: http://www.nim.nih.gov. [Accessed 2015].

[19] [Online]. Available: http://www.. [Accessed 2015].

[20] S. R. A. Shard, "Quantitative Analysis of Adsorbed Proteins by X-ray Photoelectron Spectroscopy," *Analytical Chemistry,* pp. 8659-8666, 2011.

[21] E. A. Group, "How XPS Works," Seal Laboraatories, [Online]. Available: http://www.seallabs.com/how-xps-works.html. [Accessed 2015].

[22] "Water Sanitation Health," 2011. [Online]. Available: http://www.who.int. [Accessed 2015].

[23] J. E. B. R. J. G. Dana W. Kolpin, "The Pesticide National Synthesis Project," *Environmental Science and Technology,* pp. 558-566, 1998.

[24] J. D. B. Richard H. Coupe, "Water-Soluble Pesticides in Furnished Water of Community Water Supplies," *American Water Works Association,* pp. 56-68, 2004.

[25] J. G. Svetlana Bondarenko, "Degradation and Sorption of Selected Organophosphate and Caarbamate Insecticides in Urban Stream Sediments," *Environmental Toxicology and Chemistry,* pp. 1809-1814, 2004.

[26] M. V. M. S. Anu Mailainen, "Natural Organicmatter Removal by Coagulation during Drinking Water Treatment: A Review," *Advances in Colloid and Interface Science,* pp. 189-197, 2010.

[27] H. L. J. T. T. Miguel A. Providenti, "Selected Factors Limiting the Microbial Degradation of Recalcitrant Compounds," *Journal of Industrial Microbiology,* pp. 379-395, 1993.

[28] G. L. M. Kornaros, "Biological Treatment of Wastewater from a Dye Manufacturing Company using a Trickling Filter," *Journal of Hazardous Materials,* pp. 95-102, 2006.

[29] S. S. Watson, "Adsorption of Chemical Contaminants on Pipe Material and Their Decontamination," *National Institute of Standards and Technology,* 2010.

[30] W. T. B. X. Kun Li, "Retention of Organic and Inorganic Chemical by the Drainage/Supply Piping Material," *Environmental Pollution,* pp. 397-403, 2000.

[31] W. W. e. al., "Laboratory Study on the Adsorption of Mn+2 on Suspended and Deposited Amorphous Al(OH)3 in Drinking Water Distribution Water Systems," *Water Research,* pp. 4063-4070, 2012.

[32] P. G. K. Igor M. Svishchev, "Crystallization of Liquid Water in a Molecular Dynamics Simulation," *Physical Review Letters,* pp. 975-978, 1994.

[33] D. B. P. Jeninskens, "Crystallization of Amorphous Water in the Solar System," *The Astrophysical Journal,* 1996.

[34] C. H. B. D. K. R. Scott Smith, "Evidence of Molecular Translational Diffusion during the Crystallization of Amorphous Solid Water," *The Journal of Physical Chemistry,* pp. 6123-6126, 1997.

[35] A. G. A. S. M. Surya Devarakonda, "THF-Water Hydrate Crystallization: An Experimental Investigation," *Journal of Crystal Growth,* pp. 525-538, 1999.

[36] O. J. J. B. M. Scrub, "Experimental Study and Modeling of the Crystallization of a Water Droplet," *International Journal of Refrigeration,* pp. 59-68, 2003.

[37] L. Alchin, "Copper Reaction," [Online]. Available: http://www.elementalmatter.info. [Accessed 2015].

[38] A. L. Chemistry, "Chemistry of Transition Metal Compounds," [Online]. Available: http://www.alevelchem.com.

[39] O. L. A. O. Rafi Schwartz, "Integrated Hydraulic and Organophosphate Pesticide Injection Simulations for Enhancing Event Detection in Water Distribution Systems," *Water Research,* pp. 271-284, 2014.

[40] N. Y. B. Z. Jun Li, "Occurance of Organophosphate Flame Retardants in Drinking Water from China," *Water Research,* pp. 53-61, 2014.

[41] R. S. T. P. Jaime Nacher-Mestre, "Investigation of Orgnophosphate Ester in Freshwater, Salt and Brine Samples," *Analytical Methods,* pp. 1779-1785, 2011.

[42] A. D. J. C. K. Elizabeth Flint, "Solid-Phase Microextraction of Organophosphate Pesticides in Source Waters for Drinking Water Treatment Facilities," *Journal of Chromatographic Science,* pp. 484-488, 2006.

[43] D. J. V. Snoeyink, Water Chemistry, John Wiley and Sons, Inc., 1980.

[44] J. Sangster, "Phase Diagrams and Thermodynamic Properties of Binary Organic Systems based on 1,2-1,3-1,4-Diaminobenzene or Benzidine," *Journal of Physical Chemical Reference Data,* 1994.

[45] "Linear Regression Models," [Online]. Available: http://www.people.duke.edu/~mau/rsquared.htm. [Accessed 2015].

[46] A. K.-V. S. W. G. C. J. P. Alexander V. Naumkin, "NIST X-ray Photoelectron Spectroscopy Database," 2000.

[47] S. C. R. d. B. M. F. F. C. K. Kion Norman, "Lifetime and Stability Studies," 2008. [Online]. Available: http://www.spie.org/samples/PM175.pdf. [Accessed 8 January 2015].

[48] G. P. Kimberly S. Beltran, "Acetylcholinesterase activity in Corbicula-Fluminea Mull., as a biomarker of rganophosphate pesticide pollution in Pinacanauan River, Phillipins," *Evironmental Monitoring and Assessment,* pp. 331-340, 2010.

[49] S. E. R. W. Dickinson, "Biological Warfare Agents as Threats to Potable Water," *Environmental Health Perspectives,* pp. 975-984, 1999.

[50] E. F. H.F. Hemond, Chemical Fate and Transport in the Environment, Academic Press, 1994.

[51] U. D. o. Energy, "National Iinstitute of Standards and Technology (NIST)," 2015.

[52] J. K. M. Z. C. M. U. Green, "Detection of Chemical Threat Agents in Drinking Water by an Early Real-Time Biomonitor," *Wiley Periodicals*, 2003.

[53] R. F. Chinawat Tongchat, "Determination of Partion Coefficients of Migrants between Layers used in Multi-Layer Multi-Materailstructures Intended for Food Contact," November 2015.

[54] B. N. X. Z. Churyan Hao, "Determination of Residual Carbamate, Organophosphate, and Phenyl Urea Pesticieds in Drinking and Surface Water by High-Performance Liquid Chromotography/TandemMass Spectrometry," *Journal of AOAC International*, pp. 400-410, 2010.

[55] W. F. N. Hans-Ake Lakso, "Division of NBC-Defense FOA, The Swedish Defense Research Establishment," *Analytical Chemistry*, pp. 1866-1872, 1997.

[56] L. Thibodeaux, Environmental Chemodynamics: Movement of Chemicals in Air, Water, and Soil, 2nd Edition, John Wiley and Sons, Inc., 1996.

[57] K. Newhart, "Environmental Fate of Malathion," California Environmental Protection Agency, Los Angelas, 2006.

[58] J. Schnoor, Environmental Modeling: Fate and Transport of Pollutants in Water, Air, and Soil, John Wiley and Sons, Inc., 1996.

[59] B. Logan, Environmetal Transport Processes, John Wiley and Sons, Inc., 1999.

[60] O. K. Dalrymple, "Experimental Determination of Octanol-Water Partition Coefficient for Acetophenone and Atrazine," Department of Civil and Environmental Engineering, University of South Florida, 2005.

[61] D. M. L.J. Thibodeaux, Hnadbook for Chemical MassTransport in the Environment, CRC Press, 2011.

[62] W. P. E. Fries, "Monitoring if the Three Organophosphate Esters TBP, TCEP, and TBEP in River Water and Ground Water (Oder, Germany)," *Journal of Environmental*

Monitoring, pp. 346-352, 2003.

[63] W. P. E. Fries, "Occurence of Organophosphate Esters in Surface Water and Ground Water in Germany," *Journal of Enviironmental Monitoring,* pp. 621-626, 2001.

[64] P. D. C. M. M. Steven J. Larson, "Pesticides in Surface Water: Distribution, Trendsn and Governing Factors," 1997.

[65] D. L. S. D. D. J. Ali D. Khan, "Precautions against Biological and Chemical Terrorism Directed at Food and Water Supplies," *Public Health Reporters*, pp. 3-13, 2001.

[66] H. G. T. J. G. H. D. E. B. William E. Lee, "Rapid Detection and Identification of Biological and Chemical Agents by Immunoassay, Gene Probe Assay and Enzyme Inhibition usinf a Silicon-based Biosensor," *Biosensors and Bioelectronics,* pp. 795-804, 2000.

[67] R. S. S. P. N. T. J. K. S. F. O. Y. C. S. Vinay K. Singh, "Removal of Malathion from Aqueous Solutions and Wastewater using Fly Ash," *Scientific Research,* pp. 322-330, 2010.

[68] W. P. Julia Regnery, "Seasonal Fluctuations of Organophosphate Concentrations in Precipitation and Storm Water Runoff," *Chemosphere,* pp. 958-964, 2010.

[69] J. P. A. M. J. Halamek, "Sensitive Detection of Organophosphates in River Water by Means of a Piezeoelctric Biosensor," *Analytical and Bioanalytical Chemistry,* pp. 1904-1911.

[70] A. J. Suriano, "Stdies in the Synthesis of Organophosphorus Compounds as Inhibitors of Butylcholineterase," California State University, Long Beach, 2013.

[71] S. D. Wallace.US Patent US 6200469 B1, 2001.

[72] S. G. B. A. M.-D. Velitchko G. Tzatchkov, "Water Treatment Units Residence-Time Distribution as Probabilistic Finctions," *Journal of Environmental Engineering,* pp. 1-9, 2009.

[73] M. P. C. A. M. W. C. Joseph Wang, *Analytical Chemistry,* pp. 1804-1808, 2001.

[74] O. S. University, "Malathion Technical Fact Sheet," [Online]. Available: http://www.npic.orst.edu. [Accessed 2015].

[75] "Weapons of Mass Destruction (Chem/Bio)," [Online]. Available: http://www.thewednesdayreport.com. [Accessed 2015].

[76] "Fundamental XPS Data to Assist Peak-fitting Elements, Binary Oxides and Chemical Compounds," [Online]. Available: http://www.xpsdata.com. [Accessed 2015].

[77] B. P. P. A. P. G. L. W. M. L. A. R. G. R. S. C. S. Mark C. Biesinger, "Resolving Surface Chemical States in XPS Analysis of First Row Transition Metals, Oxides and Hydroxides: Cr, Mn, Fe, Co and Ni," *Applied Surface Science*, pp. 2717-2730, 2011.

[78] D. K. A.V. Schukarev, "XPS Study of Group IA Carbonates," *Central European Science Journals*, vol. 2, no. 2, pp. 347-362, 2004.

[79] W. T. W. B. E. Y. J. P. T. C. W. V. S. D. G. M. H. J. M. M. T. H. Nohira, "Characterization of ALCVD-Al2O3 and ZrO2 Layer Using X-ray Photoelectron Spectroscopy," *Journal of Non-Crystalline Solids*, vol. 303, no. 1, pp. 83-87, 2002.

[80] Thermoscientific, "XPS Simplified," Thermo Scientific XPS, [Online]. Available: http://www.xpssimplified.com/knowledgebase.php. [Accessed 10 November 2014].

VIII. Vita

Captain William D. Flemings graduated from Antioch High School in Antioch, Tennessee. He enlisted into the United States Navy in 1997. He entered undergraduate studies at Norfolk State University in Norfolk, Virginia where he graduated with a Bachelor of Science degree in Interdisciplinary Studies in 2002. He was commissioned through the NROTC Unit at Old Dominion University as a Nuclear Engineering Officer.

His first assignment was onboard the USS Pennsylvania (SSBN-735) as the Reactor Controls Division Officer in 2004. In December 2005, he separated from the United States Navy and later was commissioned as a Logistics Captain in the United States Army in 2009. His first assignment was as the Fuel Operations Officer at the 3rd Sustainment Brigade, Fort Stewart, Georgia. While stationed at Fort Stewart, he deployed to Iraq where he served as the Fuel Operations Officer for mid and northern Iraq. After redeployment, he was assigned as the Commander of the 274th Movement Control Team at Fort Stewart, Georgia. In May 2013, he entered the Graduate School of Engineering and Management, Air Force Institute of Technology. Upon graduation, he will receive a master's of science in Combating Weapons of Mass Destruction, as well as a master's of science in Environmental Engineering and Science.

REPORT DOCUMENTATION PAGE

Form Approved
OMB No. 074-0188

PLEASE DO NOT RETURN YOUR FORM TO THE ABOVE ADDRESS.

1. REPORT DATE *(DD-MM-YYYY)*	2. REPORT TYPE	3. DATES COVERED *(From – To)*
26-03-2015	Master's Thesis	December 2013 - March 2015

4. TITLE AND SUBTITLE
Detection and Characterization of Malathion Adherence to Piping Materials Used in Water Distribution Systems

5a. CONTRACT NUMBER

5b. GRANT NUMBER

5c. PROGRAM ELEMENT NUMBER

6. AUTHOR(S)
Flemings, William D., Captain, USA

5d. PROJECT NUMBER
15V119

5e. TASK NUMBER

5f. WORK UNIT NUMBER

7. PERFORMING ORGANIZATION NAMES(S) AND ADDRESS(S)
Air Force Institute of Technology
Graduate School of Engineering and Management (AFIT/EN)
2950 Hobson Way, Building 640
WPAFB OH 45433

8. PERFORMING ORGANIZATION REPORT NUMBER
AFIT-ENV-MS-15-M-096

9. SPONSORING/MONITORING AGENCY NAME(S) AND ADDRESS(ES)
Environmental Protection Agency
National Homeland Security Research Center
26 West Martin Luther King Drive
Cincinnati, OH 45268
513-569-7321, magnuson.matthew@epa.gov

10. SPONSOR/MONITOR'S ACRONYM(S)
EPA/NHSRC

11. SPONSOR/MONITOR'S REPORT NUMBER(S)

12. DISTRIBUTION/AVAILABILITY STATEMENT
DISTRIBUTION STATEMENT A. APPROVED FOR PUBLIC RELEASE; DISTRIBUTION UNLIMTED.

13. SUPPLEMENTARY NOTES
This material is declared a work of the U.S. government and is not subject to copyright protection in the United States.

14. ABSTRACT: Protection of the public water supply is a national security priority, and as such, it is important to better understand the fate of a chemical weapons agent injection into a public water distribution system. This study investigated the adherence of malathion to pipe materials that are used in public water distribution systems, with malathion serving as a chemical representative of the organophosphorus nerve agent VX. Copper and iron specimen were exposed to malathion solutions for periods of 4, 8, and 24 hours and then tested for evidence of chemical adherence to the metal surfaces. Nonlinear desiccation profiles revealed total mass losses that were typically between 0.01-0.02% but notable mass increases were also observed during desiccation, likely due to surface reactions involving oxygen. Normalized mass differences were poorly correlated with the malathion concentrations (R2 typically < 0.6), which suggests that mass-based measurements are not sufficient to determine malathion exposure to pipe materials. X-ray photoelectron spectroscopy was also used in an effort to detect shifts in the adsorptive spectra that appeared to be attributable to the presence of trace levels of malathion on the surface of the exposed pipe materials. The spectra observed from the XPS analysis of the copper and iron specimen suggests that the presence of malathion on the surface of the pipe material can sufficiently be detected and measured by XPS analysis. To the author's knowledge, this the first study to investigate malathion adherence to pipe materials with mass measurements and XPS."

15. SUBJECT TERMS
Organophosphate, malathion, activated sludge, respiration, performance degradation

16. SECURITY CLASSIFICATION OF:			17. LIMITATION OF ABSTRACT	18. NUMBER OF PAGES	19a. NAME OF RESPONSIBLE PERSON
a. REPORT	b. ABSTRACT	c. THIS PAGE			Dr. Willie F Harper Jr. AFIT/ENV
U	U	U	UU	127	19b. TELEPHONE NUMBER *(Include area code)* (937) 255-3636, x 4528 (willie.harper@afit.edu)